2018

Defining the role of cytosolic iron-sulfur cluster assembly targeting complex in identification of iron-sulfur cluster proteins

BOSTON UNIVERSITY

GRADUATE SCHOOL OF ARTS AND SCIENCES

Dissertation

DEFINING THE ROLE OF THE CYTOSOLIC IRON-SULFUR CLUSTER ASSEMBLY TARGETING COMPLEX IN IDENTIFICATION OF IRON-SULFUR CLUSTER PROTEINS

by

AMANDA THUY VAN VO

B.A., University of Missouri, 2012
M.A., Boston University, 2014

Submitted in partial fulfillment of the

requirements for the degree of

Doctor of Philosophy

2018

Approved by

First Reader _____

Deborah Perlstein, Ph.D.
Assistant Professor of Chemistry

Second Reader _____

Karen Allen, Ph.D.
Professor of Chemistry

DEDICATION

I would like to dedicate this work to my parents, who gave me life and then supported me through it as I followed my dreams. I keep in mind daily their struggles and the sacrifices they have made so I could have the opportunities I did. I would also like to dedicate this thesis to Jessica Cosman, whose love for science continues to inspire me.

ACKNOWLEDGMENTS

First, I would like to thank my wonderful advisor and mentor Deborah Perlstein, who taught me how to think critically for myself. Without her unwavering patience and guidance, I would not be the scientist I am today. I would also like to thank my second reader Karen Allen for painstakingly editing my thesis while also providing several laughs and good spirit. A thank you also to my committee members: John Caradonna, Sean Elliott, and John (Chip) Celenza for their helpful discussions of my research and their advice over the years. I'd like to give a special thanks to Chip for his help with my yeast experiments and to Karen and Sean for their feedback on my papers.

There are countless people who helped me with my experiments. I would like to thank my collaborators mentioned in this work: Edward Brignole (MIT) and Deborah Francoleon (BU medical campus), for helping me with experiments and providing techniques to investigate interesting problems in my thesis. Also, I would like to thank the members of the CIC at BU (Jeff Bacon especially for his help with CD data), Deborah Pheasant at the BIF at MIT, and Kelly Arnett at Harvard Medical for all their help with instrumentation. Many thanks go to my awesome undergraduates Mary Froehlich, Jessica Cosman, Claudia Lee, Calina Glynn, Stephanie Esonwune, Cici Qi, and Zanub Hassan for all their contributions and hard work. I would also like to thank my labmates Melissa Marquez and Nicholas Fleischmann for their help on understanding our side of the pathway.

There are many other Perlstein lab members (previous and current) that have helped shape me as a scientist. Thank you to Xin Sun, for teaching and guiding me with a

firm hand, and inspiring me to be hard worker. Thank you also to my wonderful labmates Christa Molé and John Grossman, who have become close friends of mine and emotionally supported me through many late and rough nights in lab.

A special thank you to my significant other, James Seibel, whose encouragement, love, and support make me feel like I can do anything. Last, but not least, I want to give a big thank you to my parents, my brother Dan, my sister Kim, and my friends. I am so grateful for you all in my life and thankful for your love and support. Thank you for believing in me.

DEFINING THE ROLE OF THE CYTOSOLIC IRON-SULFUR CLUSTER ASSEMBLY TARGETING COMPLEX IN IDENTIFICATION OF IRON-SULFUR CLUSTER PROTEINS

AMANDA THUY VAN VO

Boston University Graduate School of Arts and Sciences, 2018

Major Professor: Deborah Perlstein, Assistant Professor of Chemistry

ABSTRACT

Iron sulfur (FeS) clusters are ubiquitous cofactors required for numerous fundamental biochemical processes, including DNA replication and repair, transcription, and translation. In the cell, these metallocofactors require a dedicated protein pathway for assembly. The Cytosolic Iron Sulfur Cluster Assembly (CIA) pathway is conserved across higher-level eukaryotes and is responsible for building and inserting these cofactors into the FeS proteins that need them. A major unsolved problem in the FeS cluster biogenesis field is how so many diverse FeS proteins are identified for cluster insertion. Several studies have identified a multiprotein complex containing Cia1, Cia2, and Met18 as the CIA targeting complex responsible for FeS cluster recognition and target maturation. The CIA targeting complex has been shown to associate with an FeS cluster protein, Nar1. Nar1 is a CIA factor that plays an unknown role in cluster transfer. Little information is known about the structure of the CIA targeting complex its mechanism of FeS cluster protein recognition. In this thesis, I investigate the architecture of the CIA targeting complex as well as the role each subunit plays in identification of apo-proteins and iron-sulfur cluster insertion.

Previous proteomic and cell biological studies from the Lill lab propose that the CIA targeting complex exists as a mixture of discrete complexes *in vivo*. Each of these complexes is responsible for recognizing a distinct subset of targets. Herein, we utilize affinity co-purification and size exclusion chromatography investigate connectivity of the targeting complex, identify stable subcomplexes, and define their roles in recognizing our two model targets Rad3 and Leu1. We determine the CIA targeting complex contains one Met18, two Cia1, and four Cia2 polypeptides. This complex is required to recognize Leu1. Our experiments reveal the formation of the stable subcomplexes Cia1-Cia2 and Met18-Cia2, which is sufficient to identify to Rad3. We also interrogate the role of Nar1 in binding to targets and cluster transfer, excluding the model that it acts as an adapter for cluster transfer.

Furthermore, using site directed mutagenesis, combined with our co-purification and *in vivo* assays, we map the key interfaces required to form the targeting complex and investigate how their mutations impacts CIA function *in vivo*. We identify the binding site of Cia1 on Cia2, as well as the general region in which Cia2 binds to Met18. Through these experiments, we shed light on the role these subunits of CIA targeting complex and Nar1 play in FeS target recognition and FeS cluster transfer.

TABLE OF CONTENTS

LIST OF TABLES

LIST OF FIGURES

LIST OF ABBREVIATIONS

4Fe4S	four iron, four sulfur cluster
BME	β-mercaptoethanol
BMOE	bismaleimidoethane
C18	octadecyl carbon chain bound silica column
CIA	cytosolic iron-sulfur cluster assembly
Co-IP	co-immunoprecipitation
CV	column volume
DC4	cyclic amine crosslinker
DMSO	dimethyl sulfoxide
DOX	doxycylcine
DSS	disuccinimidyl suberate
DTT	dithiothreitol
DUF59	domain of unknown function 59
EM	electron microscopy
EV	empty vector
$Fe(NH_4)_4(SO_4)_2$	ferrous ammonium sulfate
FeS	iron sulfur
FNR	fumerate nitrate reductase
FPLC	fast protein liquid chromatography
G25	desalting column
HCl	hydrochloride

HEAT	Huntingtin, elongation factor 3, protein phosphatase 2A, yeast kinase TOR1
HU	hydroxyurea
IA	iodoacetamide
IB	inclusion bodies
IDD	intrinsically disordered domain
LB	Luria broth/lysogeny broth
M1	motif 1
M2	motif 2
M3	motif 3
M4	motif 4
M5	motif 5
M6	motif 6
MALDI TOF	matrix-assisted laser desorption/ionization time of flight
$MgCl_2$	magnesium chloride
MMS	methyl methanesulfonate
MS	mass spectroscopy
Na_2HPO_4	disodium phosphate
$Na_2S•9H_2O$	sodium sulfide nonahydrate
$NaCl_2$	sodium chloride
Ni-NTA Nickel	nitrilotriacetic acid
NP40	nonyl phenoxypolyethoxylethanol
OD	optical density

PD10	desalting column
SC	synthetic complete
SDS-PAGE	sodium dodecyl sulfate polyacrylamide gel electrophoresis
SEC	size exclusion chromatography
SEC-MALS	size exclusion chromatography with multi angle light scattering
SMP	structural maintenance protein
SNAP	self-labeling fluorescent protein tag
SPR	surface plasmon resonance
Strep	Streptactin
TCEP	tris(2-carboxyethyl)phosphine
TET	tetracycline
WT	wild-type
XPD	xeroderma pigmentosum group D
YPAD	yeast, peptone, adenine sulfate, and dextrose

CHAPTER ONE: Introduction to the CIA Pathway and the Targeting Complex

1.1 Overview of FeS clusters

Iron sulfur (FeS) clusters are ubiquitous cofactors required for numerous fundamental biochemical processes in both the nucleus and cytosol, spanning from DNA replication and repair to amino-acid metabolism.[1, 2] These ancient metallocofactors are present in all forms of life including plants, animals, bacteria, and archaea and are required for essential reactions.[3] In the cell, FeS clusters require a dedicated proteinaceous pathway for their assembly.

There are several FeS cluster biogenesis pathways required to build these such as the NIF (nitrogen fixation), ISC (iron sulfur cluster), and SUF (sulfur formation) systems.[3-5] The ISC machinery is most widely present in bacteria and also present in eukaryotes. The SUF system is utilized in iron-limiting or oxidative stress conditions, while the NIF system is a dedicated pathway for maturation of an FeS nitrogenase in nitrogen fixation.[6] Notably, different domains of life have adopted specific FeS systems to provide their metallocofactors. Even in simple organisms like bacteria, there are multiple FeS biogenesis systems. For example, the SUF system is the major FeS assembly pathway for cyanobacteria, while for *Escherichia coli*, ISC is the preferred main FeS system.[4] In eukaryotes, the need for specific FeS biogenesis systems is even more complicated as they differentially localize to specific compartments. The ISC proteins are often found in mitochondria, while the SUF homologs are often found in plastid or chloroplasts.[4]

Although these FeS systems can be found in different organelles in eukaryotes

and are overall utilized differentially for different domains of life, all contain the same general steps for iron-sulfur cluster biogenesis. For each pathway, an FeS cluster is built on a scaffold. Next, this FeS cluster is trafficked and inserted into the apo-target (an FeS protein without cluster). For all biogenesis systems, the mechanism of how FeS cluster proteins are recognized is not well understood. In this thesis, I will focus on understanding how this occurs in the cytosolic iron sulfur cluster assembly (CIA) pathway in yeast.

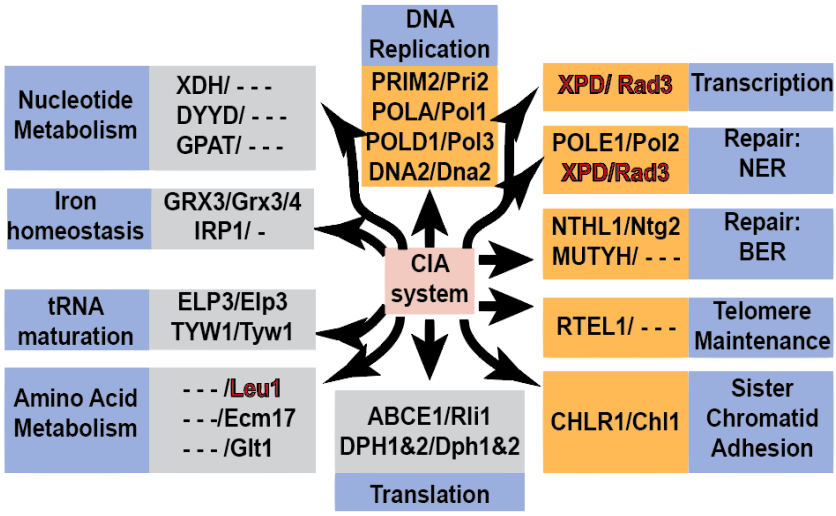

Figure 1.1. Several FeS protein targets require the CIA pathway for their biological function. Cytosolic targets are shown in grey and nuclear targets are shown in gold. This thesis work primarily focused on the helicase Rad3 required for nucleotide excision repair and the isomerase Leu1, involved in leucine biosynthesis (both shown in red).

The CIA pathway is responsible for the insertion of FeS cluster in over twenty FeS proteins, termed apo-protein targets.[7] These FeS proteins are required for essential biological functions in the cytosol and nucleus such as amino-acid metabolism, DNA replication and repair, and transcription (Figure 1.1). As insertion of these cofactors is

required for these essential biological processes, defects in the CIA pathway result in disease. Previously, studies have shown that defects in mitochondrial iron-sulfur cluster biogenesis can lead to pathologies such as Friedreich's ataxia (FRDA) and sideroblastic anemia. Defects in mitochondrial FeS biogenesis lead to nuclear genome instabilities, indicating the effects of defects in FeS biogenesis.[8] Specifically, defects in the CIA pathway have also been recently directly linked to cancer.[9, 10] As more FeS proteins are linked to transcription and DNA replication and repair, defects in the CIA pathway may be able to explain diseases associated with these FeS proteins, such as xeroderma pigmentosum and Fanconi anemia.[2, 11] Without a doubt, understanding the CIA pathway and elucidating downstream targets will identify how defects in this pathway can lead to genomic instability and other critical diseases.

1.2 Assembly of FeS clusters on the CIA scaffold

The *de novo* assembly of an FeS cluster requires sources of iron, sulfide, and reducing equivalents. For the CIA pathway it is proposed an unknown sulfur-containing source X-S is exported from the mitochondria.[1, 12, 13] Recent work has suggested that these iron and sulfur sources originate from Grx3/Grx4.[14-16] Along with an unknown iron source and reducing equivalents from the Dre2 and Tah18 complex, a 4Fe4S cluster is formed on the interface of a scaffolding complex Cfd1 and Npb35 (Figure 1.2).[17, 18] After the FeS cluster is formed on the scaffold, it is then transferred and inserted into the FeS apo-protein substrates (Figure 1.2). [18-20]

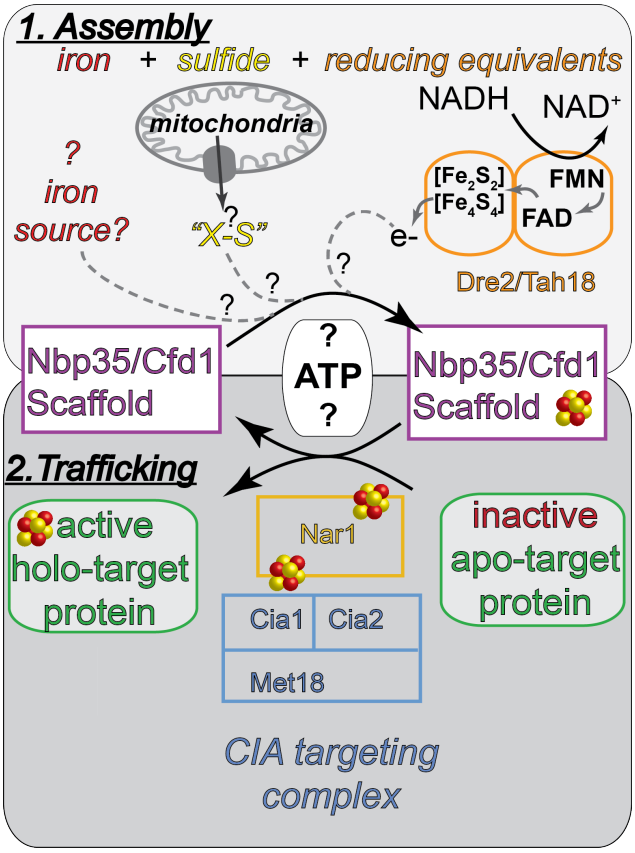

Figure 1.2 Overview of the CIA pathway.
Iron, sulfide (exported from the mitochondria), reducing equivalents (from Dre2/Tah18) are assembled on the scaffold (Nbp35 and Cfd1). The CIA targeting complex recognizes the apo-target protein and aids in cluster insertion with Nar1 to make the protein holo and active. However, it is still unknown if other accessory proteins between the scaffold and the targeting complex are required for FeS insertion.

1.3 The CIA Targeting complex

The process by which the FeS clusters are transferred to apo-protein targets remains unclear. It is still not well understood how the 4Fe4S cluster formed on the Cfd1-Nbp35 scaffold is transferred to the apo-protein targets that require the metallocofactor for their biological functions. Several proteomic studies suggest that a multiprotein complex is required to recognize FeS cluster proteins and is responsible for target maturation.[7, 21-24] The multiprotein complex contains the proteins Cia1, Cia2, and Met18

and is called the CIA targeting complex. Previous studies demonstrate that Nar1 associates with the CIA targeting complex.[25, 26] Nar1 is a CIA factor that is placed downstream of the scaffolding complex by *in vivo* studies and is required for FeS cluster insertion for CIA targets.[24, 27, 28] However, the mechanism by which the CIA targeting complex recognizes FeS proteins and the role of Nar1 are unknown. In this thesis, we explore functions of Nar1 and the CIA targeting proteins to understand how FeS clusters are identified for cluster insertion.

1.3.1 Nar1

Nar1 contains two 4Fe4S clusters and is an FeFe hydrogenase-like protein. [24, 27, 29] Nar1 is called a "hydrogenase-like" protein because of its high sequence homology to FeFe hydrogenases, but it does not produce or consume hydrogen.[30] Previously Nar1 was linked to the CIA pathway as it is essential for FeS cluster assembly on cytosolic, but not mitochrondrial FeS proteins.[24] SiRNA silencing of Nar1 does not change expression levels in Nbp35 and Cfd1, suggesting it is downstream of the scaffolding proteins.[17, 18, 24] Depletion of early acting CIA factors also reduces incorporation of FeS clusters into Nar1. However, depletion of the CIA targeting complex does not block cluster insertion into Nar1 indicating, it is upstream of the CIA targeting complex. [17, 18, 24, 25] Little is known about Nar1 in the CIA pathway and the role it plays at the interface of the scaffolding complex and the targeting complex.

Previous studies suggest that its FeS clusters important to the function of Nar1 within the CIA pathway. Eukaryotic homologs of this protein contain four cysteine residues clustered at the N-terminus and four cysteine residues scattered throughout the

center and C-terminus of the protein. Biochemical studies investigated these residues for the yeast Nar1 and noted EPR signals consistent with 4Fe4S clusters.[28] Additionally, mutations of these cysteines knock down cluster dependent activity of a Fe-S protein target, Leu1.[17, 18, 24, 27] This suggests that Nar1 requires early CIA factors for its cluster maturation and that its clusters are required for FeS insertion into apo downstream proteins.

There are many possibilities for the role of Nar1 in the CIA pathway. Nar1 could provide reducing equivalents to the scaffold. However, this model seems unlikely as previous studies demonstrate Dre2 and Tah18 provide reducing equivalents to the Cfd1-Nbp35 scaffold.[15, 17] This thesis focuses on deciphering the role of Nar1 by investigating two potential models based off previous studies that place Nar1 at the interface of the scaffolding and targeting complexes. These simple models are the most likely based off Nar1's interactions with the scaffolding and targeting proteins.

In one model, we investigate Nar1 as an adapter that joins together the scaffold and the targeting complex with an apo-target. For this model to be possible, Nar1 must be able to bind to the scaffolding complex as well as the targeting complex bound to an apo-target protein (Figure 1.3A). Previously studies have indicated that Nar1 can bind to the targeting complex proteins. [25, 26] Additionally, a newer publication observed an interaction between the scaffolding protein Nbp35 and Nar1 in plants by SPR.[31]. In chapter 3, we investigate this adapter model with our apo-protein Leu1.

Another possible model is that Nar1 is a cluster carrier that provides FeS cluster to the apo-protein targets (Figure 1.3B). In this model, the scaffold would first transfer

the FeS cluster to Nar1. Nar1 then could transfer the cluster to the apo-target protein, which is recognized by the CIA targeting complex. This model is also a possibility as previous studies suggest that mutations in the cluster ligating cysteines of Nar1 are required for cluster maturation in Leu1. [17, 18, 24, 27] We also investigate this cluster transfer model for Nar1 in chapter 3 of this thesis using Leu1 as an apo-protein target.

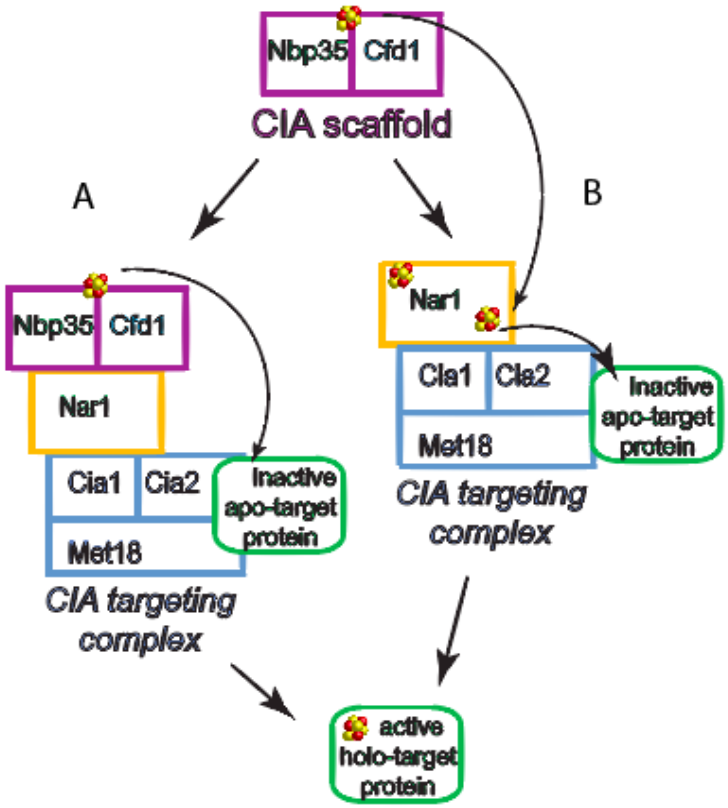

Figure 1.3. Simple most likely models for the role of Nar1.
A) Nar1 acts as an adapter between the scaffold and the targeting complex with the apo-target so that the cluster formed on the scaffold can be transferred to the apo-target protein. B) Nar1 acts as cluster carrier, trafficking the cluster from the scaffold to the apo-target protein via the CIA targeting complex.

1.3.2 Cia1

The CIA targeting complex includes the protein Cia1. Cia1 is an essential gene that in fission yeast forms a fusion protein with Cfd1. [7, 23, 32] Based off this fusion protein,

it was hypothesized that Cia1 was part of the CIA pathway. This was later confirmed when the Lill lab revealed that a depletion of the *CIA1* gene led to a decrease in enzyme activities and iron incorporation of downstream targets Leu1 and sulfite reductase.[23] Depletion of Cia1 did not result in the decrease of expression levels of Npb35 or Nar1, indicating it was downstream of these proteins.[23] Lastly, several co-immunoprecipitation (co-IP) studies place Cia1 as part of a targeting complex with Cia2 and Met18 (Figure 1.2). [7, 21-24]

The structure of Cia1 suggests its function within the targeting complex. Cia1 is a WD40 protein that contains seven propeller blades.[32] WD40 repeat proteins are involved in several types of cellular functions such as cell cycle control, vesicular trafficking, and phototransduction.[33-35] Although the cellular functions they are involved in are diverse, the "WD40 repeat" family of proteins are all involved in protein-protein interactions. Some act as hubs for large complexes and others flexibly recognize different proteins. Binding sites for the WD40 partner proteins are generally located at the central tunnel region on the top face and at one or two of the WD40 blade regions on the top/side face of the WD40 proteins (Figure 1.4, purple).[36-38] The location of the top interface is further from the side interface, suggesting Cia1 can bind to two different proteins. As Cia1 has been shown to form a targeting complex with Met18 and Cia2, one may hypothesize that it would act as a hub for binding to both these proteins. However, in this thesis we observe binding interactions with Nar1 and Cia1 and propose a different model for its role within the targeting complex.

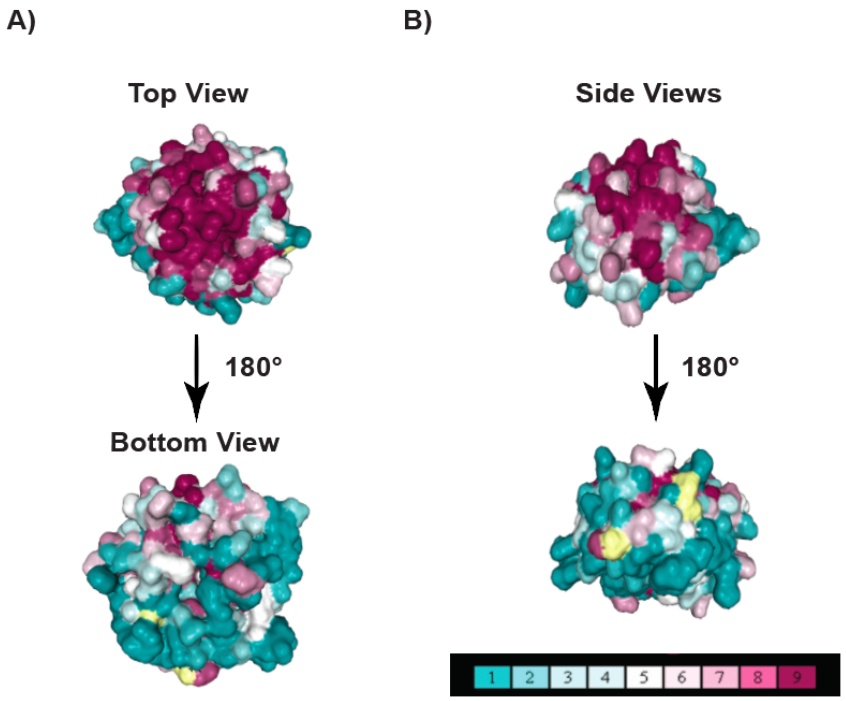

Figure 1.4 Representation of conserved amino acids at the surface of Cia1.
A) The degree of conservation is indicated by the dark pink color. The top of surface of Cia1 compared to the bottom surface is more highly conserved. B) One side of Cia1 is more highly conserved than the other. The degree of conservation was calculated using ConSurf (Landau et al., 2005).

1.3.3 Cia2

Cia2 is another component of the targeting complex. Many proteomic studies identify Cia2 as a member of the CIA targeting complex. [7, 21-24] Previous studies demonstrated that a weaker Cia2 allele exhibits lower activities of the cytosolic [4Fe-4S] enzyme aconitase and the nuclear [4Fe-4S] enzyme DNA glycosylase ROS1, indicating Cia2 is responsible for the maturation of these FeS target proteins in the CIA pathway.[39] In this thesis, we reveal that Cia 2 is the organizing center of the targeting complex involved in recognizing FeS cluster proteins for cluster insertion in the last step of the CIA pathway.[5, 40]

Cia2 contains domains that reveal its possible function within the CIA targeting complex. In humans there are two paralogs of Cia2, Cia2a (Fam96a) and Cia2b (Fam96b or Mip18). Fam96b is more structurally similar to Cia2 in yeast than Fam96a. [7] The N-terminal domain contains two conserved regions, an NxNP motif and a patch of acidic residues. This N-terminal extension is missing in bacterial and archaeal DUF59 proteins and in the Cia2a paralogs.[40] The C-terminal half of Cia2 contains a domain described as an FeS assembly domain or MIP18 family-like domain (InterPro), formerly known as the domain of unknown function 59 (DUF59).[41] DUF59 proteins are genetically linked to FeS cluster biogenesis in bacteria and archaea.[42-45] For example, a bacterial protein called SufT was recently proposed as an FeS biogenesis protein.[43] Additionally, many organisms contain a fusion of an MRP/Nbp35 type cluster scaffold and a DUF59 domain.[45] The conservation of this domain highlights the significance of the role of DUF59 domain in FeS cluster biogenesis. In chapter 4 of this thesis we will investigate residues within the DUF59 domain of Cia2.

Specifically within the DUF59 domain, studies have also shown a hyper-reactive cysteine in both yeast Cia2 (C161) and human CIA2B (C93) is critical for the function of Cia2.[46] Hyper-reactivity was defined by the Cravatt lab as cysteines with heightened nucleophilicity in their activity based protein profiling.[46] Additionally, mutations of this cysteine are lethal and dominant negative in yeast.[47] A crystal structure of Cia2a in humans forms a dimer that is present in a major form and a minor form.[48] In the minor form a conserved (C93) cysteine on the monomer of one subunit is positioned towards the cysteine of the other monomer. This suggests the possibility that two cysteines may

be required for Cia2's function in FeS cluster biogenesis. In this thesis we investigate the role of this cysteine along with other conserved amino acids to understand the function of Cia2.

1.3.4 Met18

Many proteomic studies also identified Met18 as a protein within the CIA targeting complex. [7, 21-24] Notably, Met18 is a nonessential protein unlike the other subunits of the targeting complex. However, this does not mean it plays an unimportant secondary role in the CIA pathway. Although not an essential protein, studies have indicated that Met18 is required for DNA metabolism and genomic stability.[21, 22] Mutations to Met18 show a variety of phenotypes including defects in methionine synthesis, sensitivity to genotoxic stress, and the presence of extended telomeres. [22, 49-52]. These phenotypes can be explained by the link of Met18 to the CIA targeting complex and its role in identification of FeS targets such as sulfite reductase in methionine biosynthesis, and DNA helicases, DNA demethylation mediated by glycosylases, and polymerases involved in DNA replication and repair.[22, 42, 49, 52, 53]

The tertiary structure of Met18 suggests that Met18 plays a role in FeS protein recognition. Met18 contains HEAT repeat domains that are essential for protein-protein interactions. The HEAT (Huntingtin, Elongation factor 3, protein phosphatase 2A, TOR1) domain is a di-helical domain that is separated by a non-helical region.[54-56] The proteins that this domain is defined after are mediators of protein-protein interactions and have the ability to bind to several proteins. For example, the N-terminal portion of the protein Huntingtin, has been reported to interact with more than two dozen proteins.

These interactions implicate Huntingtin in several processes such as signal transduction, transcriptional regulation, RNA splicing, intracellular trafficking and cytoskeletal function.[54] HEAT repeat domains in other proteins such as the Cullin family of E3 ligases are involved in docking large protein substrates for ubiquitinylation.[57-59] Structural maintenance proteins (SMPs) also contain HEAT repeats to identify proteins for chromosome packaging.[57] Overall, HEAT domains are shown to be important in orchestrating protein-protein interactions to diverse sets of proteins. In this thesis, we investigate the role of the Met18 HEAT repeat domains in binding to the helicase Rad3 and Cia2 as Met18 is also present in a complex MMXD (MIP18-MMS19-XPD) with Cia2 and Rad3 that is required for chromosomal segregation.[51]

Lastly, understanding the role of Met18 in the CIA pathway is significant as previous studies linked Met18 expression in esophageal squamous cell carcinoma.[10] More specifically, a recent study linked human Met18 directly to cancer, as MAGE-F1-NSE1 E3 ubiquitin ligase regulates the CIA pathway through ubiquitination and degradation of Met18, and its downregulation is a common feature in cancer.[9] Identifying the role of Met18 in the CIA pathway is required to understand how defects within this pathway can lead to cancer.

1.4 Conflicting conclusions about the CIA targeting complex interactions

In the last two decades, insight into the CIA targeting complex has been scarce as a couple of the components have just recently been identified. Furthermore, co-IP studies have led to confusing and conflicting results due to low expression levels of proteins and difficulties with detection by western-blot analysis.[25, 26, 60] A couple labs came to very

different conclusions about the binary interactions within the CIA targeting complex as well as the interactions with the CIA proteins and target proteins.

In several previous studies Cia1 has shown a strong binding interaction with Cia2.[25, 26, 40, 60-62] However, two studies dispute over if Cia1 directly interacts with Met18.[25, 26] Van Wietmarschen *et al.* observed a binding interaction between Cia1 and Met18, while Seki *et al.* did not (Figure 1.5). [25, 26] Additionally, van Wietmarschen *et al.* noted that all three CIA targeting complex proteins (Met18, Cia1, and Cia2) bound Nar1, while Seki *et al.* observed no Nar1 binding with Cia2 (Figure 1.5B).[23, 25, 26] Lastly, van Wietmarschen *et al.* observed direct binding of Met18 and Cia2 to apo-targets, but no Cia1 binding (Figure 1.5A).[26] This also conflicts with the Seki *et al.* model in which Cia1 was also able to bind to apo-targets (Figure 1.5B).[25] Additionally, the human Cia1 has also been reported to directly associate with targets including DNA polymerase δ, hRad3, and viperin.[25, 63, 64]

The conflicting conclusions of these studies indicate a new method is required to investigate these protein-protein interactions within the CIA complex as well as how the CIA components interact with Nar1 and apo-protein targets. In this thesis we utilize a co-affinity purification assay that is independent of western-blotting techniques and low protein expression levels. In chapters 2 and 3 we explore the protein-protein interactions within the CIA targeting complex as well as how apo-targets and Nar1 bind to the CIA components.

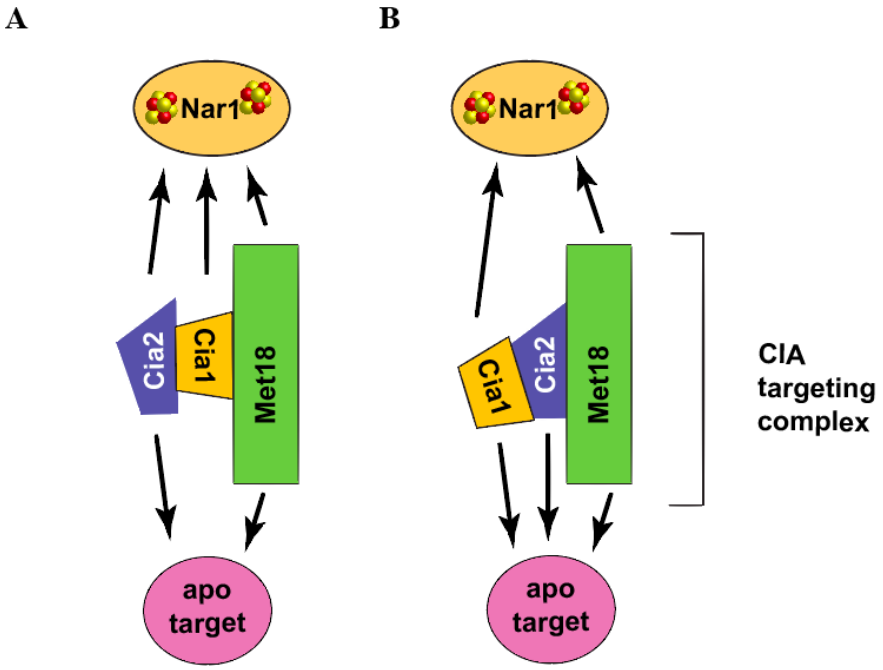

Figure 1.5 Co-IP summary of the binary interactions of proteins involved in CIA the targeting complex.
A) Using Co-IP studies, van Wietmarschen *et al.* observed by binary interactions that Cia1 was the center of the targeting complex. This publication also noted that Met18 and Cia2 had direct interactions with apo-targets and all three proteins were able to bind to Nar1. B) By the same Co-IP method, Seki *et al.* observed instead that Cia2 was the center the targeting complex and all three proteins were able to bind to apo-targets. Additionally, Seki et al. only detected binary interactions with Nar1 and Cia1 or Met18.

1.5 Identification of functional residues on the CIA targeting complex

Although it is unclear which proteins interact within the complex as well as which CIA proteins are responsible for binding to target proteins, previous studies have identified a few conserved functional residues on the CIA targeting components. The current methods to investigate the role of these residues have been limiting. In these next sections we compile the findings of previous labs for the interactions of the CIA targeting proteins and specifically the functional residues they investigate on Cia1, Cia2, and Met18 (Figure 1.6).

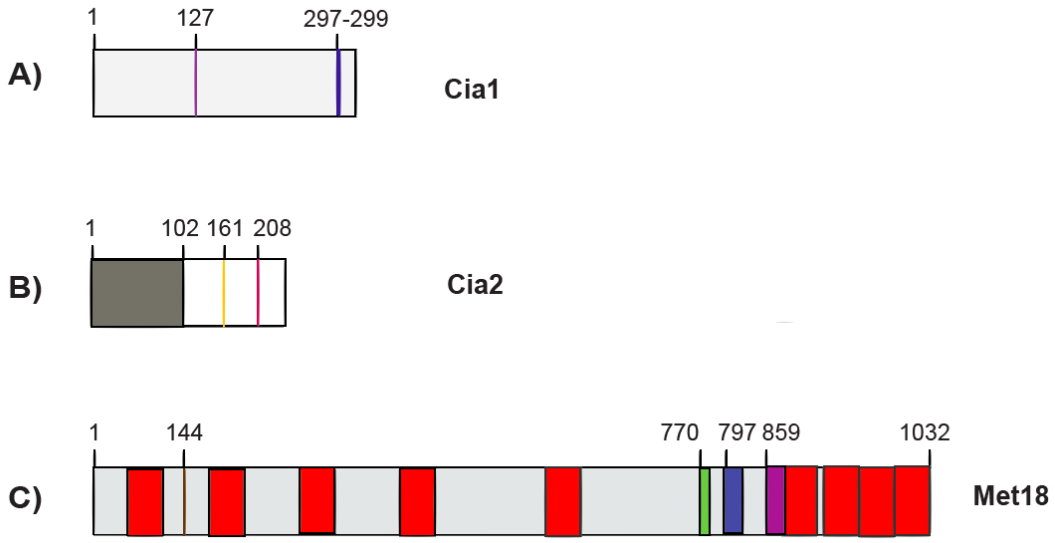

Figure 1.6. Identification of the functional conserved residues on the CIA targeting complex proteins.
A) Previous studies have investigated the R127 of Cia1 (purple) and the E297 and N299 (blue). B) Cia2 contains an N-terminal portion (1-102, dark gray) and a C-terminal DUF59 domain (52-247). Cia2 has one hyperreactive cysteine C161 (yellow) and E208 (pink) has been shown to be important for binding Met18 (Lev, *et al.*) C. Met18 contains HEAT repeat domains (red) and we investigate motif 1 (M1, R144) motif 4 (M4, residues 770-771), motif 5 (M5, residues 797-805), and motif 6 (M6, residues 859-865) in this thesis.

1.5.1 Functional residues on Cia1

Previous studies identify that the top face of the WD40 proteins is a general interface for protein binding, but the question remains for Cia1, which amino acids are participating in binding. [36, 37] Srinivasan *et al.* solved a yeast crystal structure of Cia1 (2HES) that identified a surface exposed arginine, R127 on blade 3, which showed slow cell growth and impaired CIA function via Leu1 activity (Figure 1.7A).[32] This residue is also conserved throughout eukaryotes, indicating that it may be an important residue for Cia1 in protein interactions. Wu *et al.* utilized the availability of 36 WD40 repeat protein structures to perform an in-depth analysis of WD40 structural elements, in which they identified potential amino acid residues for binding termed “hot spots” on the surface of

the proteins.[65] Through this method, Wu *et al.* was able to identify several amino acids that were potential hot spots for Cia1 (Figure 1.7B). Although there were several hot spots identified, not all were conserved throughout eukaryotes.[65] In our lab Melissa Marquez mutated conserved residues to alanines via site directed-mutagenesis and saw through co-affinity purification assays that N299 and E297 were required for binding to Cia2. Therefore, by use of the structural analysis from Wu *et al.*, she was able to identify Cia1 residues important for Cia2 binding. However, overall little is known about the residues on Cia1 that are responsible for Nar1 binding.

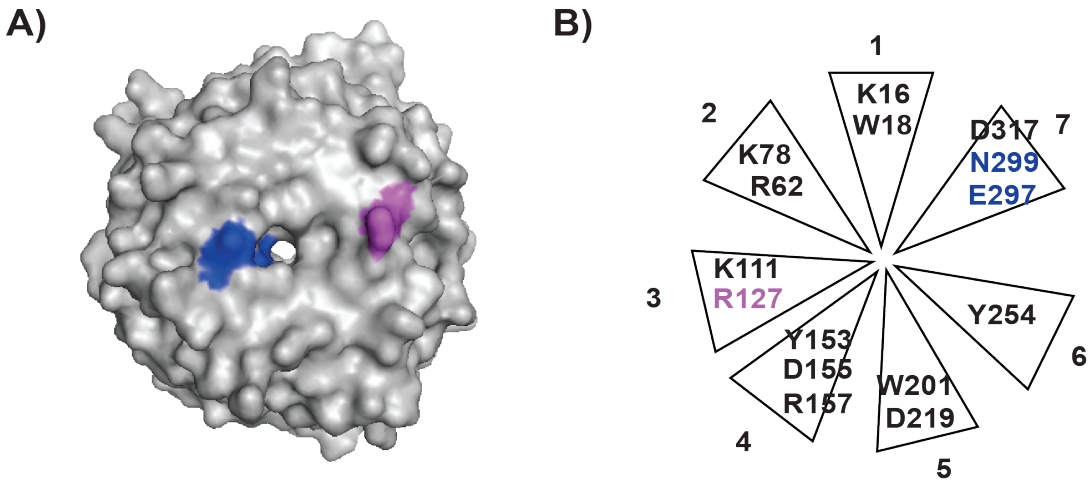

Figure 1.7 Structure of Cia1 and the amino acids investigated.
A) The surface model of the yeast Cia1 structure is shown (PDB: 2HES). The R127A identified by previous labs as surface exposed and required for CIA function *in vivo* is shown in purple. The N299 and E297 shown by Melissa Marquez in the Perlstein lab to be important for CIA binding are shown in blue. B) The Cia1 structure with its hotspots identified by Wu, *et al.* Again, the R127A shown in purple and the N299 and E297 are shown in blue.

1.5.2 Functional residues on Cia2

For Cia2 a few labs have investigated residues important for Met18 or Cia1 binding.[60, 61, 66] Specifically, Lev *et al.* showed that an E208G mutation in motif 5 on

Cia2 disrupted its interaction with Met18 by an *in vivo* reverse protein complementation assay.[66] However, Odermatt *et al.* observed that truncation of the last five amino acids on Cia2 disrupted binding to Met18 by co-IP.[60] Although identification of these residues allow for insight into the function of Cia2, little is known about which portion of Cia2 is required to bind to targets within these conserved domains. In addition to the residues that have been suggested to be important for target binding, Cia2 alignments reveal several other conserved motifs.[40] In Chapter 4, we will explore all of these residues through *in vivo* and *in vitro* assays to understand their role in Cia2.

1.5.3 Functional residues on Met18

Based upon the role of HEAT domains as protein-protein interaction scaffolds, previous labs investigated the role of human Met18 HEAT repeat domains in recognition of FeS targets. Herein, the residues in all experiments with the human MMS19, were converted to represent the homologous yeast Met18 amino acid residues by a sequence alignment generated using Clustal Omega.[67] Previously, Hatfield *et al.* identified the A, B, and C domains as having distinct functions for nucleotide excision repair and transcription.[68] Van Wietmarschen et al. designed two constructs based off this study; ΔAB construct in which the N-terminal portion of Met18 was deleted (1-284) and a ΔC construct in which the C-terminal portion of Met18 (731-1032) was deleted.[26] Both constructs contained at least 3 HEAT repeat domains. Van Wietmarschen *et al.* reported via coIP that ΔAB retained interaction with Cia1, Rad3, and other human FeS proteins RTEL1 and MUTHY (absent in yeast), whereas ΔC can only interact with Cia1. Thus, the HEAT repeat domains in the C-terminus were required for protein-protein

interactions.

Oddermatt *et al.* created four different constructs to examine binding: A(1-452), B(446-861), C(856-1032), and D(446-1032). The C-terminal constructs were able to bind to Cia2 and Cia1, as well as Pol3 and another FeS protein RTEL1 (not present in yeast).[60] The N-terminal Met18 constructs (A and B) were not able to bind to Cia2, Pol3, or RTELI, but were able to bind to Rad3. These results were conflicting with van Wietmarschen *et al.,* as this lab identified the C-terminal construct (ΔAB) as the binding site for Rad3 and the N-terminal construct (ΔC) as the binding site for Cia1.[26] These studies highlight the need for careful controlled *in vitro* studies to dissect the molecular basis for target identification.

Within this work in chapter 5, we investigated the C-terminal (748-1032) and N-terminal (1-331) domains of Met18 *in vivo* to assess their impact on CIA function (Vo *et al.*, *unpublished*, Chapter 5). We also probe the contribution of specific amino-acid residues in motif 1 (R144), motif 4 (770-7710, motif 5 (797-805), and motif 6 (857-869) in Cia2 binding with our developed *in vitro* assays as well as their *in vivo* functionality (Figure 1.6).

1.6 Motifs of target recognition for the CIA targeting complex

A major unsolved mystery for the CIA pathway is how the CIA targeting complex identifies numerous targets. If the CIA targeting complex executes target recognition via direct protein-protein interactions, what does this recognition motif look like? One such model is that a single motif on the FeS proteins is required for FeS target recognition. In the mitochondrial ISC pathway, there are a few different models for how specificity for

FeS target proteins is encoded. Previous studies identify molecular chaperones are required for insertion of FeS clusters.[69-71] For example, genetic interactions and proteomic studies indicate that the yeast proteins Ssq1 and Jac1 function with the Fe/S center assembly machinery as mutations in Jac1 cause defects in FeS enzyme activities and iron accumulation.[70] Futhermore, these chaperones were found to bind to the scaffolding protein ISCU on its LPPVK motif.[72] This reveals that these chaperones bind directly to the scaffold and aid in cluster transfer.

Another model from the Rouault lab identifies specificity factors that act as carriers to deliver FeS cluster to a subset of targets. [73] The Rouault lab observes that LYR motifs are signatures to recognize targets or accessory proteins that assist in FeS cluster transfer.[73] Furthermore, Cory *et al.* proposed that LYR proteins form lock and key interactions with acyl carrier protein (ACP), which influences the maturation of FeS proteins as ACP binds to cysteine desulfurase.[74] Recent work from the Rouault lab has also identified an LYR motif in the CIA system, on Cia1 that is required for binding to the human chaperone HSC20, which in these studies was shown to act as an adapter for the primary scaffold, ISCU1, and the cysteine desulfurase, NFS1, and the CIA targeting complex to facilitate Fe-S cluster insertion.[75]

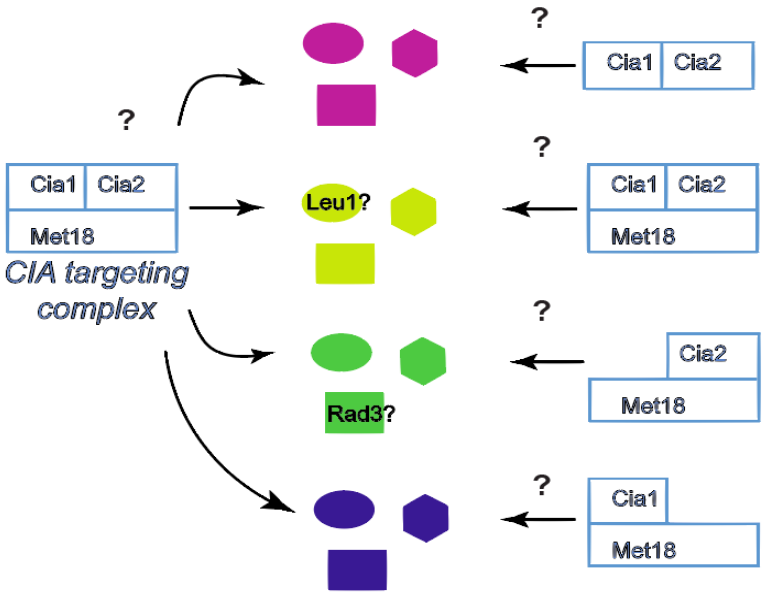

Figure 1.8 Recognition of apo-protein targets by the CIA targeting complex
Does the CIA targeting complex come together and by its different interfaces recognize different subsets of targets? (Left) Or do different subcomplexes form (right) that can each recognize a subset of targets?

For the CIA system, the Lill lab has proposed a model in which the CIA targeting complex forms different subcomplexes of the targeting complex in order to recognize these different targets (Figure 1.8). In the human system, the CIA targeting complex is responsible for the maturation of numerous Fe–S proteins such as DPYD (dihydropyrimidine dehydrogenase), ABCE1(ATP-binding cassette protein or Rli1 in yeast) and XPD(xeroderma pigmentosum complementation group D or Rad3 in yeast).[7] The Lill lab has observed that the human Met18 and human Cia1 can form a subcomplex that plays a role in recognizing DNA polymerase δ (POLD1 or Pol3 in yeast).[7] A subcomplex containing human Cia1 and human Cia2 was also shown to bind glutamine phosphoribosyl-pyrophosphate amidotransferase (GPAT).[7] If this model is valid, then it

predicts that stable subcomplexes can be formed and that the subcomplexes will differentially recognize targets.

In this thesis, we investigate the subcomplex model proposed by Lill with our two target FeS proteins, Rad3 and Leu1. Rad3 is a helicase involved in nucleotide excision repair, while Leu1 is an isomerase involved in leucine biosynthesis. [76,21-23, 77] Previous studies have identified potential recognition motifs that are identified by the CIA targeting complex. For example, the Lill lab observed a disruption of the interaction with the targeting complex when a C-terminal tryptophan was mutated in Lto1, an adaptor which tethers the target Rli1 to the CIA targeting complex.[1] Other proteins such as viperin, Leu1, and Nar1 also contain this C-terminal tryptophan (Table 1.1). In our lab, Melissa Marquez has shown that mutating the C-terminal tryptophan in Leu1 also disrupts binding with CIA targeting complex.

Table 1.1 FeS proteins with C-terminal Tryptophans

Human	Yeast	Function	Disrupted CIA interaction?/Lab
--------	Lto1	Adapter for FeS protein Rli1	Yes/Targeting complex/Lill
IOP1	Nar1	CIA component	Unknown
--------	Leu1	Isomerase in Leucine synthesis	Yes/Targeting complex/Perlstein
Viperin	--------	Interferon protein with antiviral activity	Yes/Cia1/Lill
Polδ	Pol3	Polymerase for chromosomal DNA replication	Unknown
--------	Ecm17	Sulfite reductase in sulfur metabolism	Unknown
Rev3L	Rev3	Catalytic subunit of DNA polymerase zeta; involved in translesion synthesis during post-replication repair	Unknown

Additionally, for target Rad3, Lansdorp, Uringa, and coworkers demonstrated the FeS-binding domain of Rad3, found proximal to the N-terminus of the protein, binds to Cia2 (Figure 1.8B).[26] These authors also reported that RTEL1, an ortholog of XPD (human Rad3), binds to MMS19 (Met18) via the region of amino acids 458–661, far removed from the FeS-binding domain (Figure 1.9A).[26] However, this finding conflicts with the findings of Tanaka and coworkers who propose that the C-terminal region of Rad3 is responsible for binding Met18 (Figure 1.9B).[51] In this thesis we investigate through co-affinity purification assays and SEC experiments, how the CIA targeting complex recognizes these proteins in Chapter 2 and Chapter 3. However, the challenging task of identifying different recognition motifs for all the CIA targets elucidated still lies ahead.

In this thesis in Chapter 2 we investigate the CIA targeting complex and identify protein interactions within the complex to determine its connectivity. We also utilize SEC to determine the stoichiometry of this complex. Additionally, we investigate its binding to Nar1. In Chapter 3 we interrogate how the targeting complex identifies target proteins by examining its interactions with apo targets Rad3 and Leu1. Furthermore, in this chapter we explore how apo versus holo targets are recognized and the role of Nar1 in cluster transfer. In Chapter 4 we specifically explore the biochemical role of Cia2 and identify important residues for binding to CIA components via co-affinity purification assays and assess their CIA function *in vivo*. Lastly, in chapter 5 we explore the binding interfaces of Met18 through co-affinity purification assays and the development of new *in vivo* assays.

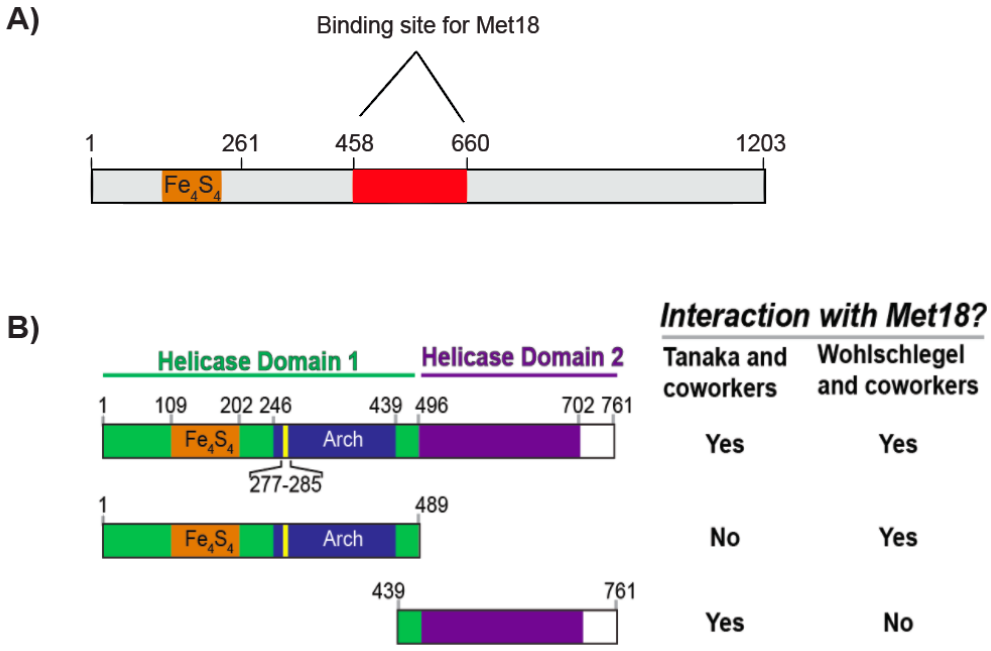

Figure 1.9 Recognition motifs on targets Rad3 and RTEL1.
A) RTEL1, a 4Fe4S helicase involved in telomere maintenance binds to MMS19 (human Met18) on amino acids 258-660 as shown by van Wietmarschen *et al.* B) Rad3 was shown by Tanka *et al.* to bind to Met18 via its Helicase Domain 2 (HD2) as opposed to Wohlschlegel *et al.*, who observed binding via its Helicase Domain 1 (HD1).

CHAPTER TWO: Identifying the protein interactions of the cytosolic iron sulfur cluster targeting complex

(*This work is a reformatted version of* **Vo** *et al., Biochemistry, accepted* **2017***)*

2.1 Introduction

Several laboratories have identified a multiprotein complex, the CIA targeting complex, as responsible for CIA target recognition and FeS cluster insertion.[7, 21-24] This complex contains Met18, Cia1, and Cia2. The CIA targeting complex has been shown to associate with an FeS cluster protein, Nar1.[25, 26] Little is known about the biochemical role of each protein. However, from the domain structures of these proteins, we can predict their potential biochemical functions. Met18 is a superhelical HEAT repeat protein and is homologous to proteins that recognize large protein substrates, such as the Cullin E3 ligases.[21, 68] Previous studies have suggested that the HEAT repeat domains on Met18 are required for FeS protein recognition.[26, 60] Cia1 is a WD40 protein, which we hypothesize is the organizing center of the targeting complex, as proteins like this serve as hubs for protein-protein interactions.[32] Cia2 contains a FeS assembly/MIP family domain, formerly known as the DUF59 domain. Proteins with this domain are frequently associated with FeS biogenesis pathways which indicates it might play some role in the FeS insertion.[48] Since Nar1 is an FeS protein that physically interacts with both scaffold and the targeting complex, this predicts it could be the provider of the FeS cluster.[27] Herein, we investigate the potential roles of these proteins and how they assemble to form the CIA targeting complex in yeast.

Previous studies investigated the binary protein-protein interactions between subunits of the human core targeting complex with Met18, Cia1, and Cia2. These data generated conflicting models about the interactions within the core targeting complex. [25, 26] Van Wietmarschen *et al.* identified Cia1 as the center of the targeting complex.[26] However, Seki *et al.* concluded Cia2 was the center, observing Cia2 binding to both Met18 and Cia1. Seki *et al.* also saw binding of Met18 to Nar1, as well as Cia1 binding to Nar1. [10] These interactions, however, were investigated by Co-IPs, which are dependent on expression levels of the proteins in cell and may not provide clear conclusions about binding interactions.

Herein, we provide a method to identify stable protein-protein interactions within the complex as well as analyze their stoichiometry by size exclusion. From our studies we observe that Cia2 acts as a bridging protein between Cia1 and Met18. By determining the molecular weight of the core complex, and the stable subcomplexes, we determine the stoichiometry of the CIA targeting complex to be one Met18, two Cia1, and four Cia2. We also present preliminary EM studies to obtain a structure of the targeting complex.

By utilizing the same methods, we also see an interaction with the CIA targeting complex and Nar1, with a size for the complex consistent with one Nar1, one Met18, two Cia1, and four Cia2. We demonstrate that Nar1 is bound to Cia1 by our co-affinity purification assays. These studies create a preliminary structure for the CIA targeting complex and allow for a platform to investigate its role in the CIA pathway.

2.2 Materials and Methods

2.2.1 Co-purification assay

The plasmid construction for the yeast proteins, which were heterologously expressed in *E. coli*, along with expression and purification of these proteins, can be found in Appendix 2. All co-affinity experiments were carried out at 4 ˚C. Bait-only and prey-only controls were performed in parallel as indicated. An affinity tagged bait protein (His or Strep tag; ~100-250 μg) was mixed with an equimolar amount of one or more prey proteins for 1h. The mixture was passed though 100-200 μL of affinity resin. Nickel IMAC columns were washed with ≥ 15 CV of 50 mM Tris, 100 mM NaCl, 5% glycerol, and 5 mM BME (Buffer A) and eluted with Buffer A with 300 mM imidazole. Streptactin columns were washed with ≥15 CV of Buffer A and eluted with Buffer A supplemented with 2.5 mM desthiobiotin. Elution fractions were analyzed by SDS-PAGE. Proteins were identified by their migration in SDS-PAGE as compared to pure standards and by Western blotting for the His- or Strep-tags as required. We also have recognized it is critical to use fresh resin for both Nickel IMAC and streptactin columns as proteins can nonspecifically bind to the resins. Additionally, the binding affinity of the streptactin resin for the tagged bait protein is decreased after a single use and it is not recommended to regenerate the resin more than five times.

2.2.2 Size Exclusion Chromatography

Each component (~10 μM final) was mixed in a final volume of 0.5 mL and incubated at room temperature for 1 h. The 0.5mL sample was injected onto a Superdex

200 Increase 10/300 GL column (GE healthcare) and eluted with 20 mM Tris, 100 mM NaCl, and 5% (v/v) glycerol at a flow rate of 0.5 mL min^{-1}. The molecular weight of each peak was determined by comparison of the elution volume to a standard curve generated with ferritin (443kDa), alcohol dehydrogenase (150 kDa) ovalbumin (66 kDa), albumin (45 kDa), and cytochrome C (12.5 kDa). At least three independent measurements of molecular weight were determined and reported as the average ± the standard deviation. Standards were analyzed immediately before experimental samples. For the Nar1 samples a standard curve generated with the Bio Rad gel filtration standard mixture 1905 containing thyroglobulin (670kDa), γ-globulin (158 kDa) ovalbumin (44 kDa), myoglobin (17 kDa), and Vitamin B_{12} (1.35 kDa).

2.2.3 Multi-angle light scattering

Size exclusion chromatography coupled with multi-angle light scattering (SEC-MALS) was performed using an Agilent AdvanceBio 300 column attached to a Dawn Heleos MALS instrument (Wyatt Technology) and an Optilab rEX detector (Wyatt Technology). ^{His}Cia1, Cia2 and Met18 were mixed and purified on IMAC before injection into SEC-MALS at a concentration of about 1 mg/mL. The column was eluted with a flow rate of 0.5 mL/min in 25 mM HEPES pH 7.5, 100 mM NaCl, and 1% glycerol. Molar-masses were calculated using the Zimm model with Astra7 software (Wyatt Technology). For analysis, the refractive index was set at a constant value of 0.185. Both peaks presented were monodisperse (Mw/ Mn < 1.01). The errors reported are fitting error generated by the Astra7 software and represent the statistical consistency of the data.

2.2.4 BMOE crosslinking

A 20 mM solution of bismaleimidoethane (BMOE) in DMSO was prepared. A 10-fold excess of crosslinker was added to each sample and the proteins were cross-linked in sulfhydryl free buffer (50 mM Tris pH 8, 100 mM Nacl, 5% glycerol, 5 mM TCEP). The BMOE was incubated with the protein for 15 minutes at room temperature and the reaction was quenched by the addition of DTT (10 mM final concentration).

2.2.5 Electron Microscopy sample preparation

The complex was prepared using the same affinity co-purification method as detailed in section 2.2.1. ^{His}Cia1 was used as the bait, mixed with un-tagged Cia2, and Met18 (with the SUMO tag cleaved off as described in Appendix 2). Different stoichiometric amounts were calculated from the protein stocks available each trial (Appendix 3). A 200μL Ni-NTA column was used to form the complex. All samples were eluted in 50 mM Tris (pH 8.0), 100 mM NaCl, 1% glycerol, and 5 mM BME. The elution fractions were pooled and concentrated with a 50kDa cutoff Amicon Ultra spin filter and the final concentration was determined by a Bradford assay. The samples were diluted accordingly for each grid and then 3 μL were spotted on each grid with different blot times (Table 2.1)

2.3 Results

2.3.1 Targeting complex subunit Connectivity and Stoichiometry

To define the yeast system's subunit connectivity and stoichiometry, we probed all possible binary interactions between Met18, Cia1, and Cia2 via affinity copurification

and determined the molecular weight of all stable complexes via SEC. We first examined the interaction between Cia1 and Cia2. Yeast two hybrid and coIP studies have identified a Cia1-Cia2 interaction *in vivo* in several eukaryotic organisms and three different groups have reported a direct interaction between the human homologues of Cia1 and Cia2 *in vitro.*[25, 26, 78-82] To determine if the yeast proteins also directly interact *in vitro*, we mixed Cia1 with Cia2 and assessed their binding via affinity copurification. Consistent with the proteomic data and reports with the human homologs, we observe an interaction between ^{His}Cia1 (His-tagged) and Cia2 (Figure 2.1A). The similar intensities of the Cia1 and Cia2 bands in the elution fraction suggested that Cia1-Cia2 was a stable, stoichiometric complex.

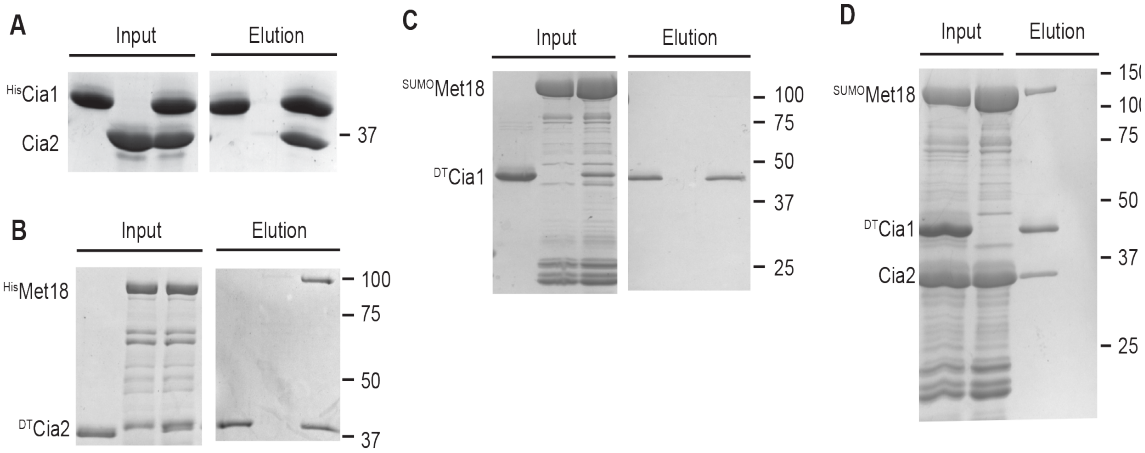

Figure 2.1. Subunit connectivity of the CIA targeting complex
SDS-PAGE analysis of affinity copurification experiments to determine subunit connectivity. A) ^{His}Cia1 and Cia2 were mixed (input) and separated via IMAC. ^{His}Cia1 can specifically retain Cia2 (elution). B) ^{DT}Cia2 and ^{His}Met18 were mixed (input) and separated via streptactin resin. ^{DT}Cia2 can specifically retain ^{His}Met18. C) ^{SUMO}Met18 and ^{DT}Cia1 were mixed (input) and separated via streptactin resin. No ^{SUMO}Met18 can be detected copurifying with the ^{DT}Cia1 bait. D) ^{Strep}Cia1, ^{His}Met18 and Cia2 were mixed and chromatographed on streptactin resin. Both ^{His}Met18 and Cia2 are retained by Cia1 (Lane 3) whereas no bands are detected in the control in which ^{DT}Cia1 was omitted (Lane 4). Molecular weight standards in kDa are shown to the right of all the gels.

We estimated the molecular weight of the Cia1-Cia2 complex via SEC to determine the subunit stoichiometry. As expected from the reported crystal structure, Cia1 on its own eluted as a monomer (Figure 2.3B, dashed line).[32] Cia2 could not be analyzed due to its low extinction coefficient and its propensity to precipitate at concentrations above 0.5 mg/mL. Since a human homolog of Cia2 was recently reported to form a dimer,[48] we examined whether the homobifunctional crosslinking reagent bismaleimidoethane (BMOE) could crosslink Cia2 via its absolutely conserved cysteine, Cys161. Incubation of Cia2 with BMOE resulted in appearance of a dimeric product whereas the C161A-Cia2 mutation significantly diminished BMOE-dependent crosslinking (Figure 2.2). We concluded that Cia2 could form a dimeric species.

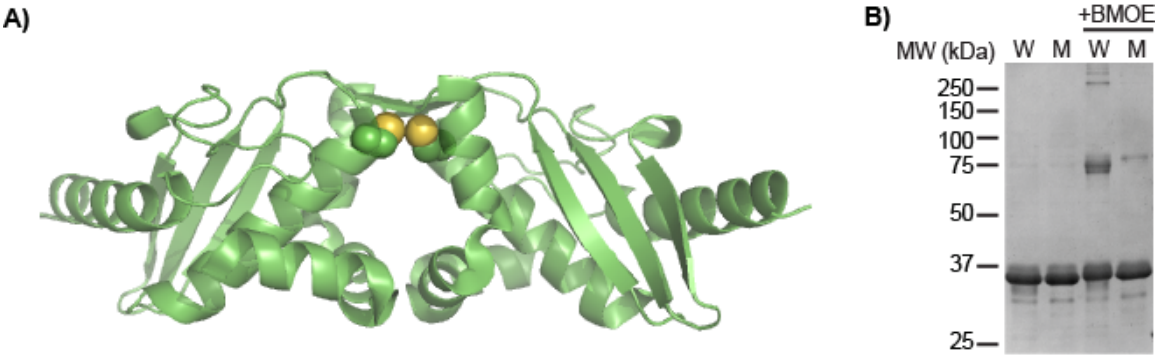

Figure 2.2 BMOE crosslinking of the Cia2 dimer
A) Crystal structure of a human homolog of Cia2 (PDB ID 3ux3) illustrating the dimeric structure where the absolutely conserved cysteine (side chain shown as spheres) is close to the same cysteine in the other protomer. B) BMOE crosslinking of the wild type Cia2 (W) and the C161A mutant (M). The first two lanes are in the absence of BMOE and the last two lanes are in the presence of BMOE as indicated.

When a mixture of Cia1 and Cia2 was analyzed via SEC, the peak for the Cia1 monomer disappeared and a new peak with a molecular weight of 90±15 kDa appeared (Figure 2.3B, solid line). Based on the sizes of ^{His}Cia1 (40 kDa) and Cia2 (25.6 kDa), we conclude that the Cia1-Cia2 complex contains one Cia1 polypeptide and two Cia2

polypeptides. Interestingly, it was previously reported that hCia1 and hCia2a can form a 1:1 and 1:2 complex with low nanomolar affinity.[48] Thus, both the yeast and the human homologs form a Cia1•Cia2$_2$ complex. This observation is consistent with the high sequence and functional conservation of CIA from yeast to humans. [5]

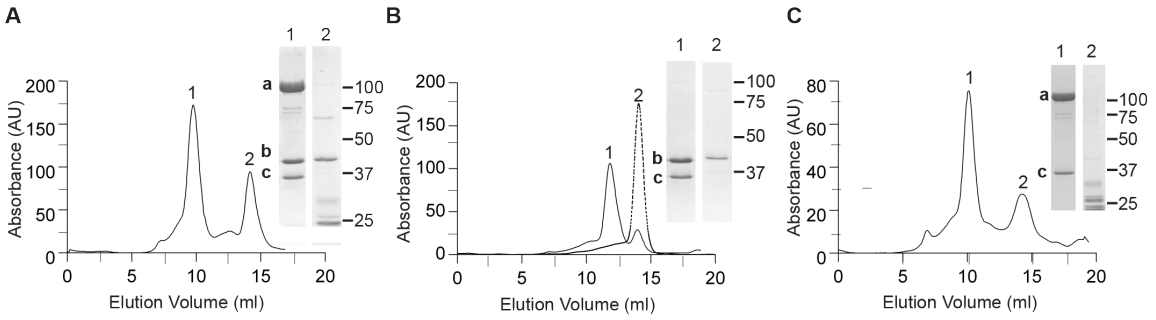

Figure 2.3. SEC of the Targeting Complex.
In all panels, the SDS-PAGE gel insets are labeled with a, b, and c to indicate migration of Met18, Cia1, and Cia2, respectfully. A) The mixture of ^{His}Cia1, ^{SUMO}Met18, and Cia2 eluted predominantly as a single, 344 kDa peak (Peak 1, Lane 1). Peak 2, eluting at 40 kDa, contains Cia1 and low molecular weight contaminants (Lane 2). B) The ^{His}Cia1 (40 kDa) and Cia2 (25.5 kDa) mixture (solid line) eluted predominantly as single, 90 kDa peak (Peak 1) containing both Cia1 and Cia2 (Lane 1). ^{His}Cia1 (dashed line) eluted as a single, 39 kDa peak (Peak 2, Lane 2). C) A ^{SUMO}Met18 (130 kDa) and Cia2 mixture eluted as a single, 245 kDa peak (Peak 1; Lane 1). The second, 25 kDa peak contains low molecular weight contaminants (Lane 2). Molecular weight standards in kDa are shown on to the right of all the gels.

Next, we investigated the Met18-Cia2 and Met18-Cia1 interactions. While previous studies with the human system were in agreement that hCia1 could interact with hCia2, these studies did not agree on whether hMet18 could form a binary complex with hCia1 or hCia2.[25, 26] When we mixed ^{DT}Cia2 (double-tagged) with ^{His}Met18 and chromatographed the mixture on streptactin resin, we observed a large amount of the Met18 prey in the elution fraction (Appendix 2). We concluded that Met18 and Cia2 form a stable complex. Using SEC, we determined that the ^{SUMO}Met18-Cia2 complex has a molecular weight of 245±6 kDa (Figure 2.3C). This molecular weight is consistent with

a complex containing one ^{SUMO}Met18 (Sumo-tagged, 130 kDa) polypeptide and four Cia2 (25.6 kDa) polypeptides. This Met18•Cia2$_4$ complex has a calculated molecular weight of 232.4 kDa, which is in good agreement with the observed molecular weight of 245 kDa.

We used a similar approach to look for a Met18-Cia1 interaction. When ^{DT}Cia1 was used as the bait and ^{His}Met18 as the prey, no Met18-Cia1 complex was observed (Figure 2.1C). We obtained the same result if Met18 was used as the bait and Cia1 as the prey (not shown). We concluded that Met18 and Cia1 does not form a binary complex or, if they do interact, their affinity is too weak for the complex's detection by copurification.

The results from our binary complex study indicate that Cia2 could be the bridge linking Met18 to Cia1 in the targeting complex. To probe the bridging function of Cia2 directly, we examined whether Cia2 could simultaneously interact with both Met18 and Cia1, or if Cia2 forms mutually exclusive binary complexes with these two interaction partners. When we mixed ^{DT}Cia1, ^{His}Met18, and Cia2 and chromatographed the mixture on streptactin resin, we observed both Cia2 and ^{His}Met18 eluting with the ^{DT}Cia1 bait (Figure 2.1D). Since Met18 does not appear to form a stable, binary complex with Cia1 (Figure 2.1C), its presence in the elution fraction when all three targeting complex subunits are present demonstrates that Cia2 is the central subunit of the targeting complex. When we analyzed this mixture via SEC, we observed a 344±4 kDa peak containing all three polypeptides (Figure 2.3A). To assign the quaternary structure, we reasoned that the Met18-Cia1-Cia2 complex is comprised of the stable Cia1•Cia2$_2$ and Met18•Cia2$_4$ subcomplexes. Therefore, we would expect the ratio of subunits observed in the binary complexes to be maintained in the full targeting complex. Based on this

hypothesis, we propose that the 344 kDa complex contains one Met18, two Cia1, and four Cia2 polypeptides. This ^{SUMO}Met18•[^{His}Cia1•Cia2$_2$]$_2$ complex has a calculated molecular weight of 312 kDa which is in good agreement with the observed molecular weight in the SEC experiment.

Given the ~30 kDa difference between the expected and observed molecular weight, we additionally analyzed the molecular weight of the Met18•Cia1•Cia2 complex via a second approach, SEC coupled to multi-angle light scattering (MALS). For SEC-MALS, we mixed ^{His}Cia1 with untagged Cia2 and untagged Met18 and purified the Cia1-containing complexes via IMAC immediately before SEC-MALS analysis. We observed two major peaks with sufficient intensity that we could determine the molecular weight of the complex via MALS (Figure 2.4). The most abundant peak elutes with a molecular weight of 94.2±0.95 kDa, which corresponds to the ^{His}Cia1•Cia2$_2$ complex, which has an expected molecular weight of 91 kDa. The next largest peak elutes with a molecular weight of 285.4 ± 1.1 kDa, which is in good agreement with the predicted molecular weight of 300 kDa for the Met18•[^{His}Cia1•Cia2$_2$]$_2$ complex. In total, the SEC-MALS data is consistent with our assigned quaternary structure for the full targeting complex in which two Cia1•Cia2$_2$ complexes dock onto a single Met18 polypeptide.

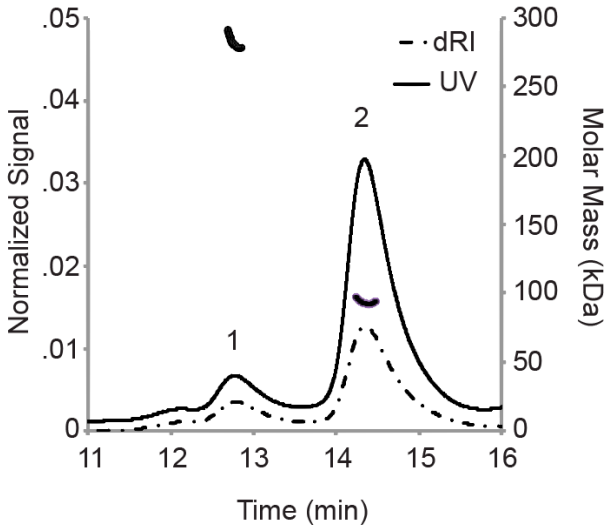

Figure 2.4. SEC-MALS analysis of the Met18•[HisCia1•Cia2]$_2$ complex.
The largest peak (2) elutes with a molecular weight of 94.2 kDa, which corresponds to the HisCia1•Cia2$_2$ complex. The next largest peak (1) elutes with a molecular weight of 285.4 kDa corresponding to the Met18•[HisCia1•Cia2]$_2$ complex. The UV trace at an absorbance of 280nm is shown as a solid line and the signal from the refractive index detector (dRI) is shown as a dashed line.

2.3.2 Nar1 binds strongly to the Targeting Complex via Cia1

To complete our investigation of the connectivity and stoichiometry of the core targeting complex, we purified the FeFe hydrogenase like protein Nar1, as in previous co-immunoprecipitation studies it showed an interaction with Cia1 and association with the targeting complex.[24, 26, 27, 60] By our co-affinity purification method we saw that Nar1 could stably bind to Cia1 (Figure 2.5, Panel A). From the SDS PAGE analysis the mixture of Nar1-Cia1 seemed stoichiometric based off the equal intensities of the bands. Previous studies on Nar1 suggest that Nar is a monomer, but hydrogenases are also able to form dimers. [27, 83] We hypothesized Nar1 would form a monomer with Cia1, as Cia1 contains two potential binding sites, one of which may be responsible for binding to Cia2.

[36, 37]

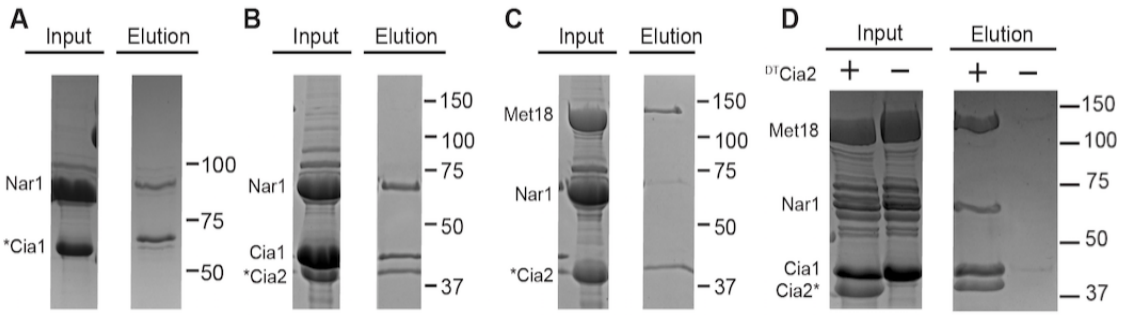

Figure 2.5 Nar1 connectivity to the CIA targeting complex
SDS-PAGE analysis of affinity copurification experiments to determine Nar1 connectivity. A) ^{His}Cia1 and Nar1 were mixed (input) and separated via IMAC. ^{His}Cia1 can specifically retain Nar1 (elution). B) ^{DT}Cia2, Cia1, and Nar1 were mixed (input) and separated via streptactin resin. ^{DT}Cia2 can specifically retain both Cia1 and Cia2. C) ^{SUMO}Met18 and ^{DT}Cia2 were mixed with Nar1 (input) and separated via streptactin resin. No Nar1 can be detected copurifying with the ^{DT}Cia2 bait. D) ^{DT}Cia2, ^{SUMO}Met18, Cia1 and Nar1 were mixed and chromatographed on streptactin resin. ^{SUMO}Met18, Cia1, and Nar1 all elute with ^{DT}Cia2 (Lane 3) whereas no bands are detected in the control in which ^{DT}Cia2 was omitted (Panel D, lane 4). Molecular weight standards in kDa are shown to the right of all the gels.

To test our hypothesis for the Cia1-Nar1 complex, we mixed Cia1 and Nar1 together in equal molar ratios and analyzed that mixture on a size exclusion column to see if that could provide a clearer picture of the stoichiometry of Nar1-Cia1 binding. For a complex with a monomer of Nar1 (56kDa) and a monomer of Cia1 (40kDa), we would estimate a molecular weight of 96kDa. If a dimer of Nar1 is binding to a monomer of Cia1 we would predict a weight of 152kDa.

However, when ran Nar1 alone, we observed a molecular weight most consistent of a dimer of Nar1 at 92kDa (Figure 2.6. solid line). To explore what quaternary state Nar1 might have in the Cia1-Nar1 complex, we mixed these two proteins and analyzed them by SEC. We observed three peaks, one with a size of 262kDa, one with size of 92 kDa, and a 40kDa peak (Figure 2.6, dashed line). We also ran the elutions for each peak on an SDS PAGE gel (Figure 2.6, Lane 1, gel inset). This allowed us to assess which

proteins were present for each peak as Nar1 alone ran as a dimer.

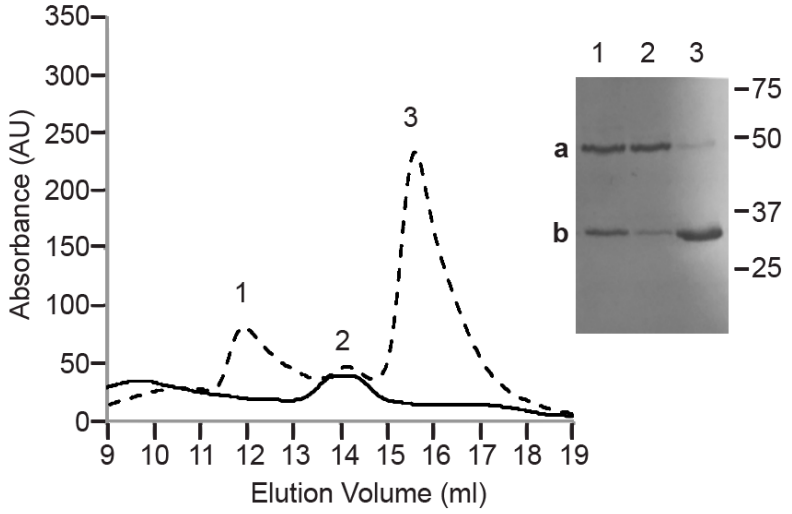

Figure 2.6. SEC of the Cia1-Nar1 complex.
The SDS-PAGE gel inset is labeled with a and b to indicate the migration of Nar1 or Cia1 respectfully. Nar1 alone (solid line) eluted at a peak with the molecular weight of 92kDa, consistent with dimer calculated molecular weight of 112kDa. The mixture of ^{His}Cia1 and ^{His}Nar1 eluted as 3 peaks (dotted line), a 228kDa peak containing Cia1 and Nar1 by SDS-PAGE analysis (Lane 1, gel inset), a 92kDa peak containing primarily Nar1 (Lane 2, gel inset) and a 40kDa peak containing mainly Cia1 (Lane 3, gel inset). Molecular weight standards in kDa are shown on to the right of all the gels.

The third peak (40kDa) was consistent with Cia1 alone and the elution fraction analyzed by SDS PAGE verified this (Figure 2.6, Lane 2, gel insert). The second peak (92kDa) was the same molecular weight as the Nar1 dimer, and from the SDS PAGE analysis this elution contained only Nar1. This indicates that this peak is the Nar1 dimer. The first peak with a weight of 262kDa, contained both Nar1 and Cia1 in the gel elution. The molecular weight does not match with either a 1:1 or 1:2 ratio of Cia1 to Nar1 binding. There are a multitude of possibilities for the molecular weight observed (as both Cia1 and Nar1 are present) including 2:3 (232kDa), 3:2 (248kDa), and 2:4 (272kDa) for a Nar1 to Cia1 ratio. Furthermore, the peak was broad and had a tailing feature. This

suggests that some higher oligomer complex of Nar1-Cia1 can be formed, but is not stable.

From our co-affinity purification we also see that Nar1 can form a Cia1-Cia2-Nar1 complex (Figure 2.5B). We analyzed this complex by size exclusion, predicting that a monomer of Nar1 would bind to a monomer of Cia1 with a dimer of Cia2 (147kDa), as previous experiments suggested only a dimer of Cia2 is able to bind to Cia1 and all three proteins were able to form a complex. This experiment was performed differently than the experiments with Cia1 and Nar1 above, as the Cia1-Cia2-Nar1 complex elution from the co-affinity purification was injected onto the column. The chromatogram showed a single peak, with the molecular weight of 228kDa. This was larger than the expected 147kDa weight. A possible composition for this complex is one Nar1, two Cia1, and four Cia2 (238kDa). This may suggest that one Nar1 can bind to two Cia1-Cia2 subcomplexes. However, this peak too had a large tailing feature indicating these higher order oligomers are not stable complexes.

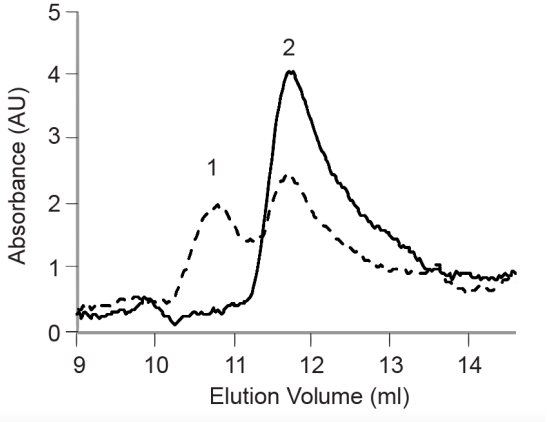

Figure 2.7. SEC of the CIA targeting complex with Nar1.
Nar1, Cia1, and Cia2 were mixed and then injected onto the sizing column (solid line). This chromatogram this showed a peak (2) with a molecular weight of 228kDa. The mixture of Cia1, Cia2, Met18, and Nar1 eluted as 2 peaks (dotted line), a 405kDa peak and a 228kDa peak (2).

Lastly, we looked at Nar1 with the targeting complex via co-affinity purification and saw Nar1 was able to bind the ternary complex. We took the elution from this interaction and injected it onto the SEC column (Figure 2.7). Interestingly, we saw two peaks, one with a molecular weight of 405kDa, and a second peak with the molecular weight of 228kDa. The 405kDa peak could be the complex of Met18•$Cia1_2$•$Cia2_4$ with one Nar1 (368kDa) or the complex with two Nar1 (424kDa), but is most likely the former, as we by the same method observed a ~30 kDa difference between the observed molecular weight for the CIA targeting complex and the calculated molecular weight, which was resolved by SEC-MALs experiments. We would expect that each Cia1 would contain a Nar1, but absence of one Nar1 subunit could be due to an insufficient concentration of Nar1. However, for both samples peak 2 at 228kDa contained a tailing feature, indicating that this species with Nar1, Cia1, and Cia2 is not stable and may be falling apart into species such as Nar1-Cia1 (96kDa) and Cia1-Cia2 (90kDa).

2.3.3 Preliminary Data for EM structure of Targeting Complex

Our co-affinity purification method also allowed for purification of the CIA targeting complex for these structural studies. The SEC experiments indicated that the targeting complex was stable and large with molecular weight of 344kDa. Although the SEC and co-affinity purification experiments allow for understanding of connectivity of the complex and subcomplexes, EM experiments will provide further insight on the structure of the CIA targeting complex and how these proteins are binding. We have initiated Electron Microscopy (EM) studies in collaboration with Edward Brignole and Catherine Drennan obtain structural information about the targeting complex by both

negative stain EM and cryo EM.

We first purified the targeting complex by CIA targeting complex by our co-affinity purification method. Utilizing Cia1 as the bait, we are able to maximize the formation of the ternary targeting complex. We underrepresented Cia1 in the mixture to saturate binding of Cia2-Met18. By this method the only potential subcomplex that might form is Cia1-Cia2, which we reasoned would be a smaller particle (90kDa) that we might not detect by EM or be able to differentiate from the ternary targeting complex. Stability studies show that when this complex is frozen and then thawed it still runs as a single peak, suggesting it is stable. (Figure 2.8) For these studies we formed the complex by co-affinity purification.

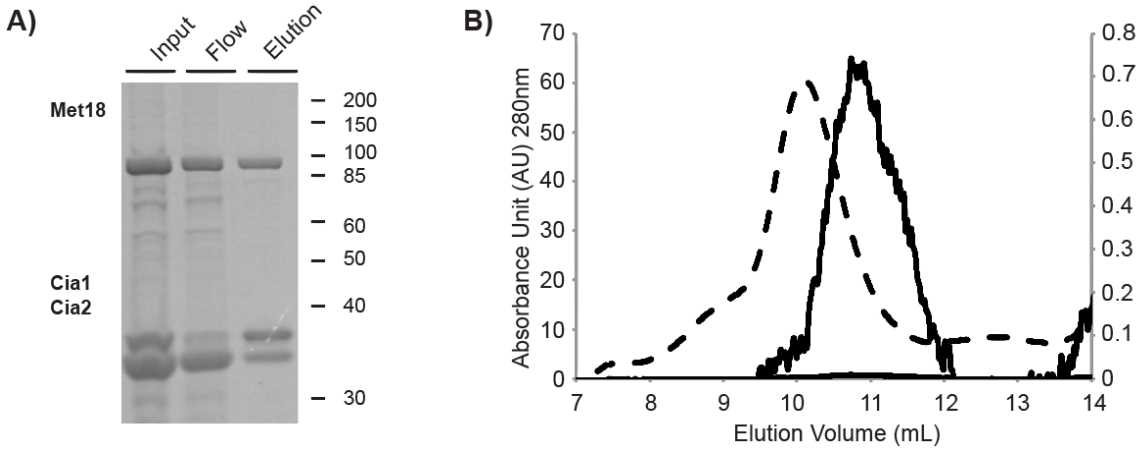

Figure 2.8. Preparation of the CIA targeting complex for EM.
A) SDS-PAGE analysis of the preparation of the CIA targeting complex by co-affinity purification. ^{HIS}Cia1, Cia2, and Met18 are mixed together, underrepresenting the amount of the ^{HIS}Cia1 bait and put on the column (Lane 1). Unbound Met18 and Cia2 flow through the column in the wash (Lane 2). The purified complex is eluted off the column (Lane 3). B) Cia1, Cia2, and Met18 are mixed together and injected onto the sizing column and elute as a single peak (solid line). The elution then is frozen, thawed, and reinjected onto the column and elutes still as a single peak (dotted line).

Next, we took the sample of the targeting complex and set cryo grids varying blot times, grid types, and concentration. Out of the cryo conditions tested, the 600 ng/μL concentration was optimal with a 6 second blot time (Table 2.1). 1627 particles from 74 of the 150 images were manually collected, aligned, and classified by Edward Brignole. The resulting averages of the images represent a different view of a consistent hook-like structure. A primary concern was that some of the classes might be Met18 alone, as Met18 is a large 118kDa protein and the particles looked hook-like consistent with Met18 threading model structure. Additionally, aggregation prevented the ability to identify more single particles from these images (Figure 2.9). Future studies are required to determine if Cia1 and Cia2 are present in this structure.

To optimize the protein sample and decrease aggregation, we have also changed buffer conditions to HEPES pH 7, 0.05% NP40, and introduced a hard centrifugal spin of the samples before setting the grids. However, the 0.05% NP40 detergent interfered with the ice formation on the cryo grids. From our co-affinity purification and SEC experiments the HEPES buffer with a low 100mM NaCl concentrations formed a stable complex we could analyze through SDS PAGE analysis as well as SEC. 100mM NaCl was sufficient and to keep the complex soluble and not disrupt the protein-protein interactions within the complex. Future studies will investigate Met18 only samples to compare to the previous structures as well as the addition of Nar1 with the targeting complex to see if Nar1 might help stabilize the targeting complex and also provide a fuller structure as a CIA component of the targeting complex.

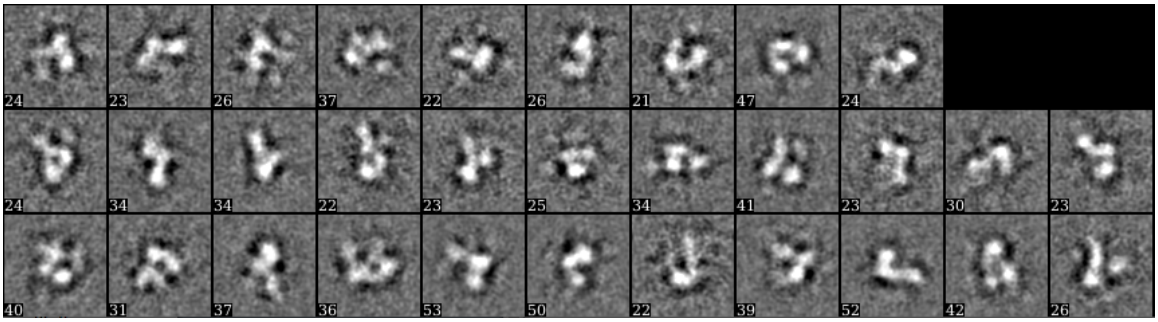

Figure 2.9. Class averages of EM particles.
Class averages appear to be similar to the overall hook-shaped structure of Met18 predicted from homology models. Number of particles in each class is indicated in the lower left corner of the average. Panels are 212 Å wide. Images were collected and particles were selected by Edward Brignole.

Table 2.1. Summary of MCC cryo-specimens prepared and screened by Edward Brignole.

Specimen	Conc.	Grid	Blot time	Result
2.1	1000 ng/µL	CFlat	6 s	-
2.2	1000 ng/µL	QFoil	6 s	-
2.3	800 ng/µL	CFlat	4 s	-
2.4	800 ng/µL	QFoil	6 s	-
3.1	600 ng/µL	QFoil	6 s	Thick ice but center holes of some squares can be shot Particles clumped/aggregated
3.2	600 ng/µL	CFlat	8 s	Bad transfer - specks of ice contaminants
3.3	400 ng/µL	QFoil	4 s	Aggregates and sparse particles, some speckle contaminants
3.4	400 ng/µL	CFlat	6 s	Good ice thickness Particle density a little sparse but still aggregated
4.1	1000 ng/µL	QFoil	8 s	Good ice everywhere, Particles clumped/aggregated
4.2	800 ng/µL	CFlat	8 s	Bent grid - discarded

2.4 Discussion

Although several proteomic and genetic studies identify Met18, Cia1, Cia2, and Nar1 as CIA downstream proteins involved in target recognition, little is known about how this CIA targeting complex is formed and the roles of these subunits. Previous Co-IP studies identify interactions between these proteins, but have discrepancies in binding

interactions that they see.[25, 26] Seki *et al.* found that Cia2 was the organizing center of the complex, while van Wietmarschen *et al.* found that Cia1 as the center. We predicted that Cia1 would be the center as WD40 proteins were shown to be docking sites for protein-protein interactions.[36, 37] To delineate the roles of the CIA components we first investigated how the complex was connected through our co-affinity purification assays.

Our *in vitro* co-affinity purification assays allow us to use large quantities of proteins (microgram to milligram amounts) to identify stable binary interactions and directly detect their interactions and qualitatively assess the degree of binding by the intensity of the bands present, compared to Co-IPs that are coupled to western blots and require transfer of the protein and binding to specific antibodies for visualization. Co-IP studies do require small concentrations of proteins for visualization, but can provide conflicting results and are also dependent on expression levels in the cell. Additionally, our method allows us to purify subcomplexes and the ternary targeting complex, which we can also analyze by SEC to assess stoichiometry. Future studies will address the physiological roles of these subcomplexes, but our *in vitro* methods allow for a basis to form these subcomplexes.

We first observed a strong Cia1-Cia2 interaction by our co-affinity purification assays. This was not surprising, as yeast two hybrid and coIP studies have identified a Cia1-Cia2 interaction *in vivo* in several eukaryotic organisms and three different groups have reported a direct interaction between the human Cia1 and Cia2 *in vitro*.[7, 25, 26, 78-82, 84, 85] However, by this method we were also able to form a stable subcomplex, which we observed by SEC a size consistent with 1Cia1 and 2Cia2. Cia2 in humans is also a dimer

of the paralogs Cia2a and Cia2b. There is high sequence and functional conservation of CIA from yeast to humans that supports the result that Cia2 is also a dimer in yeast.[86, 87]

Next, we explored the Met18-Cia2 and Met18-Cia1 interactions. Previously, two labs observed conflicting results via Co-IPs that presented two different models. [25, 26] Seki *et al.* found that Cia2 was the organizing center of the complex, while van Wietmarschen *et al.* found that Cia1 as the center. Initially, we predicted that Cia1 as a WD40 protein would act as the bridging protein for the entire targeting complex, as proteins like this are important in orchestrating complex formation by acting as docking sites for protein-protein interactions. [32, 65] However, we observed Cia2 as the bridging protein for Met18 and Cia1. The size of the Met18-Cia2 subcomplex could be determined by SEC and was consistent with 1Met18 and 4Cia2.

By the co-affinity purification method we could also form the Met18-Cia2-Cia1 targeting complex with a size consistent with 1Met18, 4Cia2, and 2Cia1 by SEC analysis. The formation of this large complex by co-affinity purification was stable and allowed for EM studies in collaboration with the Drennan lab to better understand the structure of the CIA targeting complex. By using the Cia1 protein as bait, we were able to ensure the formation of the larger Cia2-Met18 subcomplex was minimal. The particles analyzed showed different classes of a hook-like structure. A primary concern was that some of the classes might be Met18 alone in higher order oligomers. Future studies will investigate Met18 only samples to classify the particles as the CIA targeting complex or Met18.

Roland Lill's lab has proposed that the CIA targeting complex exists in multiple quaternary structures, and that each of these is responsible for FeS delivery to distinct

subpools of targets.[7] For the human homologs he observes a Cia1-Met18 subcomplex, but not a Cia2-Met18 subcomplex. However, the complexes containing Met18 appeared to be important in translation and DNA replication and repair.[7] Previous studies also show Met18 is required for genome stability, has distinct functions in nucleotide excision repair, and is present in a complex required for chromosome segregation.[21, 51, 68] From this data, we would hypothesize that Met18 containing subcomplexes in both humans and yeast are required for targets involved in these types of nuclear functions.

The Lill lab also observed Cia1 was present in every quaternary form of the CIA targeting complex, suggesting it played a role in identifying several different FeS proteins. Interestingly, our studies showed Cia2, with its FeS assembly domain, was present in all our forms of the CIA targeting complex. In the human system, there are two paralogs of Cia2, Cia2a (Fam96a) and Cia2b (Fam96b, MIP18). Studies suggest Cia2a's involvement in Fe homeostasis, while Cia2b is required for the Met18-Cia1-Cia2 targeting complex and recognition of a subset of targets.[1, 7] Yeast only contain one type of Cia2, an ortholog of Cia2b, which might explain its presence in all quaternary forms of the CIA targeting complex. Chapter 4 will explore more fully the role of Cia2 in FeS cluster biogenesis.

We also explored the role of Nar1 with components of the CIA targeting complex. Previous literature has shown that Nar1 binds to the targeting complex, but not directly to targets, indicating that it may act at the interface of the scaffold and targeting complex.[7, 21, 25, 26] Defects in Nar1 also result in a decrease in iron incorporation in downstream targets.[2, 3] These studies implicate Nar1's involvement with the CIA targeting complex

for FeS cluster insertion. We suggest two distinct models: Nar1 is either an adapter that joins together the scaffold and the targeting complex with an apo-target, or Nar1 is a cluster carrier that provides FeS cluster to the apo-protein targets. In both models, Nar1 should be able to bind to the targeting complex.

First, we investigated Nar1's ability to bind to Cia1. As we observed Cia1 binding to only Cia2, this suggests that Cia1's versatile protein interaction platform with two potential binding sites (one on the top and one on the side) is utilized for another purpose, such as target recognition or binding Nar1.[23, 25, 26 36, 37] We observed by our co-affinity purification assays that Nar1 could bind directly to Cia1 and form a complex with Cia1-Cia2. However, SEC experiments suggest multiple sizes for this complex, indicating higher order oligomers can be formed and are falling apart in solution. We also cannot rule out the fact that SEC is prone to error in observed molecular weights due to shape of the protein.

Nar1 could also bind to the ternary CIA targeting complex as a monomer. Interestingly, Nar1 did not have the ability to bind to Met18-Cia2. If stable subcomplexes are able to recognize different targets, this suggests for either Nar1 model that a consecutive cluster transfer must occur after binding to the ternary CIA targeting complex or both those models are not possible. Future experiments in Chapter 3 will more fully investigate the two models for Nar1.

In summation, our *in vitro* studies support the model the Cia2 is the bridge of the core targeting complex and that Cia1 is required for Nar1 binding (Figure 2.10). If the role of Nar1 is to provide cluster to apo-targets or act as an adapter, then we would

predict its binding might occur before the stable subcomplexes are formed and recognize targets. Through this work, we provide a platform for understanding the full structure and mechanism for the CIA targeting complex and the ability to investigate target recognition by isolation of the stable subcomplex forms.

CHAPTER THREE: Understanding the CIA targeting recognition of different FeS cluster proteins and the role of Nar1

(*This work is a reformatted version of* **Vo** *et al., Biochemistry, accepted* **2017***)*

3.1 Introduction

The cytosolic iron sulfur cluster assembly (CIA) system assembles iron sulfur (FeS) cluster cofactors and inserts them into >20 apo-protein targets residing in the cytosol and nucleus that all vary in their structure and function. Although this pathway is essential in providing this FeS cofactor for so many biological processes, little is still known about how these apo-proteins are recognized by the CIA targeting complex for FeS insertion. One possible model is that the CIA targeting complex identifies a single recognition motif on all targets, such as LYR (leucine, tyrosine, and arginine) motifs that are signatures to recognize targets or accessory proteins that assist in FeS cluster transfer in the mitochondrial system.[73]

However, previous studies suggest the alternative model that the recognition motif varies for each target or subset of targets. The Lill lab observed a disruption of their interaction with the targeting complex when they mutated a c-terminal tryptophan in the adapter Lto1, which tethers the target Rli1 to the CIA targeting complex.[1] Other proteins such as viperin, Leu1, and Nar1 also contain this c-terminal tryptophan. Additionally, for target Rad3, Lansdorp, Uringa, and coworkers demonstrated the FeS-binding domain of Rad3, found close to the N-terminus of the protein, binds to Cia2.[26] However, this conflicted with the findings of Tanaka and coworkers who proposed that the C-terminal region of Rad3 is responsible for binding Met18.[51] However, these findings still imply

each target is recognized by a different motif.

Furthermore, the Lill lab suggested the model Cia1, Cia2, and Met18 form mixtures of complexes, each capable of interacting with specific subsets of targets.[7] This model predicts that individual subunits or subcomplexes will differ in how they associate with certain targets. This model for the CIA targeting complex is consistent with the model that the recognition motif varies for each target or subset of targets. Herein we investigate the two models with our CIA targeting complex. We explore recognition of two validated CIA targets, Rad3 and Leu1, in addition to an FeS protein derived from *E. coli*, the fumerate-nitrate transcriptional activator FNR. Utilizing the CIA targeting complex and stable subcomplexes, we investigate their abilities to recognize these targets.

We also explore the aspects of cluster insertion and cluster trafficking. We would predict that the CIA targeting complex would have preferential binding for an apo-protein target. A previous study investigated the ability of the CIA targeting complex to bind to human apo-Rad3. Vashisht *et al.* utilized site directed mutagenesis to generate two mutants that were unable to bind cluster. The first, mutated a cysteine (C190S) involved in cluster binding, while the second mutant (R112H) disrupted cluster binding due to proximity to a cysteine coordinating FeS cluster binding.[62] Both these mutants were still able to bind to the CIA targeting complex and Vashisht *et al.* proposed that insertion of the cluster would trigger Rad3's release from the CIA targeting complex. Herein we look at binding of the CIA targeting complex to a chemically reconstituted holo-Leu1 compared to apo-Leu1.

To investigate cluster trafficking, we explore the role of Nar1. Previous *in vivo* experiments showed that depletion of Nar1, inhibited iron incorporation to downstream targets.[25, 28, 88] Additionally, both 4Fe4S clusters are essential for Nar1 function and cell viability. However, the role of Nar1 in the CIA pathway remains elusive. These studies indicate its involvement in cluster transfer, but still lack insight in its role in cluster insertion. In this chapter we look at the cluster associated with Nar1 and survey its potential role as an adapter or cluster carrier.

3.2 Materials and Methods

3.2.1 Chemical Reconstitution of FeS proteins

The plasmid construction, along with expression and purification of proteins can be found in the Appendix 2. The co-affinity purification method was carried out as detailed in Chapter 2.

3.2.2 Chemical Reconstitution of FeS proteins

Anaerobic water, buffer (50 mM Tris-HCl (pH 8.0), 300 mM NaCl, 10 (v/v)% glycerol) glycerol, and consumables are deoxygenated and stored in an anaerobic chamber several days before the reconstitution.[89] The night before reconstitution, 19 mg ferrous ammonium sulfate hexahydrate ($Fe(NH_4)_4(SO_4)_2$), 12 mg sodium sulfide nonahydrate ($Na_2S•9H_2O$), 77 mg dithiothreitol (DTT), and 102 mg magnesium chloride hexahydrate ($MgCl_2•6\ H_2O$) as solids were brought into the Coy chamber. The following day, add 0.5 mL anaerobic water to make the following solutions: 100 mM $Fe(NH_4)_4(SO_4)_2$, 100 mM Na_2S, 1 M (DTT), 1 M ($MgCl_2$).[90] The protein was pre-reduced

by bringing in 1 mL aliquots of 1.0-1.5 mg/mL protein in a 1.5 mL tube into the box and adding DTT from the anaerobic stock to a final concentration of 5 mM. The protein was deoxygenated as it slowly stirred with a micro stir bar for two hours on a cold block or ArmorBeads for 3 hours with the cap open. The 100 mM stocks of iron and sulfide were diluted with anaerobic water to make 10 mM working stocks in the Coy chamber. A six-fold molar excess of iron was added to protein. Iron was slowly added in small aliquots with stirring to limit high localized concentrations of the stock. The protein was incubated on a cold block for 10 minutes with gentle stirring between each addition. A six-fold molar excess of sulfide from the 10 mM Na_2S solution was added in the same manner as described for the iron. The protein was then capped and incubated with gentle stirring for two hours. During this time, the solution noticeably changed color to a yellow-brown to brown color. The supernatant to a 20 mL G-25 desalting column equilibrated with anaerobic buffer without DTT. The elution fractions were collected and protein-containing fractions were concentrated with an Amicon micro concentrator. For assessing Holo Leu1 binding to the CIA targeting complex, co-affinity purification assays were run the same way as described in Chapter 2, but with a streptactin column that had been equilibrated in the coy chamber overnight and washed with anaerobic buffer.

3.2.3 Ferrozine Assays

A sample of protein at a volume of 30 µL and around 0.5-1 mg/mL was treated by the addition of 70 µL 2 M hydrochloric acid and heated to 95˚C for 5 minutes. The precipitated protein is separated out by centrifugation at 16k xg for 12 minutes. The supernatant was added to a clean tube and 100 µL of 2M hydrochloric acid was used to

resuspend the protein pellet to extract any iron that was still bound to the protein. The sample was heated at 95˚C for 15 minutes, and then centrifuged at 16k xg for 12 minutes. The supernatant containing the liberated iron is treated with 40 µL of 75 mM sodium ascorbate to reduce the iron, 200 µL of 10 mM ferrozine (3-(2- pyridyl)-5,6-bis(4-phenylsulfonic acid)-l,2,4-triazine), 200 µL saturated (~19M) ammonium acetate, and 360 µL water is added to yield a purple species. This colored complex has a maximum absorbance at 562 nm with an extinction coefficient of 27.9 $mM^{-1}cm^{-1}$. A sample containing only buffer, treated the same way as the 30 µL protein sample above, was subtracted from the values of all the protein samples to eliminate the background absorbance for the assay. The absorption at 562 nm is used to calculate the concentration of iron in the sample.

3.2.4 Sulfide Assays

The sulfide assay is adapted from the method of Beinert, [91] and has been recently described by others in this series.[92] Based off the ferrozine assay, the protein sample should have about 20 µM sulfide in 200 µL. To the 200 µL sample, a tiny stir bar is added and stirred in 600 µL of 1% (w/v) zinc acetate dihydrate followed by 30 µL of 12% (w/v) sodium hydroxide are added and while stirred at room temperature for 45 minutes. The stirring was tired off and 150 µL of 0.1% (w/v) N,N-dimethyl-p-phenylenediamine (DMPD) was under laid in the solution and 30 µL of 23 mM iron (III) chloride was injected to form the methylene blue product. The solution was stirred vigorously for 15 minutes and then centrifuged for 20 minutes at 16k xg to pellet the protein. The methylene blue product has a known extinction coefficient of 34.5 mM^{-1} cm^{-}

[1] at 670 nm, which can be used to quantify the sulfide concentration after background subtraction of a buffer only sample prepared in the same way.

3.2.5 Leu1 Transfer Assays

Apo Leu1 and Nar1 were mixed together in a final volume 100 µL, where the final concentration of Leu1 was 3 µM and Nar1 was 10 µM. This ratio was chosen as the ferrozine assay showed Nar1 was roughly a third loaded with Fe. Leu1 activity assays were performed in 5mM DTT, 50mM Tris-HCl pH 8.0, 150 mM NaCl in a final volume of 500µL. After different time points over an hour, 10µL aliquots of the protein mixture was added to the Leu1 buffer with 4mM 3-isopropylmalate and tested for the ability to convert 3-isopropylmalate to dimethylcitraconate acid spectrophotometrically (dimethylcitraconate has an extinction coefficient of 4.35 mM^{-1} cm^{-1} at 235nm). The increase in absorbance at 235nm of dimethylcitraconate over time was used to assess the activity of Leu1. For assessing holo Leu1 binding to the CIA targeting complex, 5µL of the elution of a co-affinity purification assay was mixed in the Leu1 assays and its cluster dependent isomerase activity was measure in the same way. [90]

3.3 Results

3.3.1 The specificity of CIA recognition by the core targeting complex

To begin deciphering the rules governing target recognition, we examined the ability of the targeting complex to directly bind two validated CIA targets, Rad3 and Leu1, in addition to an FeS protein derived from *E. coli*, the fumerate-nitrate transcriptional activator FNR. Rad3 is a helicase required for nucleotide excision repair

and transcription.[93] The human homolog of Rad3 (ERCC2 or XPD; here referred to as hRad3) has been shown to associate with the CIA targeting complex *in vivo* and *in vitro.*[62, 94] Therefore, we chose Rad3 as the first target to validate our *in vitro* assay for target recognition. Since no methods to access recombinant Rad3 have been reported, we expressed Rad3 in *E. coli* and developed a method to refold the protein from solubilized inclusion bodies. CD confirmed that the refolded Rad3 has a large amount of secondary structure, consistent with successful refolding (Appendix 2). Inspection of the UV-Vis spectrum of refolded Rad3 did not reveal any features consistent with an FeS cluster, confirming Rad3 was isolated in its apo-form (not shown).

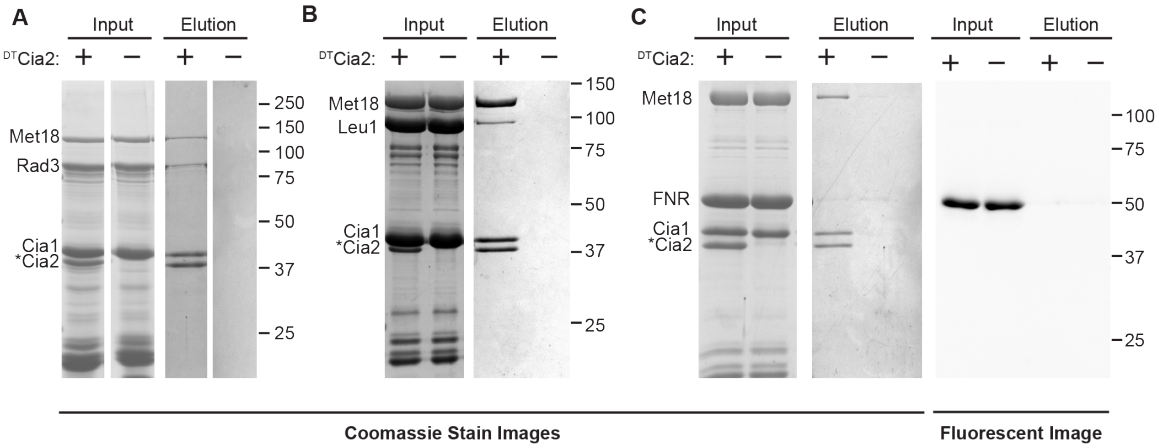

Figure 3.1. Interaction of the Met18-Cia1-Cia2 complex with targets. **^{SUMO}Met18, ^{His}Cia1 and target were mixed with the ^{DT}Cia2 bait (input) and chromatographed on streptactin resin. The bound proteins were eluted and analyzed by SDS-PAGE. Both Rad3 (Panel A) and Leu1 (Panel B) are enriched in the elution fraction specifically in the presence of the ^{DT}Cia2-bait, but not in experiments where the bait was omitted. FNR (Panel C) is not enriched in a ^{DT}Cia2-dependent manner as both Coomassie blue staining and in-gel fluorescence imaging of SNAP-FNR fusion contain similar amounts of FNR in elution fractions both in the presence (+) and absence (-) of ^{DT}Cia2. Molecular weight standards in kDa are shown to the right of all the gels.**

To validate both that the refolding procedure was successful and that our reconstituted targeting complex can execute target recognition *in vitro*, we mixed ^{DT}Cia2 (bait) with ^{His}Cia1, ^{SUMO}Met18, and apo-Rad3 and passed the mixture through a streptactin column. As shown in Figure 3.1A, a significant amount of apo-Rad3 elutes with the Cia2 bait and the other targeting complex subunits. Importantly, no bands corresponding to apo-Rad3, Cia1 or Met18 were observed in the elution when the ^{DT}Cia2 bait was omitted, showing that there is no nonspecific binding to the resin. The intensity of the apo-Rad3 band relative to those of the targeting complex subunits suggests that most of the sample contains targeting complex associated with apo-Rad3.

Having demonstrated recognition of a nuclear target, we next examined if targeting complex can recognize a very different target, the cytosolic FeS-dependent isomerase Leu1. Genetic studies have revealed that Leu1 is dependent on Cia1, Cia2 and Met18 for cofactor acquisition *in vivo.*[47] Yet, to our knowledge, no coIP, yeast two hybrid, nor protein complementation study has reported interaction between Leu1 and any component of the targeting complex. Thus, it is unknown if Leu1 is identified by the targeting complex directly, or if an adaptor is required to mediate Leu1 recognitions similar to what was recently proposed for recognition of Rli1.[95]

When we mixed apo-Leu1 with the other components of the targeting complex in our co-purification assay, Leu1 is observed in the elution fraction along with the targeting complex subunits (Figure 3.1B). However, unlike the result with Rad3, the intensity of the Leu1 band was low relative to the intensities of the Met18, Cia1, and Cia2 bands. However, the Leu1 band intensity was reproducibly above the background observed in

the control where the ^{DT}Cia2 bait was omitted. These observations demonstrate that both Rad3 and Leu1 can directly bind the targeting complex *in vitro*. They additionally suggest that the affinity for Leu1 is less than that for Rad3. This result could explain why there are numerous reports of Rad3 associating with Met18, Cia1, and/or Cia2 subunits but none reporting interaction with Leu1.

Our observation that the targeting complex can bind both Leu1 and Rad3 demonstrates that the targeting complex can flexibly recognize very different apo-targets *in vitro*. Importantly, these two targets do not share any easily detectable sequence or structural similarities. In fact, the only similarity we could find was the four cysteine residues required to bind their [Fe_4S_4]-cofactors. Therefore, we tested whether the targeting complex was able to promiscuously recognize any FeS-protein via their cluster-ligating cysteine motifs. For this purpose, we utilized the *E. coli* fumarate and nitrate reductase regulatory (FNR) transcription factor which exploits an [Fe_4S_4] cluster sensor to regulate gene expression in response to oxygen.[96]

We cloned FNR fused to a both His- and SNAP-tags. The SNAP fusion shifted the molecular weight of FNR away from that of the Cia1 and Cia2 proteins so we could continue to use SDS-PAGE for analysis. The SNAP-tag also enabled specific detection of FNR by exploiting commercially available fluorescent labels for the tag (New England Biolabs). As expected, the UV-Vis spectrum of the protein confirmed little, if any, of FNR's oxygen labile [Fe_4S_4] cluster was associated with the aerobically purified protein (not shown). However, if we introduced a cluster-stabilizing mutation, FNR purified with some FeS cluster associated demonstrating the SNAP fusion did not perturb the FNR

tertiary structure (not shown).[97]

When we examined the ability of FNR to bind the targeting complex, little FNR was observed in the elution fraction though bands for Met18, Cia1, and Cia2 were all clearly present (Figure 3.1C). Since the elution fractions from both the experimental and control samples contained a faint band close to the molecular weight of FNR, we labeled FNR with a fluorescent SNAP substrate and monitored the in-gel fluorescence (Figure 3.1C). The specific detection of SNAP-FNR revealed that there is no enrichment of the target in the interaction experiment relative to the control where the bait protein was omitted. Therefore, while the CIA targeting complex can directly bind two of validated apo-substrates of CIA, the loss of binding to FNR suggests it cannot promiscuously recognize any FeS enzyme *in vitro*.

3.3.2 The Met18-Cia2 subcomplex is sufficient for Rad3 recognition

Having established that the targeting complex can specifically identify multiple apo-targets, we wanted to pinpoint which subunit or subunits executes target recognition. We began by investigating the binary interactions between Rad3 and the individual targeting complex subunits. The results showed that Cia1 did not interact with Rad3 (Figure 3.2A, middle panel), but the data were less clear-cut for binding to Met18 or Cia2. When either ^{SUMO}Met18 or ^{DT}Cia2 was used as the bait, the elution fractions contained small amounts of Rad3 (Figure 3.2A, upper and lower panels). This result contrasts with the strong association seen for Rad3 to the full targeting complex (Figure 3.1A). Additionally, the observation of a small amount of Rad3 binding to Met18 or Cia2 was not reproducible in either case and was very sensitive to the composition of the wash

buffer and amount of wash buffer used in the copurification experiment. We concluded that Cia1 does not form a stable binary complex with Rad3, and that Met18 and Cia2 likely do bind Rad3 target but only weakly. Thus, the full targeting complex binds Rad3 with higher affinity than any of its individual subunits.

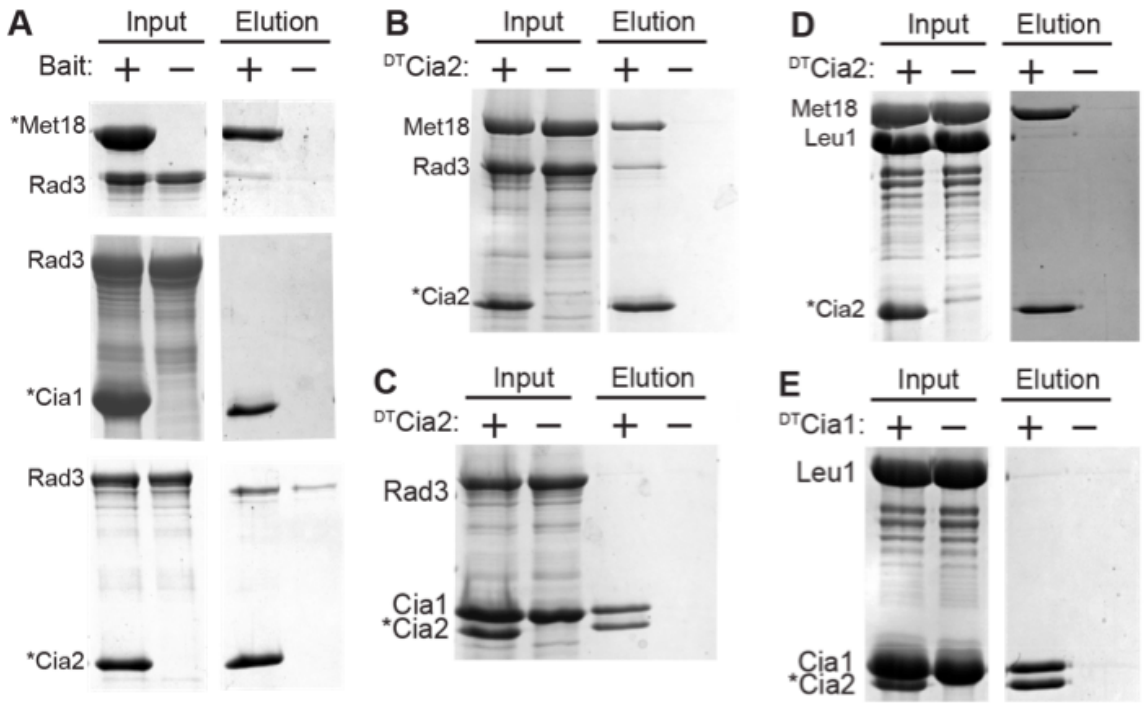

Figure 3.2 Rad3 interactions with the CIA targeting complex

SDS-PAGE analysis of Rad3's interaction with targeting complex components. Each panel shows results of the interaction tests both in the presence (+) and absence of the bait, which is marked with an asterisk to the left of each gel. A) Binary interaction tests with Rad3 (prey) and the targeting complex subunits Met18 (top), Cia1 (middle), and Cia2 (bottom). Both Met18 and Cia2 baits resulted in some enrichment of Rad3 in the elution, whereas the Cia1 bait did not. B) Rad3 and ^{SUMO}Met18 were mixed with the ^{DT} Cia2 bait (input). The streptactin column elution contains Met18, Rad3 and Cia2 demonstrating the Met18-Cia2 complex can bind Rad3. C) Rad3 and ^{His}Cia1 were mixed in the presence and absence of the ^{DT} Cia2 bait (input). The streptactin column elution contains Cia1 and Cia2 whereas little, if any, Rad3 is present.

To identify the minimal requirements for stable complex target recognition, we examined whether the Cia1-Cia2 or Met18-Cia2 subcomplexes could stably bind Rad3.

When we mixed ^{DT}Cia2 with Rad3 and either ^{SUMO}Met18 or ^{His}Cia1, we observed Rad3 co-purifying with ^{DT}Cia2 only in the presence of ^{SUMO}Met18 (Figure 3.2B). Little, if any, Rad3 was observed in the elution fraction in the presence of ^{DT}Cia2 and ^{His}Cia1 (Figure 3.2C). These results indicate that the Met18-Cia2 subcomplex is sufficient to stably associate with Rad3, whereas the Cia1-Cia2 subcomplex is not.

To determine if this result was generalizable to other apo-targets, we tested the interaction of Leu1 with both the Met18-Cia2 and Cia1-Cia2 subcomplexes, but did not reproducibly observe enrichment of Leu1 in these experiments (not shown). For both the Met18-Cia2 and Cia1-Cia2 complex, we barely detected any Leu1 that was above the background of the no bait control. Our results show that if these subcomplexes interact with Leu1, the interaction is dynamic and not observable with our co-purification affinity method. To observe recognition of Leu1 by the CIA components *in vitro*, all three proteins must be present. This observation also implies that the specificity of targeting complex recognition varies for different targets, as the affinity for Leu1 by the targeting complex is lower than Rad3 and none of the subcomplexes are sufficient to recognize Leu1.

3.3.3 Investigation of Apo Leu1 vs. Holo Leu1 binding

We investigated apo-target recognition by the core CIA targeting complex and stable subcomplex Met18-Cia2. As the function for the CIA targeting complex is to recognize apo-protein targets for cluster insertion, we were interested in exploring its ability binding to holo-protein targets. Previously, it was shown that the cysteines associated with FeS cluster binding were not the motif that was recognized by the CIA

targeting complex (Figure 3.1C). Therefore, occlusion of these cysteines is not the mechanism to recognize apo-proteins. Studies from Vashisht *et al.* suggested that the CIA targeting complex could bind to Rad3 if the cysteine associate with cluster binding was mutated.[62] We would hypothesize that the CIA targeting complex would not bind to the holo-protein forms.

We were not able to chemically reconstitute Rad3, but having established a protocol for the chemical reconstitution of Leu1, we first explored the ability of holo Leu1 to bind to the CIA core targeting complex by coaffinity purification. A 250nm to 800 nm wavelength UV Vis scan of chemically reconstituted Leu1 indicated a 410 peak consistent with a 4Fe4S cluster. From the absorbance of the cluster as compared to Leu1 protein concentration, holo Leu1 was about 50% loaded, with 2.1 ± 0.3 Fe atoms by the ferrozine assay (the sulfide assay was not performed). This chemically reconstituted Leu1 was mixed anaerobically with the core CIA targeting complex and binding of the holo Leu1 to the core CIA targeting complex was assessed by co-affinity purification. In the elution, a very small amount of Leu1 was present. However, it was unclear if the Leu1 retained on the column was apo or holo protein.

To evaluate if the Leu1 bound to the targeting complex was apo or holo, we assayed the elution for Leu1 activity. The elution sample did not contain any Leu1 activity, indicating that the Leu1 present in the sample was apo. Previously, our lower limit of detection for Leu1 activity had been shown to be a concentration of 20 nM. As Leu1 in the final protein mixture that was loaded onto the column was present at 300nM, it seems unlikely that Leu1 in the elution off the column would be less than 20 nM if the

protein were able to bind to the targeting complex. Overall, the CIA targeting complex appears to have a stronger affinity for apo Leu1, but future experiments should be able to quantify the difference in binding (Figure 3.3).

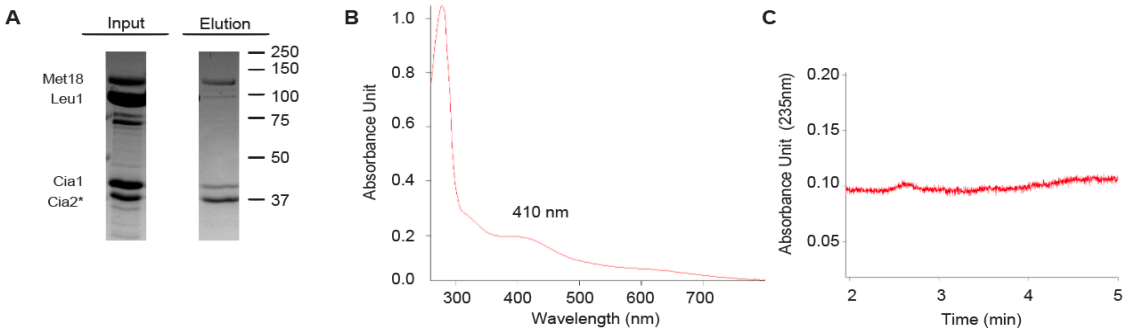

Figure 3.3 Holo Leu1 with the CIA targeting complex.
A) SDS-PAGE analysis of Leu1's interaction with targeting complex components. ^{SUMO}Met18, holo-^{His}Leu1, and ^{His}Cia1 were mixed with ^{DT}Cia2 as bait on a streptactin column. In the elution Met18 and Cia1 were retained with the Cia2 bait, but little Leu1 was present. B) A UV-VIS spectra of the chemically reconstituted protein that was used in the input of the co-affinity purification from Panel A shows a 410 peak consistent with a 4Fe4S cluster with 50% cluster loading as quantified by the ferrozine assay and calculated molar concentrations from the absorbances of the protein at 280nm and the cluster at 410 nm (using their extinction coefficients of and respectively) C) When the Elution in Panel A was assayed for Leu1's cluster dependent ability to convert to convert 3-isopropylmalate to dimethylcitraconate acid at 235 nm, over the time course of 5 minutes there is little conversion. This indicates that the Leu1 present does not contain cluster.

3.3.4 Nar1 and Leu1 do not bind simultaneously to targeting complex or transfer cluster

To fully investigate how the CIA targeting complex aids in cluster trafficking, we explored Nar1's role in CIA targeting complex. Previous *in vivo* experiments showed that depletion of Nar1, inhibited iron incorporation to downstream targets.[25, 28, 88] Additionally, both 4Fe4S clusters are essential for Nar1 function and cell viability. We investigated two possible models for the function of Nar1. If Nar1 acts as an adapter to bring the scaffolding complex to the targeting complex for cluster transfer, then Nar1

must be able to bind to both the targeting complex and targets (Figure 3.6). To test the adapter model, we mixed together Cia1, Cia2, Leu1, Met18, and Nar1 in equal molar ratios and found that only Nar1 co-eluted with the targeting complex. This co-affinity purification was compared to the binding of Nar1 and Leu1 individually with the CIA targeting complex (Figure 3.4). Leu1's inability to bind to the targeting complex while Nar1 is present suggests that the CIA targeting complex preferentially binds to Nar1 when both Leu1 and Nar1 are present and that Nar1 is unlikely to act as an adapter.

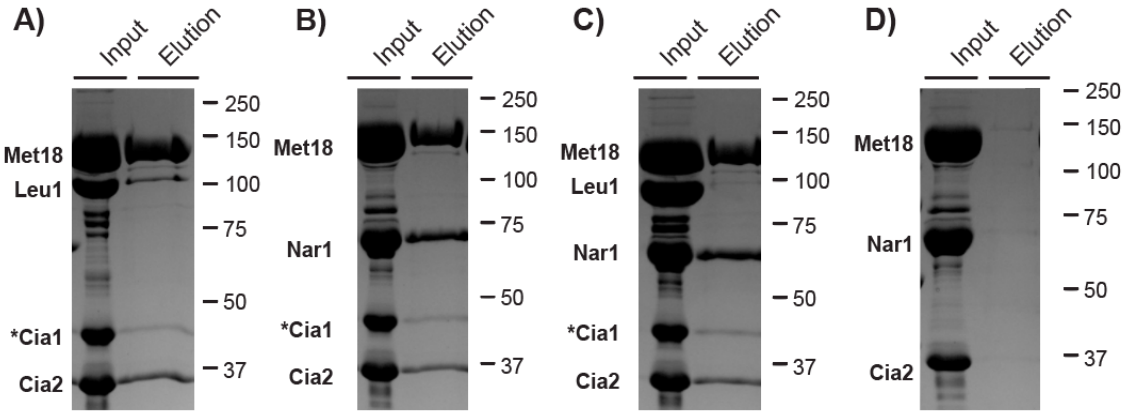

Figure 3.4. Interaction of the Met18-Cia1-Cia2 complex with both Nar1 and Leu1.
A) ^{SUMO}Met18, ^{His}Cia1, ^{His}Leu1 and/or ^{His}Nar1 were mixed with the ^{DT}Cia2 bait (input) and chromatographed on streptactin resin. The bound proteins were eluted and analyzed by SDS-PAGE. Both Leu1 (Panel A) and Nar1 (Panel B) are enriched in the elution fraction with the Met18-Cia1-Cia2 targeting complex. However, when all four proteins are mixed, only Nar1 is enriched in the elution fraction with the Met18-Cia1-Cia2 targeting complex. None of the proteins elute when the ^{DT}Cia2 bait is omitted.

Another possibility is that Nar1 is acting as a cluster carrier. Nar1 contains two 4Fe4S clusters and the fully loaded protein would contain 8 atoms of Fe and 8 atoms of S. Post purification, Nar1 appears brown, a characteristic consistent with cluster bound protein. To assess the amount of cluster loaded, we performed colorimetric assays to

quantify both iron and sulfide loading. Nar1 as purified contains 2.6 ± 0.2 Fe atoms by the ferrozine assay and by the sulfide assay, 6.1 ± 0.2 sulfide atoms, which is consistent with the as purified FeS cluster characterized in previous studies (Figure 3.5AB).[28] These studies also indicated the FeS cluster within the samples were 4Fe-4S by EPR suggesting that the as purified protein sample is a mixture of holo-Nar1 and apo-Nar1. To interrogate if this cluster could be transferred to a target we incubated Nar1 as purified with apo Leu1 and monitored Leu1 cluster-dependent activity. After assaying different time points (5, 10, 20, 30, 45, and 60 minutes) over the time course of 60 minutes, Leu1 showed no cluster dependent isomerase activity (Figure 3.5C). This mixture showed no increased specific Leu1 activity (blue diamonds), compared to a sample of holo-Nbp35 and apo-Leu1 (red squares), which showed increase in specific activity for Leu1 as the chemically reconstituted cluster on Nbp35 was transferred to Leu1 (data shown from John Grossman, *unpublished* Figure 3.5C). This result shows Nar1 as purified is not sufficient in transferring cluster to Leu1 as seen previously with chemically reconstituted proteins like Npb35 that can transfer their cluster to Leu1, which then shows specific Leu1 activity.

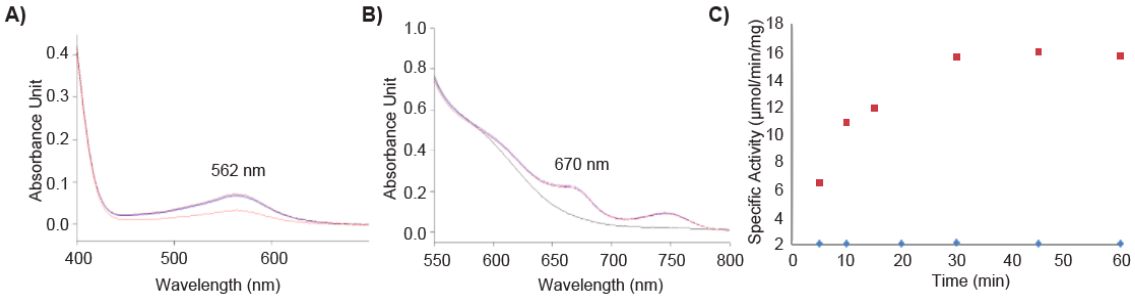

Figure 3.5 Nar1 cluster as purified cannot be transferred to Leu1.
A) Nar1 as purified contains 2.6 ± 0.2 Fe atoms by the colorimetric ferrozine assay in which the Fe in the protein sample generates a colored complex that has a maximum absorbance at 562 nm with an extinction coefficient of 27.9 $mM^{-1}cm^{-1}$. The buffer (red) is background subtracted from the samples (blue) and the resulting absorbance with the extinction coefficient is used to calculate iron concentration in the sample. B) The sulfide assay of Nar1 as purified indicates that contains 6.1 ± 0.2 sulfide atoms. The methylene blue product is generated by a reaction with the S in the protein sample and has a known extinction coefficient of 34.5 mM^{-1} cm^{-1} at 670 nm. The buffer (black) is background subtracted from the samples (blue) and the resulting absorbance with the extinction coefficient is used to calculate the sulfur concentration in the sample. C) The mixture of apo-Leu1 and Nar1 as purified was assayed over the time course of an hour. This mixture showed no increased specific Leu1 activity (blue diamonds), compared to a sample of holo-Nbp35 and apo-Leu1 (red squares), which showed increase in specific activity for Leu1 as the chemically reconstituted cluster on Nbp35 was transferred to Leu1 (data shown from John Grossman, *unpublished*).

3.4 Discussion

A major unsolved question in cytosolic FeS cluster assembly is what recognition motif is identified by the CIA targeting complex. To begin developing a mechanistic model for CIA substrate recognition, we demonstrate that two very different targets, apo-Leu1 and apo-Rad3, can both interact with the targeting complex *in vitro* (Figure 3.1AB). The simplest model to explain this result would be if apo-Leu1 and apo-Rad3 share a motif sufficient for their recognition, similar to the mechanism recently proposed for the mitochondrial FeS biogenesis system.[98] However, analysis of the Leu1 and Rad3 sequences failed to identify short regions of high homology. The only similarity we could identify is a series of cluster-binding cysteines. Therefore, we considered the possibility

that any apo-FeS protein could bind the CIA targeting complex via its cysteine-rich FeS binding motif.

To determine if the presence of an FeS binding motif is sufficient to associate with the Met18-Cia1-Cia2 complex, we investigated whether the targeting complex could identify FNR, an FeS protein derived from bacteria that does not have any eukaryotic homologs. As shown in Figure 3.1C, we could not detect an interaction with the Met18-Cia1-Cia2 complex demonstrating that the mere presence of a cluster binding site is not sufficient for target recognition. Although a cluster-binding cysteine residue could still be an element of the targeting motif, it appears likely that a more complex recognition mechanism is in play. For example, our inability to identify a shared motif between these two targets suggests there could be multiple recognition motifs, each responsible for tethering certain targets, or subsets of targets, to the targeting complex.

Other studies support the model that there are multiple recognition motifs to identify certain targets. Leu1 contains a c-terminal tryptophan similar to viperin and Lto1, which previous co-IP studies have mutated for the human homologs and saw a disruption of their interaction with the targeting complex.[1] Additionally, current Perlstein lab member Melissa Marquez has shown that mutation of the c-terminal tryptophan on Leu1 disrupts binding to the CIA targeting complex (data not shown). This recognition motif is unique from the Rad3 recognition motif proposed by reports aimed at pinpointing the region of Rad3 responsible for association to Met18.[25, 51, 62] While the published studies disagree as to what region of Rad3 is essential for binding Met18, they agree that the Met18 binding site of Rad3 lies outside of its FeS-binding domain, which supports the

model of multiple recognition motifs on targets that are identified by the CIA components.

If we predict a more complicated targeting mechanism in which there are different recognition motifs for each target protein, we would anticipate that the corresponding motif on the CIA components responsible to identify the targets would also vary for each target protein. In order to explore this model, we investigated what component or components of the targeting complex execute target recognition (Figure 3.2). Proteomics studies have suggested that Cia1, Cia2, and Met18 form mixtures of complexes, each capable of interacting with specific subsets of targets.[7] To probe this model, we investigated which subunits or subcomplexes were sufficient to bind Rad3 and Leu1. We discovered that the Met18-Cia2 subcomplex, but none of the isolated subunits nor the Cia1-Cia2 complex, was able to retain large amounts of Rad3 in the elution fraction under our elution conditions (Figure 3.2). Since both Met18 and Cia2 bound small amounts of Rad3, we think each of these subunits binds Rad3 with low affinity. These individually weak interactions synergize in the Met18-Cia2 subcomplex to increase the affinity. This model predicts that two regions of Rad3 will be required to bind the targeting complex. Indeed, Lansdorp, Uringa, and coworkers demonstrated the FeS-binding domain of Rad3, found close to the N-terminus of the protein, binds to Cia2.[26] These authors also reported that RTEL1, an ortholog of Rad3 for humans, binds Met18 via a region far removed from the FeS-binding domain.[26] This study corroborated the previously reported findings of Tanaka and coworkers who proposed that the C-terminal region of Rad3 is responsible for binding Met18.[51] However, this model was recently

challenged by the work of the Wohlschlegel laboratory who reported that a region of the Arch domain housed within Rad3's N-terminal domain is responsible for the interaction of Rad3 with Met18.[62] Since only the full targeting complex is sufficient to bind Leu1, our work reveals target-specific differences in CIA substrate recognition (Figure 3.2). Our *in vitro* studies support the model that CIA substrate recognition can be executed by the full targeting complex or by its stable subcomplexes and that these forms allow for binding to different recognition motifs on targets.

As the cysteines involved in cluster binding do not appear to be associated with target recognition, the question remained how apo and holo targets bind to the CIA targeting complex differentially. We would predict that the CIA targeting complex would bind the apo form of targets with higher affinity, as these proteins need to acquire cluster. A previous study investigated the ability of the CIA targeting complex to bind to human apo-Rad3. Vashisht *et al.* utilized site directed mutagenesis to generate two mutants that were unable to bind cluster.[62] The first, mutated a cysteine (C190S) involved in cluster binding, while the second mutant (R112H) disrupted cluster binding due to proximity to a cysteine coordinating FeS cluster binding.[62] Both these mutants were still able to bind to the CIA targeting complex and Vashisht *et al.* proposed that insertion of the cluster would trigger Rad3's release from the CIA targeting complex. However, these studies failed to investigate holo-target binding to show a decrease in affinity for the cluster bound protein and prove that their serine mutation did not bind cluster.

To explore this mechanism, we chemically reconstituted Leu1 with a 4Fe4S cluster, as we were not able to chemically reconstitute Rad3 (not shown). We saw by our

co-affinity purification assay that less Leu1 was retained with the CIA targeting complex in the holo Leu1 sample than the apo Leu1 (Figure 3.3). A Leu1 activity assay of the elution revealed that the Leu1 binding to the targeting complex was apo or too small a concentration to be detected by the assay. This experiment suggests that the CIA targeting complex preferentially binds apo-Leu1 and the interaction is lost through cluster binding. This result is consistent with the previous Rad3 studies, indicating that for multiple FeS proteins the CIA targeting complex binds tighter to the apo-form. There are two potential models for why this might be. Either the cluster occludes the binding site on the FeS proteins where the CIA targeting complex is binding, or binding to the FeS cluster creates a conformational change that alters the ability of the CIA targeting complex to bind to the target. The latter seems likely as we and other labs have determined for both Leu1 and Rad3 that the CIA targeting binding site is outside of the FeS cluster domain.[26, 61, 62, 95]

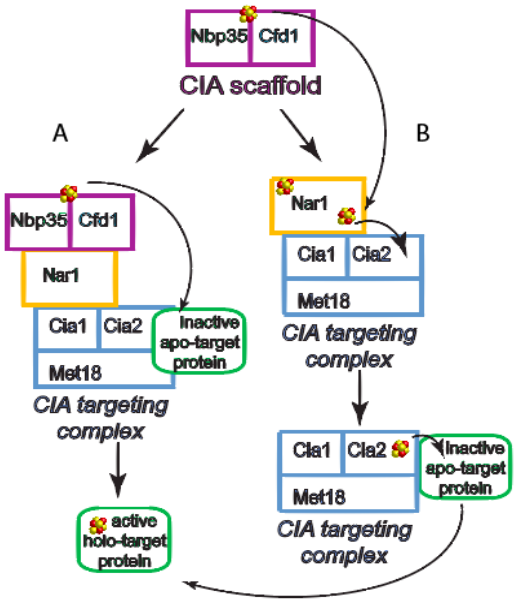

Figure 3.6. Possible models for the role of Nar1.
This figure represents the two possible models based off of *in vitro* experiments from this thesis. A) Nar1 acts as an adapter between the scaffold and the targeting complex with the apo-target so that the cluster formed on the scaffold can be transferred to the apo-target protein. B) Nar1 acts as cluster carrier, trafficking the cluster from the scaffold to the apo-target protein via the CIA targeting complex.

To further investigate cluster transfer by the CIA targeting complex we probed Nar1's role in the pathway as an adapter or potential cluster carrier. If Nar1 is an adapter, it should be able to bind simultaneously to the targeting complex as well as targets (Figure 3.6A). To test Nar1's ability to bind to both the CIA targeting complex and targets we utilized our co-affinity purification assays. Upon mixing Nar1 with the targeting complex and Leu1, we see only Nar1 co-elute with the targeting complex and not Leu1. Both Nar1 and Leu1 contain a c-terminal tryptophan. Although the c-terminal tryptophan on Nar1 has not been shown to be important for binding to the CIA targeting complex in the same manner as Leu1, this suggests that these proteins compete for the same binding site on the CIA targeting complex.

Since Nar1 cannot be an adapter, we explored its role as a cluster carrier. As purified, Nar1 contains 2.6 ± 0.2 Fe atoms by the ferrozine assay and by the sulfide assay, 6.1 ± 0.2 sulfide atoms, consistent with previous literature values in which the as purified protein contained 4Fe4S cluster by EPR with similar iron and sulfide concentrations (Figure 3.5AB).[28] Previous *in vivo* experiments showed that depletion of Nar1, inhibited iron incorporation to downstream targets.[25, 28, 88] To probe Nar1's ability to transfer cluster, we incubated Nar1 with Leu1 and assayed for Leu1 cluster dependent isomerase activity. Nar1 did not transfer its cluster to Leu1 and cannot bind simultaneously to the CIA targeting complex with Leu1. These results indicate that Nar1 does not bind transfer cluster while bound to the CIA targeting complex. However, the inability of Nar1 to directly transfer cluster to Leu1 could be due to the requirement of another substrate. For example, Cia2 could be required to transfer cluster to the apo-protein target. Cia2 could act as a cluster carrier that receives cluster or reducing equivalents from Nar1 to transfer cluster to the apo-protein target. (Figure 3.6B) As Cia2 is present in all stable forms of the CIA targeting complex, it is possible that it acts as a cluster carrier to targets. This concept will be explored in more detail in Chapter 4.

Overall, this study has provided new insights into the interactions vital for its recognition of targets. This could not have easily been developed using the cell-based assays that are frequently exploited to understand targeting in CIA. With the approach developed and experiments completed herein, hypotheses as to how apo-targets are identified can be directly tested and refined. This study has also provided insight into the role of Nar1 in cluster insertion and the ability to investigate the CIA targeting complex's

role in cluster trafficking. Finally, our work undoubtedly will enable the development of quantitative assays, which will be essential for unlocking the cryptic code utilized by CIA to identify apo-FeS proteins in the final step of cytosolic iron sulfur cluster assembly.

CHAPTER FOUR: Defining the domains of Cia2 required for its essential function *in vitro* and *in vivo*

(*This work is a reformatted version of* Vo *et al., Metallomics,* 2017*, 9 (11), 1645-1654.)*

4.1 Introduction

In this chapter we probe our understanding of the function of Cia2. Cia2 is an essential protein that is the organizing center of the targeting complex involved in the last step of recognizing FeS cluster proteins for cluster insertion.[5, 40] Therefore, we explored its conserved residues on Cia2 that may be required for its protein-protein interactions. If its primary functions are to form the CIA targeting complex and recognize targets, then mutations of these conserved residues will impact either CIA targeting complex formation, target identification, or both.

However, previous studies allude to an additional function for Cia2 in FeS biogenesis, outside of its role in protein-protein interactions with CIA components and targets. We hypothesize that mutations in conserved residues for this function will not disrupt its ability to bind other proteins, but will impair its *in vivo* functions. In order to assign the role of each of the conserved residues in Cia2, we split the protein into conserved motifs and explore the functions of these motifs through our *in vitro* and *in vivo* assays.

The N-terminal half of Cia2 contains an intrinsically disorder domain that is conserved in one set of Cia2 homologs.[40] The C-terminal half of Cia2 contains an FeS assembly/MIP18 family domain, formerly known as the domain of unknown function 59 (DUF59). As a substantial part of these experiments interrogated this domain before its

new name, we will refer to it in this work as the DUF59 domain. Proteins with this domain are genetically linked to FeS cluster biogenesis in bacteria and archea.[42-45] For example, a bacterial protein called SufT in the SUF FeS cluster biogenesis operon was recently proposed as an FeS biogenesis protein.[43] Additionally, many organisms contain a fusion of MRP/Nbp35 type cluster scaffold and a DUF59 domain.[45]

To investigate conserved portions of Cia2 and assign their functions, Deborah Perlstein and Nicholas Fleischman identified 5 conserved motifs by bioinformatics analysis (Figure 4.1).[40] Within the FeS Assembly/MIP18 domain, previous *in vivo* studies have specifically interrogated conserved residues C161 (Motif 4), E208 (Motif 5), and the last five amino acid residues of Cia2 by construct in which these are mutated Δ5C-Cia2 (Motif 5). [47, 60, 66] In this chapter, we examine these residues along with a construct with the deletion of the first two motifs (Δ102C-Cia2) and the conserved DPE (Motif 3) and to understand their role in protein-protein interactions with our *in vitro* assays, and compare these results to their phenotypes *in vivo*.

4.2 Materials and Methods

4.2.1 Co-affinity Purification

The plasmid construction, along with expression and purification of proteins can be found in the Appendix 2. The co-affinity purification method was carried out as detailed in Chapter 2.

4.2.2 Complementation Assays

For the complementation experiment, a Tet-titratable Cia2 strain (TH_3222; a BY4741 strain with the genotype MATa URA3::CMV-tTa his3-1 Leu2-0 met 15-0 Kan^R-$TetO_7$-*CIA2*) was obtained from GE Dharmacon.[99] This strain allows for repression of genomic Cia2 in the presence of doxycycline. Plasmids pRS313-ADH-CIA2-MYC, or mutations Δ102-Cia2, NPQ-Cia2, Δ5C-Cia2, C161A-Cia2, E208A-Cia2, and pRS313 for the full length Cia2, mutant alleles, or the empty vector control, respectfully, were transformed into the TH_3222 strain and selected on SC –Ura – His +G418 plates. Log phase cultures were serial diluted, applied to SD–Ura-His+G418 plates in the presence or absence of 50 μg/mL doxycycline (DOX) and in the presence of other additives as indicated, and incubated for 3 days at 30˚C before imaging. For methylmethane sulfonate (MMS) sensitivity, cells were applied to YPAD with 0.008% MMS the presence or absence of DOX. For sulfite reductase activity, cells were plated on YPAD supplemented with 0.001% (w/v) bismuth ammonium citrate, 0.003% (w/v) sodium sulfite, and 0.0003% (w/v) ferrous sulfate in the presence or absence of DOX. For hydroxyurea (HU) sensitivity, cells were plated on YPAD with 25 mM HU in the presence and absence of DOX. For NPQ-Cia2, a colony was suspended in sterile water, serial diluted and applied to plates since the strain was difficult to propagate in liquid culture.

4.2.3 Leu1 Activity Assays in vivo

The TET-Cia2 strain (TH_3222) transformed with plasmids for wtCia2 or its mutant alleles were grown overnight in SD–Ura–His+G418+DOX, diluted into YPAD supplemented with G418 and DOX (50 μg/mL), and grown to mid-log phase at 30˚C.

Crude extracts were generated in an anaerobic chamber and Leu1 assays carried out as described in Chapter 2.

4.3 Results

4.3.1 Eukaryotic Cia2 homologs share five conserved motifs

Nearly all eukaryotes encode at least one Cia2 homolog and some organisms encode a paralogous pair, referred to as Cia2a (Fam96A) and Cia2b (Fam96B or Mip18).[7] Cia2b is a general FeS assembly factor and is the ortholog of yeast Cia2. Cia2a is proposed to specifically direct maturation of iron responsive protein 1 (IRP1).[7] Through bioinformatics analysis, Deborah Perlstein and Nicholas Fleischmann identified five conserved motifs, distributed between an N-terminal acidic domain and a C-terminal domain containing the DUF59 (Figure 4.1).

The N-terminal domain has two conserved regions, an NxNP motif and a patch of acidic residues (Motifs 1 and 2, Figure 4.1). This N-terminal extension is missing in bacterial and archaeal DUF59 proteins and in the Cia2a paralogs.[40] There is little sequence conservation between these motifs except for an enrichment in polar and charged residues, suggesting this domain is intrinsically disordered.[100]

Figure 4.1. Conserved motifs of Cia2
A) The Cia2 sequence is annotated as follows: predicted regions of disorder, dark grey shading; DUF59 domain, light grey shading; Motif 1, red; Motif 2, orange; Motif 3, green; Motif 4, blue; Motif 5, purple. The positions of Leu103 (first residue of ⊗102-Cia2), Cys161, and Glu208 are each marked with a black circle. B) Surface representation of human Cia2a (PDB ID 2M5H)[25] with Motifs 3, 4, and 5 colored as in Panel A. Cys161 and Glu208 are colored yellow and red, respectfully.

The C-terminal region begins with the DUF59 domain and its characteristic motifs (Motifs 3 and 4, Figure 4.1). These motifs are close to one another (within 30 amino acids residues), forming a putative active site (Figure 4.1). Motif 5 (purple), found C-terminal to the DUF59, is missing from archaeal and bacterial sequences (Appendix). Since Motifs 1, 2, and 5 are unique to eukaryotes, they likely play a CIA-specific function, such as interaction with Met18 or Cia1. The conservation of Motifs 3 and 4 in all DUF59 proteins suggests that they play a common function in cluster biogenesis across all domains of life.

4.3.2 Cia2's intrinsically disordered domain is dispensable for its function in vitro and in vivo

Previous studies on Cia2 revealed that both the IMAC purified dtCia2 and refolded Cia2 exhibited aberrantly slow migration in SDS-PAGE. For example, dtCia2 (31 kDa) migrates with an apparent molecular weight of 44 kDa (not shown). MALDI-TOF analysis performed by Nicholas Fleishman revealed this was not due to a post-translational modification or additional residues inadvertently introduced during cloning (not shown). Since proteins with intrinsically disordered domains display this behavior[101], Deborah Perlstein and Nicholas Fleischman examined Cia2's sequence with the Multilayered Fusion-based Disorder Predictor (MFDp2) which analyzes sequences with multiple different algorithms to return a disorder propensity score.[102] This analysis revealed two regions in Cia2's N-terminal domain with a high probability of being disordered (dark grey, Figure 4.1A). Additionally, previous CD experiments performed by Nick Fleischman exhibited that the secondary structure of the N-terminal domain was consistent with an intrinsically disordered protein (not shown).

From the analysis of the inspected the sequences of Cia2 homologs, all the organisms examined have at least one Cia2b homolog with a disordered region. However, the intrinsically disordered domain is missing in the Cia2a paralogs.[40] The recent report that Cia2a/b pairs direct maturation of different targets combined with studies by Nicholas Fleischman that indicate the IDD is a distinguishing feature for this paralogous pair an investigation of whether the N-terminal domain mediates interaction with targets.[7] Using an affinity copurification assay, the ability of Cia2 and Δ102-Cia2 to bind to

Met18, Cia1, and Rad3 was assessed. When we mixed the double-tagged Cia1 (dtCia1, with both Strep- and His-tags) bait with SUMOMet18, Rad3, and Cia2, we observed similar amounts of each prey protein in the streptactin column elution fraction regardless of whether Cia2 or Δ102-Cia2 was used in the assay (Figure 4.2A). Thus, the IDD is dispensable for Cia2's interactions *in vitro*.

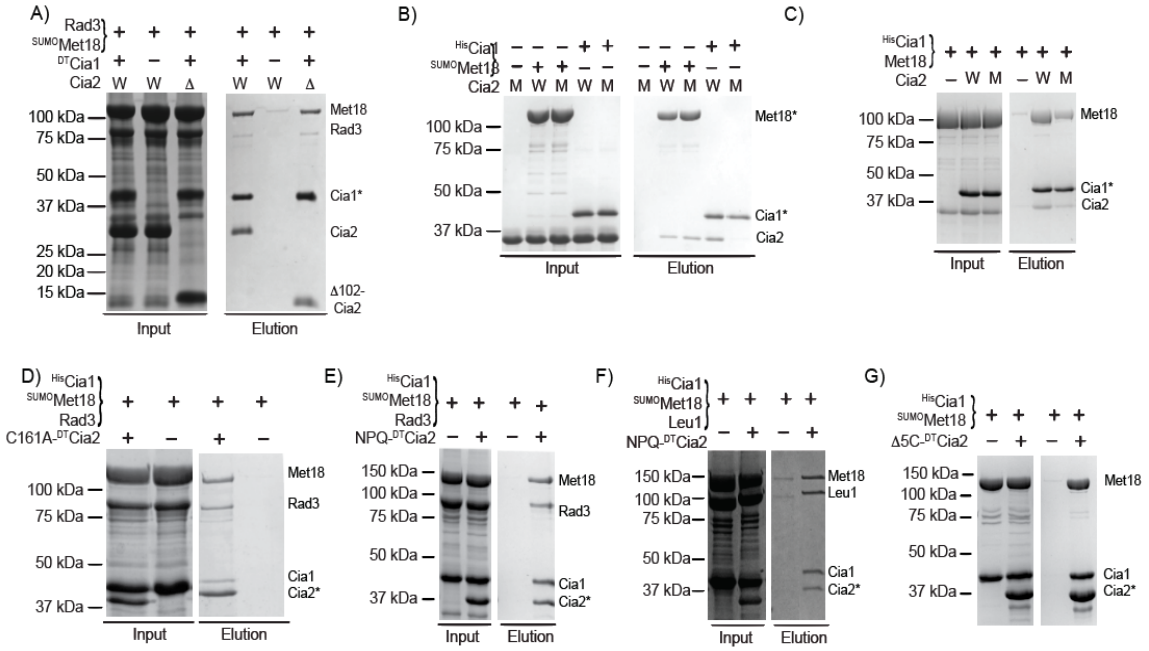

Figure 4.2. SDS-PAGE analysis of affinity copurification assays.
In all panels, a bait (*) is mixed with one or more prey proteins as indicated (Input) and passed through an affinity resin specific to the tag appended to the bait, either IMAC (Panel B and C) or Streptactin (Panels A, D, E, F, and G). The column is washed then the bound proteins are eluted and analyzed by SDS-PAGE (Elution). A negative control omitting the bait is also included in each panel. Panel A compares the ability of wt-Cia2 (W) and Δ102-Cia2 (Δ) to tether Rad3 to the DTCia1 bait. Panel B compares the ability of wt-Cia2 (W) and E208A-Cia2 (M) to form the Met18-Cia2 or the Cia1-Cia2 binary complexes. Panel C compares the ability of wt-Cia2 (W) and E208A-Cia2 (M) to scaffold the targeting complex by simultaneously binding Met18 and Cia1. Panel D demonstrates C161A-Cia2 can both form the targeting complex and bind Rad3. Panels E and F demonstrate NPQ-Cia2 can both form the targeting complex and bind Rad3 or Leu1. Panel G shows the ability of the Δ5C-Cia2 to form the targeting complex with Met18 and Cia1. The relative migration of MW standards and positions of CIA targeting complex subunits and Rad3 are indicated to the left and to the right in each panel, respectively. The data shown are representative of at least three independent experiments.

We next wanted to know if the N-terminal domain is required for Cia2's essential function *in vivo*. For this experiment, we used a commercially available strain in which Cia2's promoter is replaced with a Tet-regulated promoter.[99] In the absence of a plasmid-born Cia2, this TET-Cia2 strain cannot grow in the presence of doxycycline (DOX), which represses expression of the essential genomic Cia2. We introduced plasmids bearing Cia2 and Δ102-Cia2 into this strain and found that both constructs were able to complement the doxycycline-induced growth defect whereas the empty vector (EV) control could not (Figure 4.3A). Thus, the C-terminal domain is sufficient to support CIA function *in vivo*.

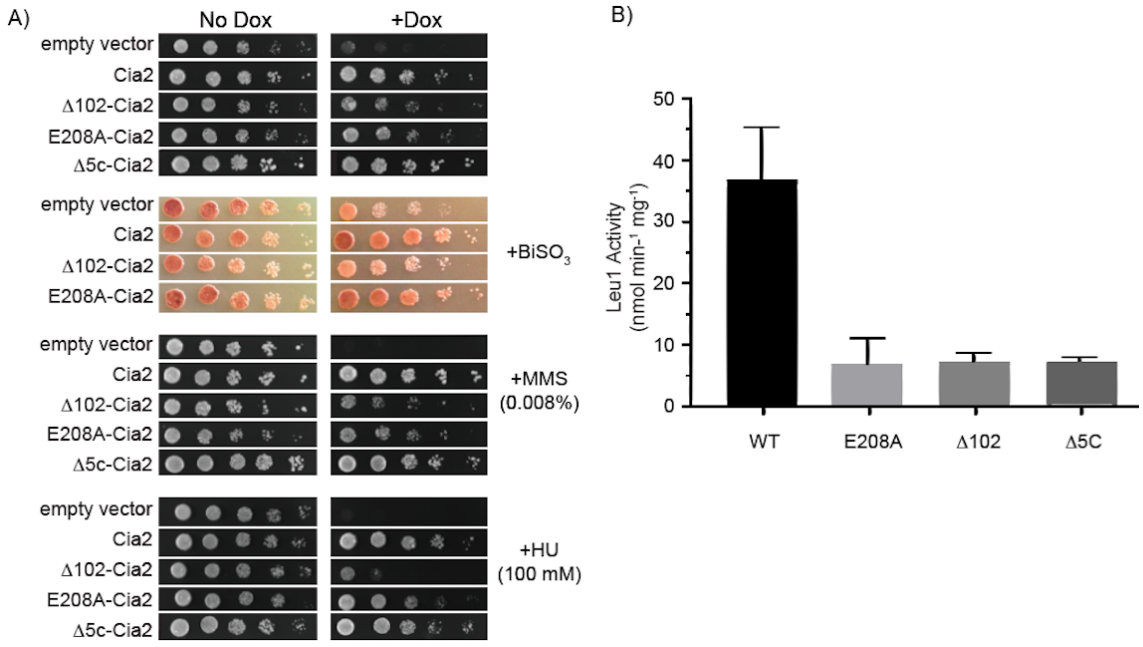

Figure 4.3 Assays to assess functionality of Cia2 mutants *in vivo*.
A) For the complementation analysis, the Tet-Cia2 strain was transformed with plasmids for expression of Cia2, either wt or mutant alleles under control of an *ADH* promoter, or the empty vector (EV) control as indicated. The inclusion of 50 µg/mL doxycycline (+Dox) represses expression of the genomic Cia2. Yeast were grown to mid-log phase in SD-Ura-His media and spotted on YPAD supplemented with additives as indicated. B) Leu1 activity in the soluble cell extract generated from Tet-Cia2 strain expressing the indicated Cia2 allele was compared. Yeast were grown to mid-log phase in the presence of DOX. The cells were collected, lysed and the soluble extract was assayed for Leu1 activity. The data shown represent the average ± the standard deviation of at least three independent determinations.

To probe the functionality of Δ102-Cia2 more deeply, we examined the activity of the FeS-dependent sulfite reductase by growing the complemented strains on media supplemented with bismuth sulfite. Active sulfite reductase results in formation of the brown Bi2S3 precipitate. As sulfite reductase is an FeS cluster protein, its activity can be linked to CIA function. Although the additives appeared to interfere with the DOX inhibition leading to slow growth of the empty vector control, we observed that the Δ102-Cia2 complemented strains were similar in color to the empty vector control on the plates containing doxycycline and lighter in color than the strain complemented with wt-Cia2

(Figure 4.3A, second panel). This suggested Δ102-Cia2 might have compromised functionality. To quantitatively assess target maturation, we compared the activity of the cytosolic FeS protein Leu1. We found a significant decrease in the Leu1 activity in extracts derived from the Δ102-Cia2 complemented strain as compared to the wild-type control (Figure 4.3B).

To also assess cluster targeting to nuclear FeS proteins, we examined the Δ102-Cia2 strain's sensitivity to the DNA damaging agent methyl methanesulfonate (MMS) and the DNA replication inhibitor hydroxyurea (HU).[2, 25, 42, 62, 103, 104] We observed diminished resistance to both reagents compared to the strain complemented with wt-Cia2 (Figure 4.3A, bottom panels). Western blotting revealed that both the full length and the truncated Cia2 are expressed (Figure S4). However, the expression level of Δ102-Cia2 appeared smaller than that of the full-length protein. Together, these results demonstrate that Δ102-Cia2 is sufficient to support cell viability but with a diminished ability to support CIA target maturation possibly due to lower stability of this construct *in vivo*.

4.3.3 Glu208 of Motif 5 is required for the Cia1-Cia2 interaction.

The C-terminal half of Cia2 comprises the DUF59 domain and ~40 additional amino acids which house Motif 5 (purple, Figure 4.1). Motif 5 is unique in eukaryotic DUF59 proteins suggesting it could be important for formation of the targeting complex.[40] In fact, an *in vivo* protein-protein interaction study previously found that Glu208 found within Motif 5 (red, Figure 4.1B) is important for the interaction between Met18 and Cia2.[66]

To pinpoint the function of Motif 5, we examined E208A-Cia2's interactions via affinity copurification. When wt-Cia2 or E208A-Cia2 was mixed with the ^{SUMO}Met18 bait, we were surprised to find similar amounts of the Cia2 prey in the elution fractions (Figure 4.2B). This unexpected result prompted us to examine the mutant protein's ability to bind to Cia1 and found that the E208A mutation disrupts the Cia1•Cia2 complex (Figure 4.2B). Consistent with Cia2's role as the bridge linking Met18 to Cia1 in the targeting complex,[25] we also found that E208A-Cia2 was able to tether less ^{SUMO}Met18 to the ^{His}Cia1 bait as compared to the wt-Cia2 control (Figure 4.2C). We concluded that E208A-Cia2 has a defect in its ability to bind Cia1, but has no observable defect in its ability to bind Met18.

Since this result is at variance with the conclusions of Lev *et al.*,[66] we additionally examined whether E208A-Cia2 could complement depletion of wt-Cia2 in the TET-Cia2 strain. In agreement with the previous study, E208A-Cia2 can support viability (Figure 4.3A). We additionally examined the sulfite reductase activity and the HU and MMS sensitivity of the E208A-Cia2 complemented strain. We observed little, if any effect, of the E208A mutation on the color of the colonies grown on bismuth sulfite media and a slightly increased sensitivity to HU and MMS compared to wt-Cia2 control (Figure 4.3A). The modest effects observed in the qualitative assays prompted us to quantitatively assess maturation of the Leu1. We observed the E208A mutation results in a 6-fold reduction in Leu1 activity (Figure 4.3B) while Western blotting revealed an expression level comparable to that of wt-Cia2 (Figure 4.4). All together our results are consistent with E208 being important for association with Cia1 and that destabilization of

the Cia1-Cia2 complex can negatively impact CIA function *in vivo.*

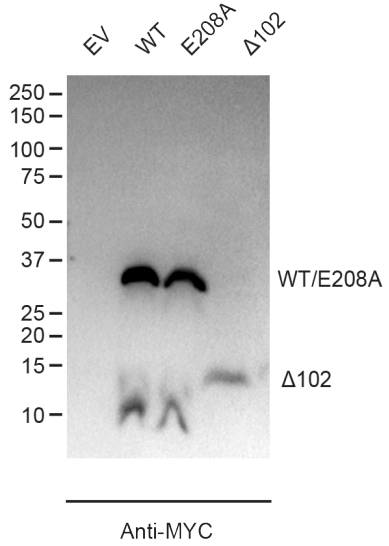

Figure 4.4. Anti-MYC Western of Cia2 constructs.
Anti-MYC Western of empty vector (EV), wild-type (WT), E208A, and Δ102 Cia2. WT and E208A have bands at around 37kDa, consistent with the SDS-PAGE weight for Cia2. Δ102 Cia2 contains a 15kDa band.

4.3.4 DUF59 motifs are essential for Cia2's function in vivo but are dispensable for its protein-protein interactions in vitro

The two remaining motifs, Motif 3 and 4, are found within Cia2's DUF59 domain. It was previously reported that mutation of C161 within Motif 4 results in a dominant negative phenotype, but not mutations of Motif 3 have been reported.[47] We mutated "DPE" sequence of Motif 3 to "NPQ" and examined how this mutation affects CIA function via the complementation assay. Although we could obtain transformants, the NPQ-Cia2 strain grew slowly in the absence of DOX and it failed to grow on plates supplemented with DOX (Figure 4.5). Since it was difficult to propagate the NPQ-Cia2 complemented strain due to the apparent growth inhibitory effect of this mutant allele, we could not assess its sensitivity to HU or MMS or its effect on Leu1 activity. However, on

plates supplemented with bismuth sulfite, we observed that the NPQ-Cia2 strain was significantly lighter in color as compared to the strain expressing wt-Cia2. We concluded that NPQ-Cia2 is a nonfunctional allele and has a growth inhibitory phenotype similar to that previously reported for the C161A allele.[47]

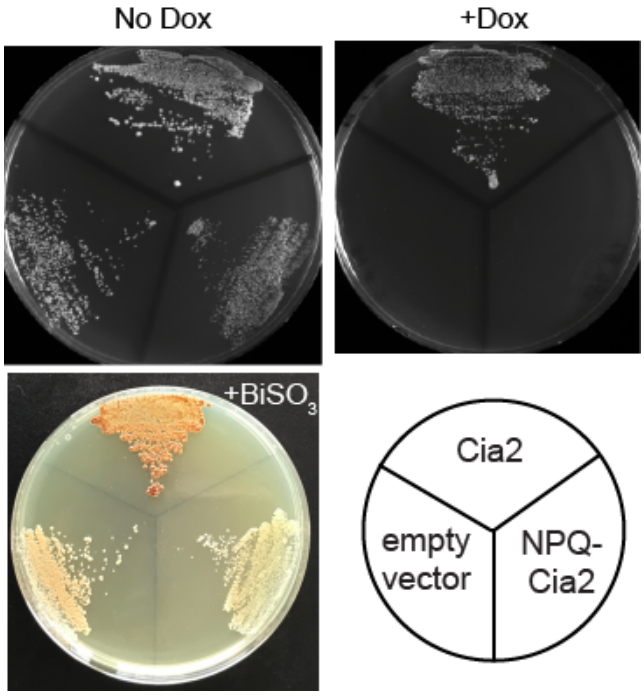

Figure 4.5. NPQ *in vivo* complementation
The Tet-Cia2 strain was transformed with plasmids for the indicated Cia2 allele grown in the presence or absence (left) of doxycycline or bismuth sulfite (bottom).

Next, we tested whether the residues of Motifs 3 or 4 were required for any of Cia2's protein-protein interactions *in vitro*. We reasoned that if the DUF59 domain is a privileged scaffold for association with apo-FeS proteins, this could explain the common function of this domain in cluster biogenesis. When we mixed the C161A-dtCia2 bait with SUMOMet18, HisCia1, and Rad3 prey proteins, we found all three prey proteins in the elution fraction (Figure 4.2D). We observed a similar result when the NPQ variant was used in the copurification assay (Figure 4.2E) or if Leu1 was used as the model apo-

target in place of Rad3 (Figure 4.2F). We concluded that neither DUF59 motif is vital for any of Cia2's interactions *in vitro*.

The only validated biochemical function of Cia2 is mediation of interactions essential for formation of the targeting complex and binding apo-targets. Therefore, it was surprising that mutation of the invariant residues of the DUF59 domain did not affect Cia2's interactions, especially given that mutation of the invariant residues within the DUF59 domain are nonfunctional *in vivo* (Figure 4.3).[43] This observation suggested to us that Cia2 might have an additional function in target maturation. In fact, we noticed during our bioinformatics analysis that the DUF59 domain (PFAM family PF01883) belongs to the same PFAM clan as the "NifU domain" (PFAM family PF01106).[105] NifU is a three-domain protein that serves as the FeS cluster scaffold for nitrogenase metallocofactor maturation.[106, 107] PF01106 corresponds to NifU's C-terminal domain and it is also found in Nfu FeS cluster carriers. These Nfu carriers bind a cluster at their homodimeric interface via a conserved CxxC motif (Figure 4.6A). A structural alignment of Arabidopsis Nfu (CnfU) and the human Cia2a paralog reveals these two domains share the same fold (Figure 4.6).[106, 108] The alignment in the Dali server returned a z value of 2.7, indicating a highly similar fold.[109] Moreover, the cysteine of the DUF59 domain (C161 of Cia2) aligns in three-dimensional space with the second cysteine in Nfu's cluster-ligating CxxC motif (Figure 4.6).

The structural similarity between Nfu carriers and DUF59 proteins and the conservation of one of the two cluster ligating ligands prompted us to examine whether Cia2 binds an FeS cluster. The UV-Vis spectra of some Cia2 preparations purified by

IMAC and performed by Eric Camire had absorption features in the low 400 nm region which were suggestive of [Fe2S2] or [Fe4S4] binding (not shown). However, the intensity of this feature was always significantly lower than one would expect for stoichiometric FeS cluster binding. Furthermore, the intensity of these features in the as isolated protein varied between different preparations of the same construct. We tried unsuccessfully to increases cluster loading in the as-isolated protein via several approaches including anaerobic expression and purification, expression in iron supplemented media, and by coexpression with ISC operon or with the other targeting complex subunits Met18 and Cia1. We also attempted to chemically reconstitute a cluster on the refolded Cia2 or the Cia1-Cia2 complex. However, Cia2's instability and propensity to precipitate during or immediately following chemical reconstitution prevented us from isolating and characterizing an FeS-bound form of the protein.

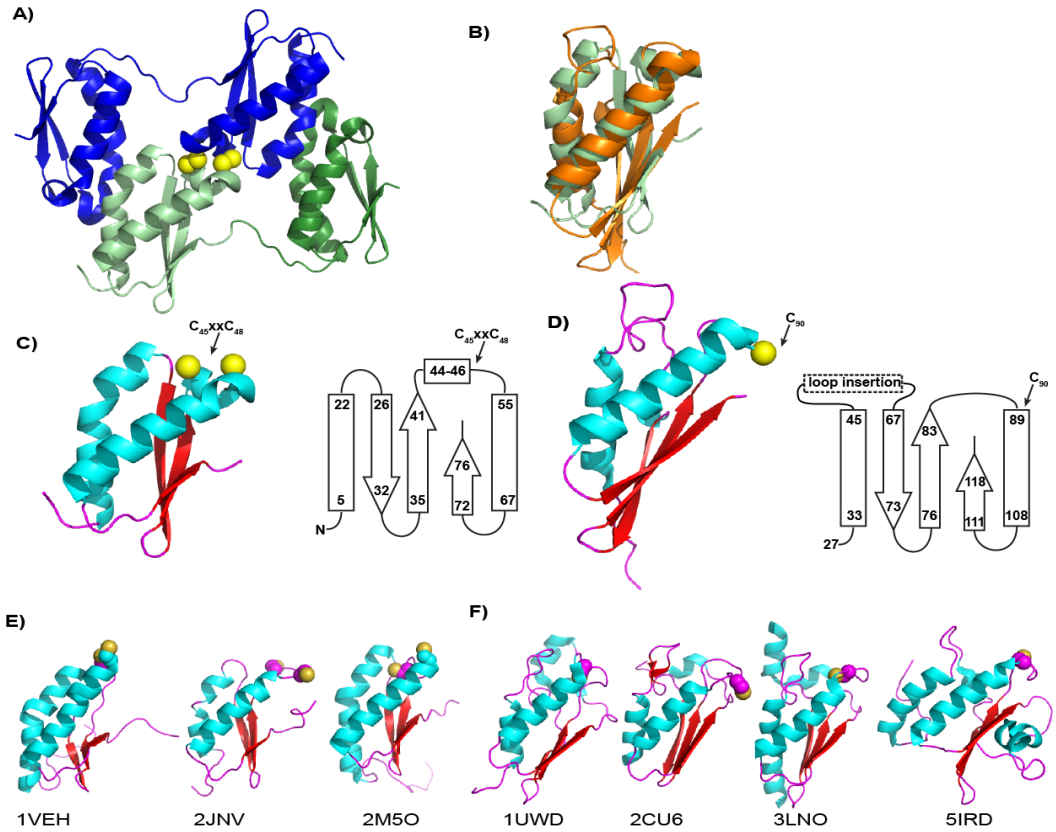

Figure 4.6. The structural similarity of NFU-domain proteins and DUF59 proteins.
A) The structure of arabidopsis CnfU iron sulfur cluster biosynthesis protein[110] (PDB 2Z51). The FeS-binding cysteines, two from each polypeptide, are yellow spheres. The two polypeptide chains are colored blue and green. Each CnfU polypeptide has two NifU domains, colored light and dark green in the green colored polypeptide, where the N-terminal NifU domain has the CxxC motif. B) The FeS binding domain of CnfU (light green in panel A) overlaid with human Cia2a[111] (2M5H, orange). C) The FeS binding domain of CnfU colored by secondary structure and secondary structure map. The location of the CxxC motif is indicated and cysteine sulfurs are yellow spheres. D) Cia2a DUF59 domain (residues 27-119) colored by secondary structure and its secondary structure map. The absolutely conserved cysteine of the DUF9 domain is shown as a yellow sphere. E) All of the known Nfu structures in the protein data bank including the mouse (1VEH), rice (2JNV), and human (5M5O) Nfu proteins. The cysteines of the CxxC motif is shown as spheres. F) All of the known Duf59 structures in the protein data bank including *T. maritima* (1UWD), *T. thermophiles* (2CU6), *B. anthracis* (3LNO), and *M. tuberculosis* (5IRD). The cysteine corresponding to the absolutely conserved cysteine of the DUF59 domain is shown as spheres.

4.3.5 Deletion of the last five amino acids produces no observable phenotype

We were surprised that none of the identified motifs were found to be vital for the Cia2-Met18 interaction. Since Gari and coworkers recently proposed that the last 5 amino

acids of Cia2 house the Met18 interaction site,[60] we tested whether their deletion also affects formation of the Met18-Cia2 complex *in vitro* or CIA functionality *in vivo*. Using our copurification assay, we assessed Δ5C-Cia2's interactions but we observed that it formed the CIA targeting complex with a similar efficiency as the wt-Cia2 control (Figure 4.2G). The Δ5C-Cia2 complemented strains were indistinguishable from wt-Cia2 complemented strains based on their ability to complement the DOX-induced growth defect or sensitivity to MMS and HU. However, the Leu1 activity in crude extracts was knocked down from that of the WT (Figure 4.3B). Because the C-terminal MYC tag was removed by our primer design, we were unable to check expression of Δ5C-Cia2. We concluded that the last 5 amino acids of Cia2 do not significantly contribute to its protein interactions *in vitro*, but further experiments will be needed to understand CIA function, specifically the knockdown in Leu1 activity, with the ability to complement the DOX-induced growth defect and no sensitivity to MMS or HU.

4.4 Discussion and Future Directions

Previous studies have shown Cia2 to be the center of the targeting complex, but little information is known about the biochemical function of this protein in the last step of cytosolic iron sulfur cluster assembly. To further understand its function, we began by identifying the conserved motifs of Cia2 and probing their roles through *in vitro* and *in vivo* assays. Upon sequence analysis, we saw that all eukaryotes shared at least one Cia2 homolog with an intrinsically disordered domain at the N-terminus (Figure 4.1). We hypothesized that this IDD might provide flexibility for promiscuous protein-protein

interactions, as this is a common function of this domain type.[101] However, we found that this domain is dispensable for Cia2's interaction with Met18, Cia1, and target Rad3 in our coaffinity purification assays. We also found that it is dispensable for its essential function *in vivo*, as this mutation was able to complement the DOX-induced growth defect and showed little sensitivity to MMS and HU. However, the knockdown in Leu1 activity and lack of brown color on the sulfite reductase activity plates indicates that CIA function is compromised.

The IDD does not appear to be involved directly with protein-protein interactions, but we cannot rule out its ability to bind to other targets aside from Rad3. A previous studied revealed that human Cia2a/Cia2b paralogs bind to different targets.[7] Cia2b, containing the IDD is responsible for binding to the CIA targeting complex and recognition of targets such as Rli1 and Rad3 in humans, while Cia2a can only bind to Cia1 and appears responsible for an iron related regulatory function, as it is associated with Iron Regulatory Protein-1 (IRP1).[7]

Another possibility is that this domain is required for a regulatory function such as a site for post-translational modification. A previous study highlighted that depletion of the human Cia2a/Cia2b paralogs, differentially affects iron homeostasis.[7] Additionally, it was recently reported that Cia2b appears to be the key factor for regulation of CIA by its degradation in the absence of Met18.[60] Expression levels of the Δ102 Cia2 appear lower than the wild-type, indicating that this N-terminal domain may have a regulatory function. This role can now be further explored, as we know that the IDD is not responsible for protein-protein interactions with other CIA components or the target

Rad3.

After examining the N-terminal domain, we were interested in identifying the interfaces on Cia2 that interact with Cia1 and Met18 for formation of the targeting complex. We investigated first the E208 residue on Cia2 as previous *in vivo* studies have reported the E208G disrupts Cia2's interaction with Met18.[66] This E208 is located in motif 5 with a patch of charged amino acids (Figure 4.1). Surprisingly, our findings showed from our *in vitro* studies that the E208A mutant disrupts the interaction with Cia1, but not with Met18 (Figure 4.2B). Additionally, recent experiments in the Perlstein lab have identified the adjacent K207 and D206 (Marquez, M., Esonwune, S., *unpublished*, not shown). These experiments provide additional evidence that this motif is the binding site for Cia1.

There are several possibilities for why we might have observed the disruption of the Cia1interaction with the E208A Cia2 mutant, while Lev *et al*. observed a disruption in the interaction with Met18.[40, 66] It can be challenging to distinguish direct effects from indirect effects with *in vivo* protein interaction assays like the protein complementation approach employed by Lev *et al*. These authors also reported that depletion of Cia1 diminished the Met18-Cia2 interaction.[112] Several studies have noted that depletion or overexpression of one targeting complex subunit can affect the concentrations of the other subunits, which could indirectly affect the amount of complex observed in co-IPs from extracts.[25, 51, 60] We think it is likely the E208G mutation destabilizes the Cia1-Cia2 complex, which in turn affected in the amount of Met18-Cia2 complex detected via protein complementation.

We also employed *in vivo* assays to identify this mutant's effect on CIA functions. Our *in vitro* assay identified the Cia1-Cia2 binding site on Cia2, however our *in vivo* assays showed that this mutation is viable, with little HU and MMS sensitivity. The sulfite reductase activity shows color similar to that of the wild-type, while Leu1 activity is knocked down (Figure 4.3). We suggest the mild effect in phenotypes is due to the ability of Cia2 to still form the ternary targeting complex, despite the destabilization of the Cia1-Cia2 interaction. However, the knock down in Leu1 activity does indicate that the E208A mutation impairs CIA function.

Now that we had identified the binding site of Cia1, we decided to explore residues that are critical for Met18 binding. We investigated the last 5 amino acids of Cia2 as Gari *et al.* proposed this to be the binding site to Met18.[60] Our *in vitro* assays showed that Δ5C formed the CIA targeting complex with a similar efficiency as the wt-Cia2 control (Figure 4.2G) and that this mutation was able to complement the DOX-induced growth defect and showed little sensitivity to MMS and HU (Figure 4.3A). However, we observed a knock down in Leu1 activity for the Δ5C-Cia2 extract, which was unexpected as it had mild phenotypes and bound to Met18 and formed the targeting complex (Figure 4.3B). One explanation is that *in vivo* expression for this mutation low, resulting in an overall lower Leu1 activity. Indeed, in the Gari studies, expression of this mutation in Co-IP studies appeared lower than that of the wild-type.[60] Another possibility is that the C-terminal end may contribute to target binding, which seems unlikely due to its proximity to the Cia1 binding site on Cia2. A construct was designed to add back the C-terminal MYC tag on the Δ5C mutation so that expression levels can

be assessed along with sulfite reductase activity (Appendix) for a more thorough investigation of this mutation. Overall, we have determined that the Δ5C is still able to bind to other CIA components, and the last five amino acids are not required for Met18 binding.

We also investigated conserved residues in Motifs 3 and 4, which surprisingly did not disrupt Cia2's interaction with Cia1, Met18, or Rad3 (Figure 4.2D and 4.2E). Motif 3 results in a dominant negative phenotype similar to that reported for the C161 reactive cysteine in Motif 4 (Figure 4.5).[47] This demonstrates that these mutants compete with wt-Cia2 and create a nonfunctional CIA targeting complex that cannot be recovered by the presence of wt-Cia2. There is a possibility that these regions could be involved in binding to another interaction partner not tested, such as other targets. However, the dominant negative phenotype is extreme compared to the E208A mutation, which disrupted Cia1-Cia2 binding (Figure 4.5).

One possibility is that Cia2 is directly a cluster carrier. Previous studies show functional overlap between a DUF59 domain protein SufT and Nfu in bacteria.[43] Additionally, our alignment with the DUF59 domain of an Nfu carrier (PDB 2Z51) and the DUF59 domain of Cia2 (2M5H) demonstrates that the C161 conserved cysteine aligns with the cluster-binding residue of the Nfu carriers (Figure 4.6).[110, 113] This structural alignment is a good fit as the Dali server returned a z value of 2.7.[109] Although Cia2 contains a single cysteine, the structures for the human homologues demonstrate the formation of Cia2 dimers or higher order oligomers and we saw from Chapter 2 studies that Cia2 exists as a tetramer in the targeting complex.[40, 48] Additionally, dimeric

monothiol glutaredoxins can ligate to an FeS cluster by a single cysteine, which provides a precedent for this type of ligation.[114]

Although the bioinformatic and genetic evidence suggest Cia2 is a cluster carrier, we have been unable to successfully reconstitute FeS bound Cia2. This observation could be due to the fact that the cluster may be unstable or require another substrate to stabilize the cluster. This supports the other model that Cia2 is not a direct FeS donor or carrier, but may contribute in interacting with the nascent FeS cluster perhaps transferred from Nar1.

Our *in vitro* and *in vivo* studies on the defined conserved motifs of Cia2 allowed us to identify the key E208 residue for Cia1 binding and analyze other conserved motifs for binding to the CIA components. We have also highlighted the importance of motif 3 and 4, which are not required for binding to CIA components, but are vital CIA function *in vivo*. The ability to assemble the targeting complex with Cia2 mutants for *in vitro* analysis and compare this binding to *in vivo* functions is a vital first step toward defining the function of Cia2 and its role in FeS biogenesis.

CHAPTER FIVE: Understanding the role of Met18 in the CIA Pathway

5.1 Introduction

In the previous chapters, we investigated the conserved residues of Cia2 and identified the E208 residue as part of the Cia1 binding site on Cia2.[40] We have also established that Met18 binds to Cia2, forming a stable subcomplex that can recognize the helicase target Rad3.[61] In this chapter, we probe the residues on Met18 that are responsible for Cia2 and Rad3 binding, develop *in vivo* methods to assess CIA function of these residues, and optimize an approach to identify the binding interface of the Cia2-Met18 subcomplex. Identifying these interfaces and probing their functionality *in vivo*, will allow for understanding of how the targeting complex forms and recognizes targets for FeS cluster insertion.

Met18 contains HEAT repeat domains. The HEAT (Huntingtin, Elongation factor 3, protein phosphatase 2A, TOR1) domain is a di-helical domain that is separated by a non-helical loop region.[54-56] Other HEAT repeat proteins appear to bind protein substrates. For example, the Cullin family of E3 ligases, are involved in docking large protein substrates for ubiquitinylation and structural maintenance proteins (SMPs), which play a role in chromosome packaging by binding to other proteins.[57-59] HEAT proteins typically bind to other protein substrates via their loop regions.[115] Previous studies also indicate that the N-term and the C-term HEAT repeat domains of Met18 are essential for protein-protein interactions.[21, 22]

Two labs have investigated the conserved portions of human Met18 (MMS19) and their role in binding to CIA factors and targets using co-IP and siRNA studies

(Figure 5.1).[25, 26, 60, 61, 68] Van Wietmarschen *et al.* made two constructs, an ΔAB construct in which the N-terminal portion of Met18 was deleted (1-284, containing 3 HEAT repeats) and a ΔC construct in which the C-terminal portion of Met18 (731-1032, containing 4 HEAT repeats) was deleted (Figure 5.1, red-brown box).[26, 67, 116] These constructs were based on the results of a previous study, which identified the A, B, and C domains as having distinct functions for nucleotide excision repair and transcription.[68] Van Wietmarschen *et al.* reported via co-IP that ΔAB retained interaction with Cia1, Rad3, and other human FeS proteins RTEL1 and MUTHY (absent in yeast), whereas ΔC can only interact with Cia1.[26]

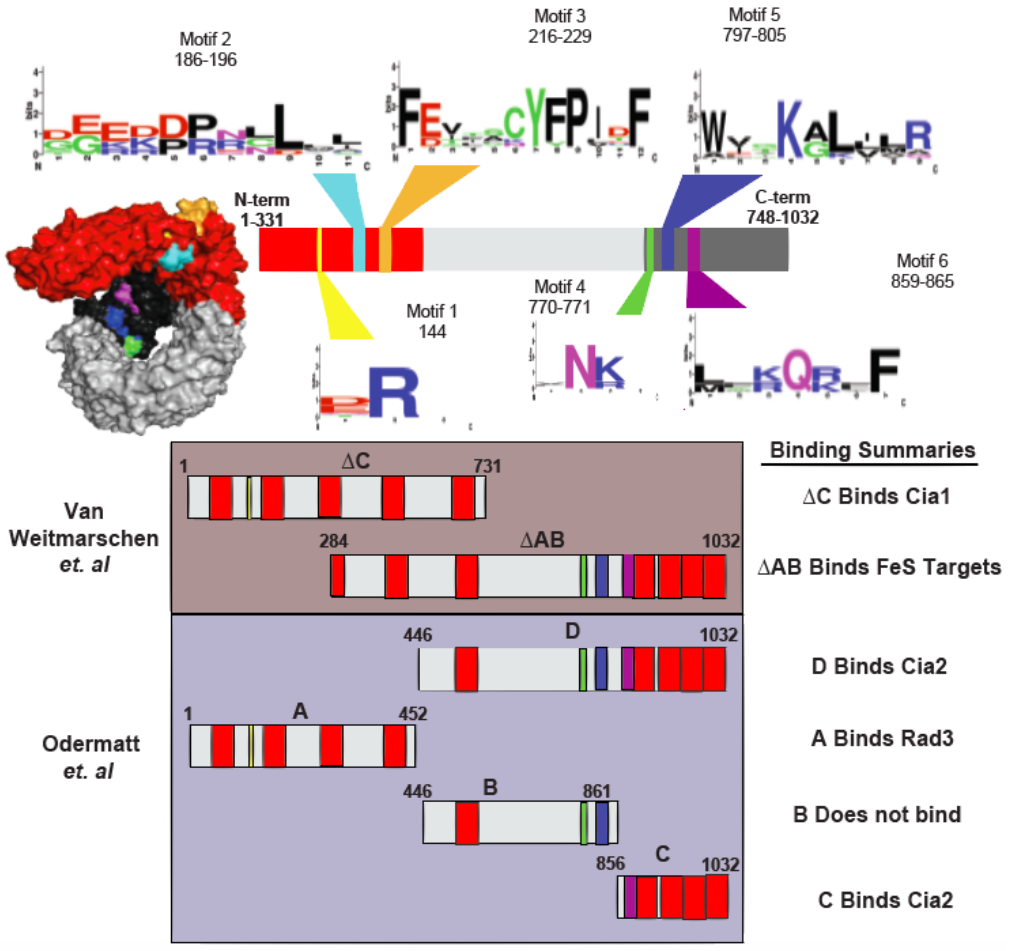

Figure 5.1. Met18 conserved residues.
Surface representation of Met18 (Threading model I-TASSER) with Motifs 1, 2, 3. 4, 5, and 6 colored in yellow, cyan, orange, green, blue, and purple, respectively. A sequence alignment generated by Clustal Omega identified conserved residues, which are then represented by Weblogo. The N-terminal construct is colored in red, and the C-terminal construct is colored in dark grey. In the purple box are the A, B, C and D constructs made by Odermatt *et al.*, with the HEAT repeat domains shown in red. The brown-red box shows the ΔAB and ΔC constructs made by Wietmarschen *et al*. The residues in all experiments with the human MMS19, were converted to represent the homologous yeast Met18 amino acid residues by a sequence alignment generated by Clustal Omega.

Odermatt *et al.* investigated four truncated Met18 constructs: A(1-452), B(446-861), C(856-1032), and D(446-1032) (Figure 5.1, purple box). They observed C-terminal constructs were able to bind to Cia2 and Cia1, as well as Pol3 and another FeS protein RTEL1 (not present in yeast) (Figure 5.1).[60] The N-terminal Met18 constructs (A and B)

were not able to bind to Cia2, Pol3, or RTELI, but were able to bind to Rad3. These results were conflicting with van Wietmarschen *et al.,* as this lab identified the C-terminal construct (ΔAB) as the binding site for Rad3 and the N-terminal construct (ΔC) as the binding site for Cia1.[26] The residues in all experiments with the human MMS19, were converted to represent the homologous yeast Met18 amino acid residues by a sequence alignment generated by Clustal Omega.[67]

Herein, we investigate the C-terminal (748-1032) and N-terminal (1-331) domains of Met18 *in vivo* to assess their impact on CIA function. We also probe the contribution of specific amino acid residues in motif 1 (R144), motif 4 (770-771), motif 5 (797-805), and motif 6 (859-865) in Cia2 binding. Additionally, their *in vivo* functionality is assessed through our developed methionine biosynthesis and Leu1 activity assays (Figure 5.2). Overall, we find that the N-terminal R144 is required for Rad3 binding and the C-terminal motifs are required for Cia2 binding. We investigate the Met18-Cia2 binding interface by crosslinking, proteolysis, and mass spectroscopy to pinpoint the specific Met18 interface required to bind to Cia2. Eventually, we will utilize this method to map how the Rad3 N-terminal domain binds to Met18-Cia2. Mapping the binding interface on Met18 will allow for identification residues responsible for Cia2 binding and Rad3 recognition. Pinpointing these binding interfaces will allow for understanding of how FeS proteins are recognized by the CIA pathway and insight on how the CIA targeting complex associates to recognize these proteins.

5.2 Materials and Methods

5.2.1 Complementation Assays

For the complementation experiment, a Met18 deletion (ΔMet18) strain (TH_12287; a BY4742 strain with the genotype MATalpha his3-1 leu2-0 lys2-0 ura3-0 *met18Δ::KanMX*) was obtained from GE Dharmacon.[117] In this strain, *MET18* is deleted and replaced with a KanMX cassette, making the strain G418 resistant. The *MET18* or *met18* mutations (N-term, C-term, M4, M5, or M6) were inserted into the pRS316 vector via Gibson Assembly (Appendices 1 and 2). This vector contains an *URA3* selection marker. Additionally, the plasmid contains an HA epitope tag that will be placed in frame with the Met18 gene to be on its C-terminus. The full length Met18, Met18 mutations, or the empty vector control were transformed into the TH_12287 strain and selected on SC –Ura +G418 plates (200μg/mL). For complementation analysis, log-phase cultures were serially diluted and applied to SC –Ura, +G418 in the presence or absence of Met.

5.2.2 Leu1 Activity Assays in vivo

The *MET18* deletion strain (TH_12287) transformed with plasmids *MET18-HA* or its mutant alleles.The resulting transformants were grown overnight in SC–Ura–+G418 in a 5 mL culture. The culture diluted into YPAD supplemented with G418 to an optimal density with an absorbance of 0.3 at 600 nm (OD600 of 0.3), and grown to mid-log phase (OD600 of 1.0)at 30 ˚C. Crude extracts were generated in an anaerobic chamber and Leu1 assays were carried out as described in Chapter 4.

5.2.3 Co-affinity Purification

The plasmid construction for the Met18 constructs heterologously expressed in *E. coli*, along with expression and purification of proteins can be found in the Appendix. The co-affinity purification method was carried out as detailed in Chapter 2 in 2.2.1.

5.2.4 Western Blotting for Met18 expression

The extracts were also run on a 10% SDS-PAGE gel and transferred onto a PVDF membrane at 100V for one hour on ice in an optimized buffer containing 25 mM Tris, 192 mM glycine, 10% methanol, and 0.1% SDS. The membrane was blocked for one hour at room temperature with 5% (w/v) non-fat dry milk in TBST (50 mM Tris pH 7.6, 150 mM NaCl, 0.1% Tween-20) and washed with TBST. The blot was then incubated with a 1:1000 dilution of HA antibody (Cell Signaling Technology) for one hour at room temperature and washed again with TBST. The blot was incubated with a 1:1000 secondary antibody, an HRP-linked mouse antibody for one hour at room temperature. After incubation, the blot was washed with TBST and the ECL imaging kit (Thermo Fisher) was used to image Met18 expression.

5.2.5 DSS and DC4 Crosslinking

Samples were buffer exchanged by a PD10 column into a phosphate buffer (50 mM Na_2HPO_4, 100 mM $NaCl_2$, 5% (v/v) glycerol, 5 mM BME, pH 8) to remove any cross-reactive amines from the original Tris buffer. A disuccinimidyl suberate (DSS) stock was made at 25 mM in DMSO. A 25-fold molar excess of DSS was added to a mixture that contained 15 μM of each protein (Cia2 and Met18) in about a 100 μL

sample. The DSS was incubated with the protein mixture for 30 minutes and then the reaction was quenched with a Tris buffer (50 mM final concentration). A 10 mM DC4 stock solution was made in DMSO. A 25-, 50-, and 100-fold molar excess of DC4 was added to a mixture that contained 15 μM of each protein (Cia2 and Met18) in about a 100 μL sample. The DC4 reactions were incubated and quenched in the same way as described above for DSS and stored at -80 ˚C.

5.2.6 Mass Spectroscopy Sample Preparation

The DSS cross-linked sample (about a 100 μL sample) was injected onto a Superdex 200 Increase 10/300 GL column (GE healthcare) and eluted with 20 mM Tris, 100 mM NaCl, and 5% (v/v) glycerol at a flow rate of 0.5 mL min^{-1}. Fractions (1mL each) were collected and analyzed by SDS-PAGE. The following steps were performed in a clean room in which buffers were filtered as keratin can contaminate peptide samples. Tips, gloves, and other consumables were stored in special containers away from contaminating dust particles. The fraction containing the desired crosslinked band was then collected. DTT (10 mM final) and 2 M ammonium bicarbonate (300 mM final) were added to the DSS and DC4 cross-linked samples. The samples were incubated for 1 hour at 50 ˚C. The samples were then cooled to room temperature and alkylated by adding 200 mM stock of iodoactamide (20 mM final) and incubating for one hour at 37 ˚C in the dark. The alkylation reaction was quenched with DTT (10 mM final).

Samples for use in gel digestion of the DC4- and DSS-treated samples were also prepared. Each sample (37.5 μL) was mixed with 12.5 μL of 4x dye (Bio-rad) for a final volume of 50 μL. The samples were loaded onto a 4-12% gradient SDS-PAGE gel,

subjected to electrophoresis, and the gel bands around 250 kDa were excised with a clean razor. The gel bands were cut into small cubes about 1 mm thick. The gel cuts were washed with a 50:50 mix of acetonitrile and 100 mM ammonium bicarbonate to remove the Coomassie stain. The gel cuts were then reduced and alkylated as described above. Following alkylation, the gel samples were washed with 100 mM ammonium bicarbonate by incubating the gel samples with the solution for 10 minutes. The supernatant was removed, followed by a wash with acetonitrile in the same way. The ammonium bicarbonate and acetonitrile wishes were repeated 3 times, the supernatant was removed, and then the gel pieces were dried for 10 minutes in the speedvac at 60˚C.

Trypsin Gold (Promega, Catalog number V5280) was resuspended in 50mM acetic acid to make a stock solution with a final concentration of 200 ng/ µL. The stock solution was aliquoted out into 10 µL aliquots. Trypsin was added to the cross-linked samples. In the final mixture the proteins were in 50 fold molar excess to the trypsin. Ammonium bicarbonate (100 mM from a 2M stock solution) was added to the samples to neutralize the samples and activate the trypsin. The samples were digested overnight (16h) at 37 ˚C. After the incubation, TFA was added at a final 0.5% (v/v).

The MS interfering small molecule contaminants in the DSS in solution sample and gel samples were removed using 100 µL C18 tips, while the DC4 sample was cleaned on a 500 µL C18 cartridge (Thermo Fisher). The tips or cartridges were wetted three times with 1 CV of a 50% (v/v) of acetonitrile and then equilibrated with 1 CV of 0.1% (v/v) TFA solution three times. The sample was loaded on 1 CV at a time. The tips were then washed with 1 CV of a 0.1% (v/v) TFA and 5% (v/v) acetonitrile solution three

times. All samples were eluted in 100 μL with a 0.1% (v/v) TFA and 65% (v/v) acetonitrile. In collaboration with the Costello lab, Boston University School of Medicine, Deborah Francoleon collected the data for the masses of the fragmented peptides on the Q Exactive HF Hybrid Quadrupole Orbitrap MS (Thermo Fisher). A programming script, developed by Christian Heckendorf, analyzed the peaks and selected possible precursor masses of peptide pairs based off of the sequences of Met18 and Cia2 and the mass of the crosslinker. These peptide pairs were then compared to a database generated in MASCOT to confirm the identity of the peptide sequences. To validate the peptide pairs, the raw MS^2 data were analyzed for the monoisotopic masses of each amino acid fragment.

5.3 Results

5.3.1 Identification of conserved Met18 motifs

Our approach was to identify conserved residues on the surface of Met18. Next, these residues could then be mutated to alanines. The binding of these variants to Cia2 and Rad3 could be investigated by co-affinity purification assays. Lastly, we would explore the ability of these variants to support CIA function in vivo. First, a Clustal Omega alignment with 10 eukaryotic organisms was performed to identify conserved residues. This alignment revealed that within the C-terminal portion, there were strings of conserved amino acid motifs: motif 4 (M4, residues 770-771), motif 5 (M5, residues 797-805), and motif 6 (M6, residues 859-865).[67] The N-terminal region contained three conserved motifs: motif 1(M1, a highly conserved R144), motif 2 (M2, residues 186-196), and motif 3 (M3, 216-229) (Figure 5.1). These motifs were consistent with studies

from previous labs that had identified the C-terminal region and the N-terminal region as the most conserved.[26, 60, 68, 104] Therefore, we divided the protein into two segments, the N-terminal region (1-331) and the C-terminal region (748-1032) (Figure 5.1).

Next, as there is no three-dimensional structure for this protein, a Jpred secondary prediction server was utilized to ensure the protein was not cut in the middle of a helix.[118] Additionally, a homology model of Met18 generated by ITASSER, which revealed that these conserved amino acid residues were present on the surface (similar results were obtained by generating a homology model using Phyre2, which enhanced our confidence in the model) (Figure 5.1).[119, 120] For our truncations, the homology models confirmed that we were cutting at connecting loops or regions of low sequence conservation. The other motifs containing conserved amino acids were alanine-scanned. However, motif 2 and motif 3 were rather large motifs (greater than eight amino acids), and were not the focus of the alanine scans.

5.3.2 Met18 N-terminally binds Rad3 and C-terminally binds Cia2

In collaboration with Claudia Lee, we were able to express and purify N-terminal region of $Met18^{N}$ (1-331) . The N-terminus of Met18 was not able to bind to Cia2 via co-affinity purification (Figure 5.2A). These data are consistent with that of Odermatt *et al.* that the C-terminal end of Met18 is responsible for the interaction with Cia2 (Figure 5.2A, Claudia Lee).[60] These results also suggested that the N-term was required for Rad3 binding. To investigate this, we mutated a conserved arginine in the N-terminus, R144 to an alanine. By co-affinity purification, binding to Rad3 was disrupted, but the R144A mutant maintained its binding interaction with Cia2 (Figure 5.2B, Claudia Lee). These

results suggest that R144 is required for binding to targets, specifically Rad3.

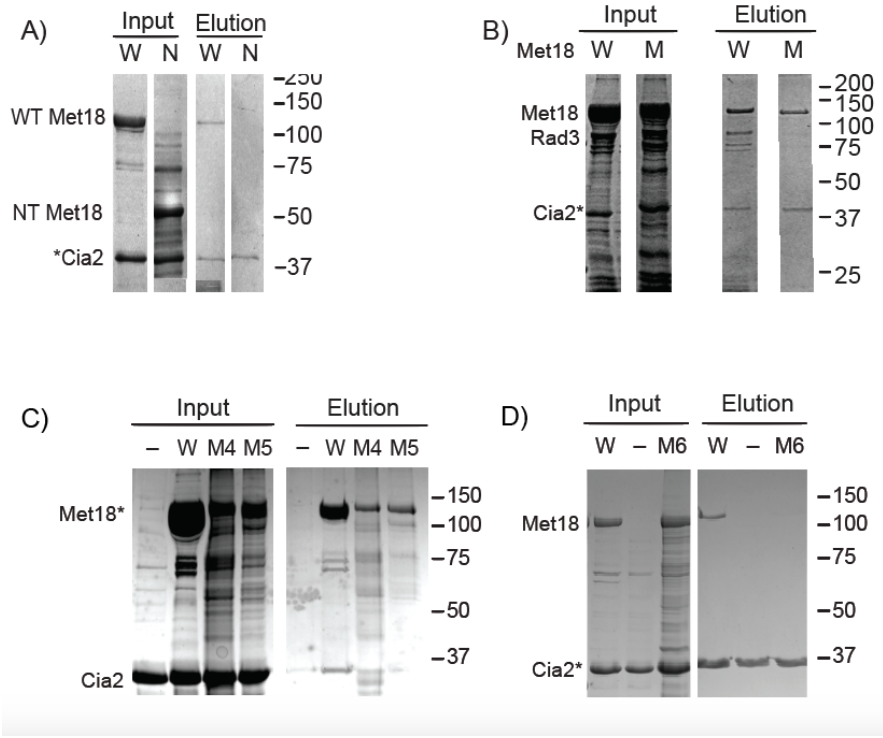

Figure 5.2. Determining Met18 variants ability to binding to Cia2 and Rad3
SDS-PAGE analysis of affinity copurification experiments to determine Met18 to Cia2 and Rad3. A) ^{SUMO}Met18 (WT Met18) or NT Met18 (N-terminal Met18 1-331) and ^{DT}Cia2 were mixed (input) and separated via streptactin resin. ^{DT}Cia2 can specifically retain ^{SUMO}Met18, but not NT Met18 (elution). B) ^{DT}Cia2 and Met18 (W, wild-type or M, mutant R144A) were mixed (input) and separated via streptactin resin. ^{DT}Cia2 can specifically retain W Met18 (W, wild-type) with Rad3, but Rad3 is not retained with ^{DT}Cia2 with M Met18 (M, mutant R144A) . C) ^{SUMO}Met18 (W (wild-type), M4 (Motif 4), or M5 (Motif)) and Cia2 were mixed (input) and separated via IMAC. Cia2 can only be detected copurifying with the ^{SUMO}Met18 W (wild-type) bait. No bands are detected in the control in which ^{SUMO}Met18 was omitted (Lane 5). D) ^{DT}Cia2 and Met18 W (wild-type) or Met18 M6 (Motif 6) were mixed and chromatographed on streptactin resin. Only Met18 W (wild-type) is retained by ^{DT}Cia2(Lane 4) whereas no bands are detected in the control in which ^{DT}Cia1 was omitted (Lane 5). Molecular weight standards in kDa are shown to the right of all the gels.

To probe the function of the C-terminal region of Met18, we investigated the C-terminal domain truncation of Met18. However, we were unable to purify this construct due to lack of expression in *E. coli* cells. Instead, we looked at the ability of the motifs bearing alanine replacements to bind Cia2 via coaffinity purification assays. We

predicted that if a variant was responsible for the Met18 interaction with Cia2, we would see a disruption in binding with Cia2 for that variant. These alanine-scanned variants expressed in inclusion bodies and were refolded. However, a CD scan of these variants showed they maintained their alpha helical structure (Appendix 2.3). Interestingly, all three motifs, M4, M5, and M6 were unable to bind to Cia2 by our co-affinity purification assay (Figure 5.2CD). This suggests that all of these motifs contain amino-acid residues required for Cia2 binding. Overall, these findings support the model that the C-terminal segment of Met18 is essential for binding to the CIA components.

5.3.3 Development of a complementation assay for Met18

Development of an in vivo assay for Met18 is required to test how these variants affect CIA function. In the previous chapter, we utilized an assay to assess Cia2 functionality via viability screen since Cia2 is an essential protein.[40] However, Met18 unlike the other CIA targeting components is not an essential protein. A different approach is required to assess the in vivo functionality of Met18 mutations compared to wild-type Met18. Although Met18 is nonessential, defects in the protein have shown a variety of phenotypes, such as defects in methionine biosynthesis, methyl methanesulfonate sensitivity, and increased length of telomeres.[22, 49-52] We reasoned we could exploit one of these phenotypes to develop an in vivo screen to assess Met18 mutations, specifically mutant defects in methionine biosynthesis.

Met18 was identified as a protein required for methionine biosynthesis. Mutations in this protein have resulted in impaired sulfite reductase activity as well as methionine auxotrophy, which is what lead to the discovery of this protein and its name.[121] To

develop our assay, we obtained a commercially available Met18 deletion (ΔMet18) strain. In this strain, genomic Met18 ORF is deleted and replaced with a KanMX4 cassette. The KanMX4 cassette gives this strain G418 resistance. This strain, obtained from GE Dharmacon, had the genotype MATalpha his3-1 leu2-0 lys2-0 ura3-0 Kan^R-ΔMET18)[117]. A yeast shuttle vector pRS316 that harbored a URA3 marker was utilized to select for the vector in ΔMet18 strain. We transformed this yeast shuttle vector pRS316 containing wild-type (WT) Met18 with an HA tag into the ΔMet18 strain, as well as an empty vector (EV) control with no Met18 gene inserted to use as controls.

To test the functionality of our assay, we plated the ΔMet18 strain, EV, and WT Met18 on SC-Ura plates with and without methionine. For this assay to be successful, nonfunctional Met18 must not be able to complement the loss of wild-type. From our plating assays, we observed that EV, and WT Met18 both grow on the SD-Ura plates, while the ΔMet18 strain does not. This indicates that the URA selective marker is working for the EV and WT Met18 and that these strains are able to grow on plates containing methionine. For the plates that did not contain uracil or methionine, we observed that EV and the ΔMet18 strain did not grow, but the WT Met18 did (Figure 5.3A). This demonstrates that the WT Met18 complements the lack of this nutrient, while the EV containing no Met18 gene is not viable. We concluded that this assay allowed us to assess the in vivo functionality of Met18 as the deletion of this protein clearly produced dependence on methionine for growth.

To assess the mutants with our new in vivo assay we transformed N-terminal (1-331), C-terminal (748-1032), M4, M5, and M6 mutations in the pRS316 plasmid into the

ΔMet18 strain. When spotted on the plates without methionine, the N-terminal and C-terminal Met18 were not viable (Figure 5.3B). However, the M4, M5, and M6 mutations grew on the plates without methionine. A Western blot for the HA tag on the Met18 constructs was required to confirm that the proteins were expressing. The anti HA blot revealed that M4, M5, and M6 were expressed (Figure 5.3C), while the N-terminal and C-terminal Met18 constructs did not (not shown). This assay allows assessment of the in vivo functionality of Met18 mutations and revealed that, although M4, M5, and M6 were required, as shown by in vitro assays for Cia2 binding, strains bearing these mutations are still functional in vivo in conditions dependent upon CIA function. The development of this assay allows for assessment of the Met18 mutations in the context of the cell.

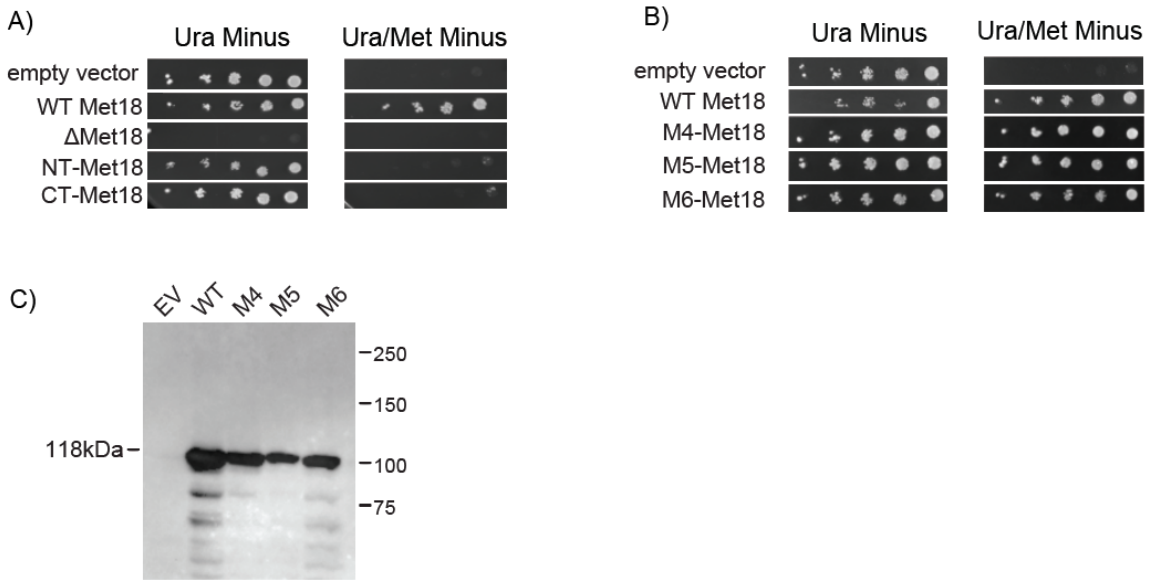

Figure 5.3 Development of a complementation assay.
A) For the complementation analysis, the ΔMet18 strain was transformed with plasmids for expression of Met18, either wt or mutant alleles under control of an *ADH* promoter, or the empty vector (EV) control as indicated. The absence of methionine causes death in those cells with no functional Met18. Yeast were grown to mid-log phase in SD-Ura media and spotted on SC plates supplemented with additives as indicated. The N-term (1-331, NT) and C-term (748-1032, CT) also did not grow on the plates without methionine (Met minus). B) The M4 (Motif 4, 770-771), M5 (Motif 5,797-805), and M6 (Motif 6 859-865) grew on the plates without methionine (Met minus).

5.3.4 Quantitative assessment of in vivo functionality of the Met18 mutations by Leu1 activity assays

Although the development of the *in vivo* Met18 screen allowed for assessment of the mutations *in vivo*, this assay has limitations. Cells can still be viable yet have compromised CIA activity. For example, the Walden lab observed yeast growth for mutations in Cfd1 in the CIA scaffold in which the CIA function measured via IRP1 aconitase activity was severely compromised.[122] The Leu1 activity of the cells with these mutations was knocked down by ~90% compared to wild-type, yet the cells were still

able to grow.[122] The methionine assays did not report on the extent by which CIA is compromised, but this quantitative assay for CIA function is helpful in discriminating between fully functionally and partially functional alleles.

To quantitatively assess the CIA function of our mutations, we turned to Leu1 assays. In Chapter 4, we had utilized this assay to investigate CIA function for TET-regulated Cia2.[40] However, to apply this approach to Met18 mutations, it is important to ensure that the ΔMet18 strain had little to no background Leu1 activity. If the Leu1 activity of the ΔMet18 strain is high, assessing the functionality of the mutations by loss of activity would be difficult. When we investigated the Leu1 activity of the ΔMet18 strain and a strain with WT Met18 we saw that ΔMet18 strain contained no measurable Leu1 activity compared to WT BY4741 cells, which contained an activity of 147 ± 15 nmol IPM/min/mg extract. Despite a similar protein concentration for the ΔMet18 strain extract to the wild-type protein extract, we were not able to detect any activity for the ΔMet18 strain (Figure 5.4A).

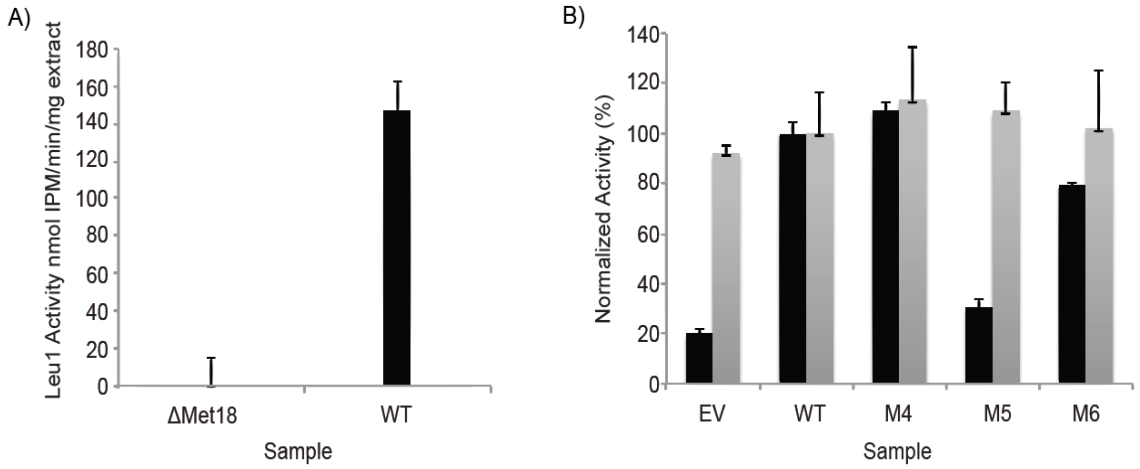

Figure 5.4 Leu1 activity assays for the yeast extract of the Met18 constructs.
Yeast were grown to mid-log phase in SD-Ura media. The cells were collected, lysed and the soluble extract was assayed for Leu1 activity. A) The empty ΔMet18 strain contained no activity compared to the WT Met18 strain extract (BY4741) which showed an average activity of 147 ± 15 nmol IPM/min/mg extract. B) The ΔMet18 strain was transformed with plasmids for expression of Met18, either wt or the mutant alleles M4 (Motif 4, 770-771), M5 (Motif 5,797-805), and M6 (Motif 6, 859-865) under control of an *ADH* promoter, or the empty vector (EV) control as indicated and the extract was assayed for Leu1 activity (black bars) as before. ADH activity (gray bars) was assessed for all constructs as a control to show all the constructs were treated the in the same manner.

Next, we exploited this assay to interrogate the CIA function of Met18 mutations. The Motif 5 mutant was significantly decreased compared to wild-type, with 70%±3.4% less activity than that of wild-type. The Motif 6 mutant had a small decrease in activity (20%±0.5%) (Figure 5.4). The Motif 4 mutant had similar Leu1 activity to wild-type, indicating that this motif is not important for CIA function *in vivo* (Figure 5.4B). All mutations showed greater activity than the EV control, which showed 80%±2.0% less activity than that of wild-type. This assay allows assessment of the degree to which these mutations impair target maturation for CIA function.

5.3.3 DSS and DC4 Crosslinking and Mass Spectroscopy can be used to identify the Cia2- Met18 binding site

While successful, our approach of identifying protein-protein binding interfaces via targeted site directed mutagenesis has disadvantages. Our previous experiments allowed us to explore the roles of conserved regions of Met18. From the co-affinity purification assay it can be surmised that motifs in the C-terminal region of Met18 are required for Cia2 binding. Mutations of these motifs lead to an impairment of CIA function as shown by *in vivo* assays. However, these mutations contained several amino acids, spanning a large region within the C-terminal portion of Met18. Although we can conclude the binding site for Cia2 likely is located within the C-terminus of Met18, the specific amino acid residues contributing to Cia2 binding are still not identified. Single point mutations of each of these motifs would be illuminating, but very time consuming.

Additionally, in Chapter 4 we identified a single amino acid responsible for Cia1 binding on Cia2 (E208), but observed the five amino acids on the C-terminal end of Cia2 were not responsible for binding to Met18 as proposed by a previous lab.[60] Thus, the site on Cia2 where Met18 is binding, is also still largely unknown. To approach this problem, we collaborated with the Costello lab to utilize cross-linking coupled with mass spectroscopy to identify the residues involved in Cia2 and Met18 binding. By this method, we crosslinked the proteins, digested them with a protease, and used mass spectroscopy to analyze the peptides from both proteins linked by the crosslinker.

This method required optimization of the crosslinking reaction. We first used a DSS amine cross-linker to crosslink Met18 with Cia2. The C-terminal end of Cia2,

contains a patch of positively and negatively charged amino acids which we hypothesized were important for binding to Met18. First, we had to optimize our crosslinking reaction. The correct ratio of crosslinker to protein is required. Too much crosslinker will lead to inter-complex proteins and a large crosslinked aggregate that would not yield any information about the amino acids involved in the binding interface. To optimize these DSS amine crosslinker reactions, we first titrated crosslinker, at different molar ratios, into Met18-Cia2. We used 5-, 10-, 25-, and 50- fold excess and observed high molecular weight bands upon SDS-PAGE analysis of the crosslinked samples (Figure 5.5A). These crosslinked reactions contained Met18, Cia2, and multiple higher molecular weight bands. We predicted that some of these higher molecular weight products were over reacted crosslinked proteins that may not have any true binding significance. We were able to select for the desired cross-linked product from the over reacted and unreacted smaller molecular weight proteins by using size exclusion chromatography (Figure 5.5B, *X-link product). We purified our cross-linked Met18-Cia2 product (Figure 5.5B, solid line) as it eluted at the same elution volume as the Met18-Cia2 subcomplex we had collected in previous experiments (Figure 5.5B, dashed line). This gave us confidence that any crosslinked peptides identified are likely to be physiologically relevant as they are not likely to come from overly crosslinked (inter-complex) reactions.

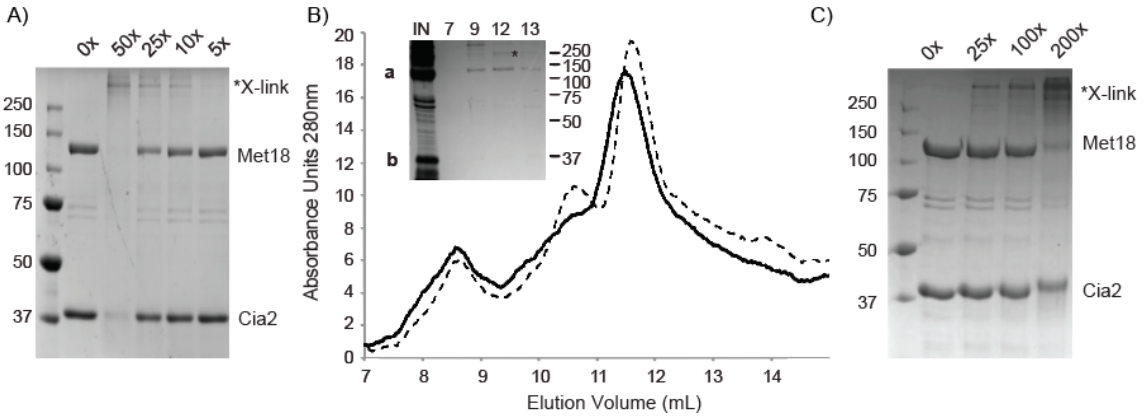

Figure 5.5. Optimization of Crosslinking with DSS and DC4.
A) Different concentrations, 5-,10-,25-, and 50- fold molar excess of DSS crosslinker are tested with a mixture of Met18 and Cia2. The desired cross-linked product is labeled (*X-link). B) Met18 is denoted as (a) at 130kDa and Cia2 is denoted as (b) at 25kDa for the inset gel. DSS cross-linked sample (solid line) that was injected onto the SEC (IN, gel inset) and fractions from the elution volumes of 7 mL, 9 mL, 12 mL, and 13 mL were collected and analyzed by SDS-PAGE (gel inset). The chromatogram was similar to the Met18-Cia2 sample containing no crosslinker (dashed line), indicating the peak collected at 12mL (12*, gel inset) was the Met18-Cia2 subcomplex. C) Different concentrations DC4 crosslinker, 25-, 100-, and 200- fold excess are tested with a mixture of Met18 and Cia2. The preferred cross-linked product is labeled (X-link*). All molecular weight standard sizes are shown beside the gels.

In addition to the DSS crosslinker, we used a DC4 mass cleavable crosslinker to crosslink Met18 with Cia2. The DC4 reaction was optimized by titration of 25-, 100-, and 200- fold molar excess crosslinker to protein complex. We obtained a maximal yield of the Cia2-Met18 cross-linked product using the DC4 amine cross-linker in 200 fold molar excess (Figure 5.5C). The DC4 crosslinker includes two positive charges, by which the crosslinked peptides fragment into individual peptides from each protein by ionization from mass spectrometry.[123] Fragmentation on either side of the positive charges on the crosslinker allow for the peptides to be identified as pairs containing defined masses depending on how the crosslinker was cleaved.[123] A peptide pair may have the short portion or a long portion of the DC4 crosslinker, with its own unique mass based on

cleavage (Figure 5.6).

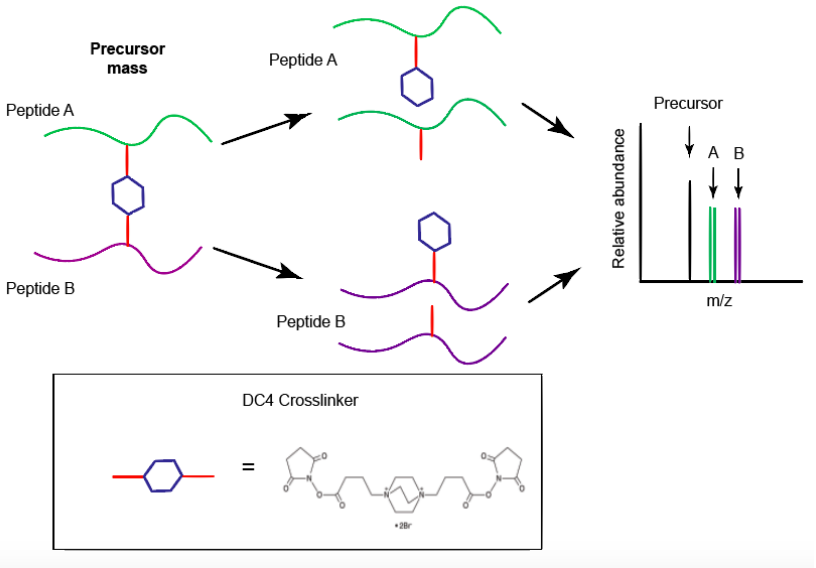

Figure 5.6. Schematic of DC4 Crosslinking.
Peptide A (green) is crosslinked to Peptide B (purple) with a DC4 crosslinker (red sticks and blue hexagon). The peptides can fragment with the short portion of the DC4 crosslinker (red stick only) or long portion of the DC4 crosslinker (red stick with blue hexagon). All these mass peaks may be observed in the spectra of the raw data

To test if we could optimize the purity of the crosslinked solution, both DSS and DC4 samples were run on an SDS-PAGE gel. The band containing the desired Met18-Cia2 cross-linked was excised from the gel for each sample and the crosslinked protein was extracted from the gel. However, gel extractions commonly contain little protein. In addition to the gel extracted samples of the DSS and DC4 crosslinked proteins, we analyzed the samples from reaction in solution with DSS and DC4. We predicted one of these conditions might generate cross-linked peptide pairs for analysis. All four DSS and DC4 cross-linked samples (in solution and in gel) were digested with trypsin, cleaving the proteins at amine residues. Small molecule MS contaminants were removed by C18 tips. In collaboration with the Costello lab, Deborah Francoleon collected the data for the

masses of the fragmented peptides on the Q Exactive HF Hybrid Quadrupole Orbitrap MS (Thermo Fisher).

The raw data for each sample contained several mass peaks of fragmented peptides. A programming script, developed by Christian Heckendorf, analyzed the peaks and selected possible precursor masses of peptide pairs based on the sequences of Met18 and Cia2 and the mass of the crosslinker. The program script for the DC4 crosslinker also utilizes the masses associated to the charged short or long arm of the crosslinker as a parameter for identifying the precursor masses of the peptide pairs. The fingerprint of the DC4 crosslinker allowed more accurate selection of the crosslinked peptides. However, the DSS crosslinker does not contain a charge. The mass of the DSS crosslinker was used to select for precursor peptides, which are modified by the mass of DSS. However, the lack of cleavage of the DSS crosslinker makes it difficult to ensure that the peptides identified are indeed connected to the crosslinker. These peptides chosen by the script are more likely to be other peptide fragments with a similar mass to a peptide reacted with DSS.

The script returned 15 cross-linked peptide pairs for the DC4 in solution sample, no peptide pairs for the DC4 in gel solution sample, 43 peptide pairs for the DSS solution sample, and 654 peptide pairs for the DSS in gel sample. The DSS crosslinked samples contained the greatest number of peptide pairs. However, due to the high number of peptide pairs in both DSS samples, it seems most likely that the majority of these peptide pairs were other random peptide fragments.

Using MASCOT, a server running a protein identification algorithm, the peptide sequences were compared to a peptide database containing the sequences of Cia2 and Met18 as well as *E. coli* proteins.[124] MASCOT showed that the top hits for the DSS in solution sample contained keratin contamination. All the other samples contained an *E. coli* metal-binding protein glutamine fructose-6 phosphate aminotransferase as a top hit for the sequences in the sample. This protein is a common contaminant that binds nonspecifically to Ni-NTA columns and elutes with proteins purified in this manner.

Because the DSS in solution sample had a high level of false positives and keratin contamination, we focused on the 15 cross-linked pairs for the DC4 in solution sample (Table 5.1). Each peptide pair had a theoretical computed precursor mass. The raw data was searched for a peak with this theoretical precursor mass. The observed mass peak in the raw data was then compared to the theoretical precursor mass to make sure the peak was within the mass tolerance of the instrument(error less than 5 ppm). If the peak fit this criterion, we searched the MS^2 for the y and b series fragmentation to identify peaks that we could assign as amino acid fragments of each precursor peptide. If each peak could be found within the raw data, that peptide was deemed a valid hit.

Pre Mass (m/z)	Pre (z)	Met18 Sequence	Cia2 Sequence	Valid?	Reason
684.5424	6	EVLEGFAALAPMKYVSINEIAQLLR	MLVTCKGRR	No	Wrong precursor monoisotopic mass
1254.616	5	IINLMALQLYNFDK	GALEVLFQDPGYQDPMMSEFLNENPDILEENQLPTRK	No	MS2 does not match
767.8154	5	LFEVFVMDISSLKK	ERVAAACENEQLLGVVSK	No	MS2 does not match
687.116	4	K	EDSTKDLLLGGFSNEATLERR	No	MS2 does not match
532.0646	4	ILDTPNVLAISYAK	GRK	No	MS2 does not match
527.296	4	IINLMALQLYNFDK	K	No	MS2 does not match
811.7783	3	LMEAFAKRQGK	MLVTCKGR	No	MS2 does not match
783.7299	3	QK	GTHDSENQVNKQLNDK	No	MS2 does not match
783.7296	3	QK	GTHDSENQVNKQLNDK	No	MS2 does not match
714.7332	3	GLIMQNSLESSEIAKK	K	No	MS2 does not match
576.3555	3	KALTCLTTILAK	K	Yes	---
576.3549	3	KALTCLTTILAK	K	Yes	---
466.6466	3	K	FRITTILLK	Yes	---
466.6466	3	K	FRITTILLK	Yes	---
401.8994	3	LMEAFAK	K	No	MS2 does not match

Table 5.1. Summary of DC4 Crosslinked Peptides Identified

The validated peptide pairs included a Met18 sequence on the N-terminus of Met18 and a peptide sequence on the C-terminus of Cia2 that were not the sequences

predicted to be involved in peptide binding (Table 5.1). Additionally, these peptides were each coupled to a lysine residue that could be any accessible lysine residue in either protein; that is- no unique lysine was identified. From these experiments, the purity of the protein samples must be optimized.[125] Future experiments can include use of the NiCo strain (NEB), which allows for removal of metal binding contaminants such as glutamine fructose-6 phosphate aminotransferase. Moreover, a different protease can be used to cleave the peptides, as the amine cleavage site targeted by trypsin may be reacted with DC4. However, from these preliminary experiments, we found the DC4 crosslinker to be optimal for mass spectroscopy analysis of crosslinked peptides compared to samples that were crosslinked using DSS. Additionally, these experiments create a platform for developing this method to identify the interacting peptides of Met18 and Cia2.

5.4 Discussion and Future Directions

Within the CIA targeting complex, Met18 plays a critical function as a large protein-docking site for Cia2 and FeS target proteins. However, the binding sites of these proteins on Met18 remain elusive. Pinpointing these binding interfaces will allow for understanding how FeS proteins are recognized by the CIA pathway and insight on how the CIA targeting complex associates to recognize these proteins.

To identify the binding sites on Met18 we focused on the two regions that are the most highly conserved throughout eukaryotes: a C-terminus containing four HEAT repeat domains (748-1032), and an N-terminal portion containing three HEAT repeat domains (1-331).[26, 42, 60, 68] These constructs were similar to those made by van Wietmarschen *et*

al., an ΔAB construct in which the N-terminal portion of Met18 was deleted (1-284) and a ΔC construct in which the C-terminal portion of Met18 (731-1032) was deleted (Figure 5.1).[26] These constructs were based upon a previous study, which identified the A, B, and C domains as having distinct functions for nucleotide excision repair and transcription.[68] Van Wietmarschen *et al.* reported via co-immunoprecipitation (Co-IP) that ΔAB retains interaction with Cia1, Rad3, and other human FeS proteins RTEL1 and MUTHY (absent in yeast), whereas ΔC can only interact with Cia1.[26]

Another lab published conflicting results, indicating that the C-terminal region of Met18 is required for binding to the CIA components, not targets. Odermatt *et al.* truncated the human Met18 in four ways, A(1-452), B(446-861), C(856-1032), and D(446-1032) and saw that the C-terminal constructs are able to bind to Cia2 and Cia1, as well as Pol3 and another FeS protein RTEL1 (not present in yeast) (Figure 5.1).[60] Moreover, the study from Odermatt *et al.* showed the N-terminal Met18 constructs (A and B) are not able to bind to Cia2, Pol3, or RTELI, but are able to bind to Rad3.

Our results by co-affinity purification were most consistent with Odermatt *et al.* The construct containing the N-terminal portion (1-331) of Met18 did not interact with Cia2. Furthermore, alanine scanning of the motif 4 (770-771), motif 5 (797-805), and motif 6 (859-865) in the C-terminal region of Met18 all disrupted the binding interaction with Cia2. This result was consistent with what Odermatt *et al.* had observed for their D construct, as our M6 variant was not able to bind to Cia2. However, our M4 and M5 variants were also not able to bind to Cia2, suggesting that these motifs also contributed to Cia2 binding. Odermatt *et al.* did not observe binding to M4 and M5 as their B

construct did not bind to Cia2.

It is possible that upon truncation of the protein Odermatt *et al.* may have generated a construct that could not be properly folded as truncating the protein compromised tertiary structure. Additionally, this construct in the cell shows low expression levels, which could be why there was no observed interaction with construct B and Cia2.[60] However, our confidence in the refolding of our own M4 and M5 Met18 constructs was high as the CD analysis showed they maintained their alpha helical structure like that of wild-type Met18 (Appendix A.2).

For the N-terminal function of Met18, our results were consistent again with Odermatt *et al.* We observed that the R144A mutant in motif 1 disrupted binding to Rad3, but not Cia2, which supported the concept that the N-terminal region of Met18 is responsible for binding to FeS proteins, specifically Rad3. Rad3 is a helicase involved in nucleotide excision and repair.[50, 62] Odermatt *et al.* observed human Rad3 binds directly to the N-terminal region of Met18, but other targets such as human Pol3, a polymerase, bind to the C-terminal end of Met18 with Cia2. However, we observe that Cia2 is required for Rad3 binding to Met18. One possibility is that there are two distinct binding sites for Rad3 on Met18 and Cia2. Future binding studies are required to observe if binding is similar for all targets.

Both Odermatt *et al.* and our lab have conflicting results with van Wietmarschen *et al*. Similarly, our result that Cia2 was the bridging protein did not match van Wietmarschen *et al.*, as in their experiments Cia1 directly interacts with Met18. One possibility for this discrepancy is that the yeast system may be different than that of the

human orthologs. However, this possibility seems unlikely as Odermatt *et al.* observe results similar to ours for the human orthologs. Odermatt *et al.* suggests that the *in vitro* translated Met18 or Cia2 from van Wietmarschen *et al*. might not fold properly and hence displays a different binding behavior than what is observed by other labs for the Cia2 and Met18 interaction. We favor the model that Met18 may weakly bind to Cia1, which we may not be able to observe via our co-affinity purification studies.

Although Co-IP and our co-affinity studies allow for conclusions about which portions of Met18 bind to Cia2 or Rad3, little is known about how these mutations affect CIA function in the cell. If the C-terminal motifs are the binding site for Cia2, we might expect that mutation of these residues *in vivo* would diminish CIA function if the Met18-Cia2 complex is important for CIA function inside the cell. These conclusions cannot be made solely from the binding of the proteins *in vitro*.

To address this issue, we developed an approach to analyze the effect of mutations in Met18 on CIA function. However, viability screens, such as those employed in Chapter 4, can only be used for essential proteins and Met18 is nonessential.[40] However, defects in Met18 result in phenotypes such as methionine biosynthesis, methyl methanesulfonate sensitivity, and increased length of telomeres.[22, 42, 49, 50, 52] Specifically, mutations in this protein have resulted in methionine auxotrophy.[121] We exploited this defect to assess CIA function *in vivo*. Our results from these *in vivo* assays reveal that the M4, M5, and M6 variants that are required for Cia2 binding are functional *in vivo*.

Previous studies have also shown cells can still be viable yet have compromised CIA activity. For example, the Walden lab observed yeast growth for mutations in Cfd1

in the CIA scaffold in which the CIA function measured via IRP1 aconitase activity was severely compromised.[122] The activity of the cells with these mutations was knocked down by 88% compared to wild-type, yet the cells were still able to grow.[122] This indicates a quantitative assay for CIA function is helpful in understanding the extent to which the mutants compromise CIA activity *in vivo*. We also exploited Leu1 activity to assess the CIA functionality of our Met18 mutations.

We observed that the Motif 5 mutant had significantly lower activity compared to wild-type, with 70%±3.4% less activity. The Motif 6 mutant had a small decrease in activity (20%±0.5 lower) (Figure 5.4). The Motif 4 mutant had similar Leu1 activity, indicating that this motif is not important for CIA function *in vivo* (Figure 5.4). All mutants had activity above the EV control, which showed 80%±2.0 less activity than that of wild-type.

These results suggest that Motif 5 contains amino acids required for CIA function, which also are required for Cia2 binding. This result was surprising as Odermatt *et al.* observed direct binding with M6 and this motif had a small decrease in Leu1 activity. As we see M4, M5, and M6 all disrupt Cia2 binding, this suggests for our studies that M5 has a more dominant role in binding to Cia2 than the other motifs. These results allowed for a quantitative assessment of the extent to which Met18 mutations impair CIA function, but future studies may quantify this binding contribution. Future studies will investigate the R144A and other conserved amino acid residues, but this preliminary work provides a platform for assessing the functionality of Met18 mutations *in vivo*.

Lastly, we optimized a method using crosslinking coupled with mass

spectroscopy for pinpointing the Cia2-Met18 binding interface. Our previous experiments allowed us to explore the roles of conserved regions of Met18. However, these mutations contained several amino acids, spanning a large region within the C-terminal portion of Met18. Although we can conclude that the binding site for Cia2 is most probably located within the C-terminus of Met18, the specific amino acid residues contributing to Cia2 binding are still not identified. Single point mutations of each of these motifs would be very time consuming. Additionally, in Chapter 4 we identified a single amino acid on Cia2 responsible for Cia1 binding (E208), but observed the five amino acids on the C-terminal end of Cia2 were not responsible for binding to Met18 as proposed by a previous lab.[60] Thus, the site on Cia2 where Met18 is binding, is also still largely unknown.

From our studies, we are able to crosslink Cia2 to Met18 by amine crosslinkers, indicating that the binding interface is indeed a charged interaction. Our experiments also indicate that DC4 is the optimal cross-linker for identifying interacting peptides by mass spectroscopy. Although the DSS crosslinker allows for production of the preferred crosslinked product that can be purified by SEC, the lack of cleavability on the DSS crosslinker precludes analysis of the interacting peptides by mass spectroscopy. These preliminary studies indicate that that for this method, we should focus on developing experiment with the DC4 crosslinker.

Additionally, these experiments determined that there is much contamination from the Ni-NTA purification. The purity of our crosslinking samples can also be improved by expressing our samples in the NiCo strain (NEB), to remove the primary

contaminant, glutamine fructose-6 phosphate aminotransferase, an *E. coli* metal binding protein. We will then optimize the crosslinking reaction with the pure protein and digest using a protease such as chymotrypsin, which cleaves at an amino acid residue other than an amine.

Overall, these studies identify important motifs for Cia2, develop *in vivo* methods to determine how mutations on Met18 impair CIA function, and optimize an approach to identify the Cia2-Met18 binding site. Previous studies have not exploited use of *in vivo* assays to investigate Met18 mutations. The work in Chapter 5 creates a basic platform to explore Met18 binding interactions with Cia2 and Rad3, as well as *in vivo* screens that can assess how these interactions affect CIA function.

CHAPTER SIX: Major conclusions and future directions

Previously, there has been a dearth of knowledge for the CIA targeting complex and the process by which it identifies apo-protein targets. Studies from the Seki *et al.* and van Wietmarschen *et al.* publications prior to this thesis conflicted in the binary interactions they observed through co-IP experiments.[25, 26] Utilizing our method of co-affinity purification assays allowed for the determination of the connectivity of the targeting complex without the unclear results due to western-blotting detection and low expression levels. We found Cia2 to be the center of the CIA targeting complex. By the co-affinity purification method we could also form the Met18-Cia2-Cia1 targeting complex with a size consistent with 1Met18, 4Cia2, and 2Cia1 by SEC analysis. We were also able to form stable subcomplexes that could differentially recognize the targets Rad3 and Leu1.

The purification of these proteins allowed for preliminary experiments to set EM grids. Future studies to optimize the purification of this CIA targeting complex with Nar1 will allow us to obtain an EM model that will give structural insight regarding the targeting complex. Additionally, future experiments to quantify binding of Cia1-Cia2, Cia2-Met18, and Cia1-Met18 by Kds will provide insight on the formation of this complex within the cell.

In this work we also investigated the role of Nar1 within the CIA pathway. We ruled out the possibility that Nar1 could act as an adapter between the scaffolding complex and the targeting complex with an apo-target protein, as Nar1 could not bind simultaneously to the CIA targeting complex while Leu1 was bound. This result

suggested that Nar1 may compete with Leu1 for binding to the CIA targeting complex. Future work to quantify Nar1 binding to Cia1 as well as Leu1 binding to Cia1 will help to understand this competition.

Additionally, in this work we observed that Nar1 was unable to transfer cluster to the apo-Leu1. Future studies will investigate the role of Nar1 by exploring its interaction with the scaffold and any effect it may have on the ATPase activity of the scaffold. Lastly, more conditions can be scouted to fully reconstitute Nar1 to look at the role its FeS clusters might play in the CIA pathway. Future studies will work to understand the effect of apo and holo Nar1 on ATPase activity, as well as the effect of apo and holo Nar1 on target recognition.

This work identified several key residues on Cia2. In chapter 4 we identified that the E208 on Cia2 was required for binding to Cia1. We also demonstrated that the C161 was not required for protein-protein interactions and had an alternate biochemical function that we proposed had to do with a cluster-carrying role. Future studies must identify on Cia2 the residues that are important for Met18 binding.

In chapter 5 we also identified that the N-terminal portion of Met18 was responsible for binding to apo-target Rad3. Future studies will investigate the effect this mutation has on binding to other apo-targets such as Leu1. Additionally, these studies should address the conserved residues in motifs 2 and 3 that are also located within the N-terminus of Met18. In chapter 5 we also observed that the C-terminal portion was required to bind to Cia2 and specifically motif 5 had significantly lower activity Leu1 compared to wild-type, with 70%±3.4% less activity. Future quantitative binding

experiments can compare these alanine scanned motifs to more clearly identify the binding contribution of each motif.

In chapter 5 we also initiated crosslinking experiments coupled with mass spectroscopy to identify the binding interfaces between Cia2 and Met18. These experiments must be optimized by use of the NiCo strain to purify the proteins from the metal binding contaminant proteins after the IMAC purification. Additionally, a new protease that cleaves at other amino acid residues (not arginine like trypsin) will allow for better peptide cleavages during the digestion of the crosslinked proteins. Once these parameters are optimized, we can apply this method to identify the binding interfaces between other proteins such as the CIA component with targets to identify recognition motifs.

Overall, this thesis has developed the basis for which the CIA targeting complex can be investigated by *in vitro* and *in vivo* experiments. Purification of these proteins allows for a platform to understand the unsolved question of how FeS proteins are recognized by the CIA targeting complex. As defects in this pathway lead to cancer, understanding the basis of this pathway could lead to development of cancer therapeutics.

APPENDICES

Appendix 1: Primer Sequences

1.1 Table of Primer Sequences

Table A1.1 Primer Sequences

Name	Backbone	Gene/Use	Sequence (5'→3')
AV03	pRSFduet	^{HIS}Met18	AGCCATCACCATCATCACCACAGCCAGGA TCCGAATTCGATGACACCAGACGAACTAAAT
AV04	pRSFduet	^{HIS}Met18	TGTTCGACTTAAGCATTATGCGGCCGCAAG CTTGTCGACTTACTCGAACGGGATTTGGC
AV05	pRSFduet	Nar1	AGTTAAGTATAAGAAGGAGATATAC ATATGATGAGTGCTCTACTGTCCGAG
AV06	pRSFduet	Nar1	CGCAGCAGCGGTTTCTTTACCAGACT CGAGTTACCAGGTGCTCCAACAGA
AV11	None	Met18	GCCGAAGATGCTTATAGC
AV12	None	Met18	TCAGCCCTTTAGTCAACC
AV13	pRSFduet	Rad3	AGTTAAGTATAAGAAGGAGATATAC ATATGAAGTTTTATATAGATGATTTACCA
AV14	pRSFduet	Rad3	CGCAGCAGCGGTTTCTTTACCAG ACTCGAGTCACTGCATTTCTATATCTTC
AV15	pETduet	^{HIS}Cia1	CATCATCACCACAGCCAGGATCCG AATTCGATGGCGTCTATCAATCTG
AV16	pETduet	^{HIS}Cia1	TTCTGTTCGATTAAGCATTATGCG GCCGCCTACGCTGCTTTTTCTAG
AV26	pRSFduet	^{SUMO}Met18	AGCCATCACCATCATCACCACAGCCAGGA TCCGAATTCGATGGCTAGCGGATCGGAC
AV27	pRSFduet	^{SUMO}Met18	ATTTAGTTCGTCTGGTGTCATCCGA ATTCGACCACCAATCTGTTCTCT
AV30	pETduet	^{DT}Cia1	CCAGGCGTGGAGCCACCCGCAGTTCGAAAA GGGAGGAGATCCGAATTCGATGGCGTCT
AV31	pETDuet	^{DT}Cia1	ACTGCGGGTGGCTCCAGCCCTGGAAATA CAGGTTTTCCGGATCCTGGCTGTGGTG
AV32	None	Cia2 E208A	CAACTAAATGATAAGGCACGTGTAGCAGCTGCA
AV33	None	Cia2 E208A	TGCAGCTGCTACACGT GCCTTATCAATTAGTTG
AV34	pRSFduet	^{SUMO}Met18 C-term	ATGACACCAGACGAACTAAAT
AV35	pRSFduet	^{SUMO}Met18 C-term	ATCCTGGCTGTGGTGATGATG
AV49	pRS313	Δ102 Cia2^{MYC}	CTATAGGGCGAATTGGAGC
AV50	pRS313	Δ102 Cia2^{MYC}	TATGGGTACAATCCACCTAA CTTACAAGTCACTAACATC

AV67	pRS313	Δ5C Cia2^{MYC}	GAACAAAAACTTATTTCTGAAG
AV68	pRS313	Δ5C Cia2^{MYC}	CATCTTAGAGACTACACC
AV71	pRS316	Met18^{HA}	TTCGATATCAAGCTTATCGAT ATGACACCAGACGAACTAAAT
AV72	pRS316	Met18^{HA}	GACGTCGTATGGGTACTTTAC CTCGAACGGGATTTGGCCT
AV73	pRS316	N-term Met18^{HA}	GACGTCGTATGGGTACTTTACC TGTTGGTCTTTATTGTACGGA
AV74	pRS316	C-term Met18^{HA}	TTCGATATCAAGCTTATCGA TCATGCTCCAAGAATGACG
CL01	pRSFduet	^{SUMO}Met18 N-term	TAAGTCGACAAGCTTGC
CL02	pRSFduet	^{SUMO}Met18 N-term	CGGATTTAGTAGAGTGTT
CL03	pRSFduet	Met18 R144A	GCATCAACTGCACTGTGGCC
CL04	pRSFduet	Met18 R144A	CAAATGCTGGCCTTGTTGATAG
CL13	pRS316/ pRSFduet	Met18^{HA} Met18^{HIS}	GCAGCAGCCGCCGGTGA CATTTTTCAAACAC
CL14	pRS316/ pRSFduet	Met18^{HA} Met18^{HIS}	TGCCGCCGCGATTTTA ACGGTATTATTCCA
CL15	pRS316/ pRSFduet	Met18^{HA} Met18^{HIS}	GCAGCATTCGTCTCTG AAAAAGATGTGATA
CL16	pRS316/ pRSFduet	Met18^{HA} Met18^{HIS}	TGATAAGACCAA CAGCAATTCCA
CL17	pRS316/ pRSFduet	Met18^{HA} Met18^{HIS}	GCAGGGGCGGCAGCGGC AAACTCATTAGAGTCATCA
CL18	pRS316/ pRSFduet	Met18^{HA} Met18^{HIS}	TGCCGCCGCAACCATCACTTCAAGATT
ZH01	pRSFduet	Met18^{STREP}	TTTCCAGGGCCATAGCCAGGATCCTGGAGCCACC CGCAGTTCGAAAAGATGGCGTCTATCAATCTGATT
ZH02	pRSFduet	Met18^{STREP}	TCGACTTAAGCATTATGCGGCCGCAA GCTTCTACGCTGCTTTTTCTAGAGA

Appendix 2: Methods for Expression and Purification of Proteins

2.1 Table of Plasmids Used For Expression

Table A2.1 Plasmids Used for Expression

Name	Gene	Vector	Selection	Primers Used
pAV02	^{HIS}Met18	pRSFduet	Kanamycin	AV03 and AV04
pAV03	Nar1	pRSFduet	Kanamycin	AV05 and AV06
pAV08	Rad3	pRSFduet	Kanamycin	AV13 and AV14
pAV10	Cia1	pETduet	Ampicillin	AV15 and AV16
pAV13	^{SUMO}Met18	pRSFduet	Kanamycin	AV26 and AV27
pAV15	DTCia1	pETduet	Ampicillin	AV30 and AV31
pAV20	Δ102 Cia2^{MYC}	pRS313	Ampicillin/His	AV49 and AV50
pAV28	Δ5C Cia2^{MYC}	pRS313	Ampicillin/His	AV67 and AV68
pAV29	Met18	pRS316	Ampicillin/Ura	AV71 and AV72
pAV30	M4 Met18	pRS316	Ampicillin/Ura	CL15 and CL16
pAV31	M5 Met18	pRS316	Ampicillin/Ura	CL17 and CL18
pAV32	M6 Met18	pRS316	Ampicillin/Ura	CL13 and CL14
pAV34	N-term Met18	pRS316	Ampicillin/Ura	AV71 and AV73
pAV35	C-term Met18	pRS316	Ampicillin/Ura	AV72 and AV74
pAV37	M4 Met18	pRSFduet	Kanamycin	CL15 and CL16
pAV38	M5 Met18	pRSFduet	Kanamycin	CL17 and CL18
pAV39	M6 Met18	pRSFduet	Kanamycin	CL13 and CL14
pJG01	Cia2	p15	Ampicillin	YHR122-p15 forward and YHR122-p15 reverse
pJG04	^{DT}Cia2	pET52	Ampicillin	YHR122-p15 forward His and YHR122-p15 Strep backwards
pJG15	^{DT}C161A	pET52	Ampicillin	YHR122 C161A forward and YHR122 C161A backwards
pHG01	Δ102 Cia2^{HIS}	pET24		EC033 and EC034
pJDG04	FNR	p15b	Ampicillin	JDG03 and JDG04
pCG05	SNAP FNR	pSNAP-tag(T7)-2	Ampicillin	JDG16 and JDG17
pMM01	^{His}Nar1	pRSFduet	Kanamycin	JC02 and MM01
pMM03	Cia2 NPQ	pET52	Ampicillin	MM05 and MM06
pMM08	Δ5C Cia2	pET52	Ampicillin	M15 and M16
pNF01	Cia2 E208A	p15	Ampicillin	AV33 and AV34
R144A Met18	Met18 R144A	pRSFduet	Kanamycin	CL03 and CL04
CL01	N-term Met18	pRSFduet	Kanamycin	CL01 and CL02

2.2 Expression and purification of Wild-type Met18 in vitro

N-terminally His-tagged Met18 (^{His}Met18) was created by amplifying Met18 from genomic DNA using primers AV03 and AV04 (Appendix Table 1.1) and inserting Met18 between the *EcoR1* and *SalI* sites of the pRSF-Duet vector via the Gibson DNA assembly method, creating pAV02. [126] His-SUMO Met18 (^{SUMO}Met18) was created by insertion of the SUMO coding sequence at the *EcoR1* site of pAV02 using primers AV26 and AV27 (Appendix Table 1.1) and Gibson assembly to create pAV13. Double-tagged (^{DT}Met18) was created by the addition of a C-terminal TEV protease and Strep-II tag to pAV13 via Q5 Mutagenesis Kit (NEB) using primers ZH01 and ZH02 (Appendix Table 1.1). These constructs, as well as all other constructs reported herein, were confirmed via DNA sequencing. ^{His}Met18 expressed in *E. coli* Rosetta2 (DE3) grown at 37˚C to an OD_{600} of 0.7-0.8. IPTG (1 mM) was added and the cells were collected 4 h later. ^{SUMO}Met18 and ^{DT}Met18 were grown by autoinduction.[127]

For purification, the cell paste was resuspended in Buffer A (50 mM Tris (pH 8.0), 100 mM NaCl, 10% glycerol) and 5 mM -mercapoethanol supplemented with protease inhibitors and DNase nuclease. Cells were lysed by sonication and the soluble extract was added to TALON affinity resin (Clontech). The column was washed with 50 column volumes (CV) Buffer A supplemented with 5 mM imidazole and eluted with Buffer A supplemented with 300 mM imidazole. Met18 was dialyzed overnight against Buffer A, concentrated to 1.0 mg/mL, and stored at -80˚C. Purification of ^{DT}Met18 proceeded as described above except the TALON elution was loaded onto a streptactin column which was washed with 10 CV of Buffer A and eluted with Buffer A

supplemented with 2.5 mM desthibiotin.

Untagged Met18 was accessed by cleavage of the SUMO tag from ^{SUMO}Met18. The SUMO-tag was removed with the addition of SUMO protease (0.6 mg/mL). After an overnight incubation at 4℃, the mixture was passed over a HisBind column and Met18 was recovered from the flow-through.

Biochemical and biophysical studies of the CIA targeting complex require milligram quantities of protein, but no methods are currently available to access Met18.[21, 22] Therefore, we developed a method to purify recombinant Met18 following overexpression in bacteria. While we could purify His-tagged Met18 from the codon enriched *E. coli* Rosetta(DE3) cell line, the yield was improved using an N-terminal SUMO tag along with autoinduction expression conditions (Figure A.1). The low molecular weight contaminants of ^{SUMO}Met18 could be removed by the use of a double tagged construct with an N-terminal His-tag and C-terminal StrepII tag and tandem affinity purification (Figure A.1A, Lane 3).

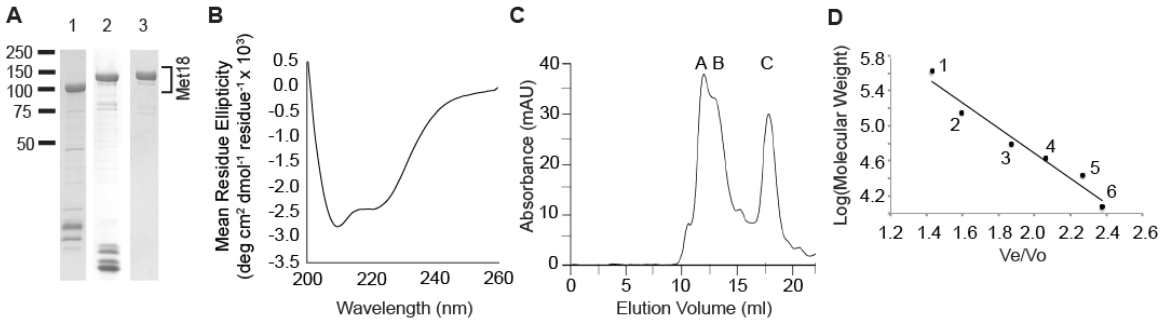

Figure A.1. Purification of Met18.
A) SDS-PAGE of ^{His}Met18 (Lane 1), ^{SUMO}Met18 (Lane 2), and ^{DT}Met18 (Lane 3). Migration of MW standards (in kDa, left) and Met18 ^{128} are indicated. B) CD spectrum of ^{SUMO}Met18 (2 μM) in 10 mM KPO_4 and 100 mM NaCl buffer demonstrating the protein's alpha helical character. C) SEC analysis of ^{SUMO}Met18 (130 kDa) which elutes as two overlapping peaks with corresponding to molecular weights of 558 and 298 kDa for Peaks A and B, respectively. Peak C (25 kDa) contains low molecular weight contaminants seen in Lane 2 of Panel A. D) A representative standard curve used to determine molecular weight from SEC. Standards used were apo-ferritin (1, 443 kDa), alcohol dehydrogenase (2, 150 kDa), albumin (3, 66 kDa), ovalbumin (4, 45 kDa), carbonic anhydrase (5, 29kDa), and cytochrome c (6, 12.4kDa).

To ensure that the tags added did not impact the native fold of Met18, we characterized the recombinant protein via circular dichroism (CD) and size exclusion chromatography (SEC). Met18 is predicted to be an all alpha helical HEAT (*h*untingtin, *e*longation factor 3, subunit *A* of protein phosphatase 2A, and *t*arget of rapamycin) repeat protein.[129] Consistent with this domain structure, ^{SUMO}Met18 has a CD spectrum that one would expect for an alpha-helical protein (Figure A.1B). We also determined the quaternary structure via SEC. ^{SUMO}Met18 eluted as two overlapping peaks with molecular weights of 558 kDa and 298 kDa (Figure A.1C). Since the ^{SUMO}Met18 polypeptide is 130 kDa, our results are most consistent with a Met18 forming a mixture of dimers and tetramers. We concluded from these biochemical experiments that the recombinant Met18 was suitable for *in vitro* protein-protein interaction analysis.

2.3 Refolding Met18 Mutations in vitro

Primers CL01 and CL02 were used to delete the C-terminal domain of Met18 in pAV13 plasmid to create N-terminal Met18 (1-331) via Q5 mutagenesis (NEB Biolabs). CL15 and CL16 were used to mutate Met18 in pAV13 via Q5 mutagenesis (NEB Biolabs) to create the M4 Met18 mutant, pAV37. CL17 and CL18 were used to mutate Met18 in pAV13 via Q5 mutagenesis (NEB Biolabs) to create the M5 Met18 mutant, pAV38. CL13 and CL14 were used to mutate Met18 in pAV13 via Q5 mutagenesis (NEB Biolabs) to create the M6 Met18 mutant, pAV39.

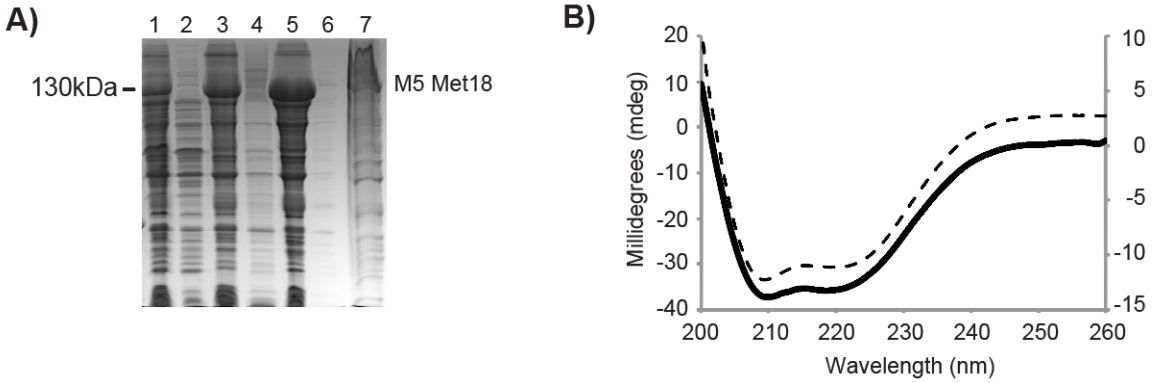

Figure A.2 Denaturation and CD analysis of refolded Met18 constructs.
A) An SDS PAGE gel shows Met18 cells were lysed (Lane 1), then centrifuged and the supernatant was discarded (Lane 2). The resulting pellet (Lane 3) was resuspended and excess protein was discarded in wash (Lane 4). This was repeated (Lane 5 and Lane 6). The protein was then denatured in GndHCl (Lane 7), which was then refolded. B) The CD spectrum of Met18 M4 (dotted line) and Met18 M6 (solid line) was acquired in 10 mM KPO_4 and 100 mM NaCl buffer and demonstrates a significant amount of secondary structure content consistent with proper refolding of Rad3.

To refold N-terminal Met18 (1-331), Motif 4 Met18, Motif 5 Met18, and Motif 6, the cell paste was resuspended, lysed, and centrifuged as described for ^{His}Met18 (Figure A.2A, Lanes 1-2). The pellet was washed with Buffer B (50 mM Tris (pH 8), 100 mM NaCl, 1 mM EDTA, 1 mM DTT, and 5% glycerol) supplemented with 0.5% Triton X100

and subsequently with Buffer B (Figure 2.3.1A, Lanes 3-6). The pellet was resuspended with 50 mM Tris (pH 8), 200 mM NaCl, 2 mM EDTA, 7 M guanidinium•HCl, centrifuged, and passed through a 0.2μm filter (Figure A.2A, Lane 7). Solubilized inclusions (1 mL) were added drop-wise to 49 mL of 50 mM Tris (pH 7.5), 10 μM betamercaptoethanol, 800 mM arginine, 100 mM NDSB 195 and 100 mM NaCl. The solution was incubated with gentle agitation for 2h, centrifuged, exchanged into Buffer B, concentrated, and stored at -80˚C.

The refolded protein was assessed by circular dichroism (CD) to show the protein was properly folded and not random coil (Figure A.2B). Spectra were acquired on an Applied Photophysics CS/2 Chirascan. Spectra were acquired in a 1 mm path length quartz cuvette at 1.2 s/nm with a 1 nm spectral bandwidth. The samples (0.3-0.5 mg/mL protein) were prepared in 10 mM potassium phosphate (pH 8.0), 100 mM potassium chloride, and 0.5 mM DTT. Multiple spectra of the same protein were collected, averaged, smoothed and background subtracted using the Chirascan software.

2.4 Expression of Met18 constructs in vivo

A yeast shuttle vector to express Met18 with a C-terminal HA tag from an *ADH* promoter was created by amplifying Met18 from pAV13 (Appendix) using primers AV71 and AV72 (Appendix Table 1.1). The pRS316 plasmid containing the ADH promoter and HA tag was used from the Walden lab. The plasmid was digested with BsaBI to cut out the Nbp35 gene. The resulting Met18 PCR product and digest were ligated by the Gibson Assembly method. The successful construction of pRS313-ADH-MET18-HA was confirmed by sequencing. The M4, M5, M6, R144 mutations were

generated by using AV71 and AV72 to amplify the mutated Met18 genes off pAV37, pAV38, pAV39, and R144 Met18 respectively. The N-terminal Met18 construct (1-331) was amplified off pAV29 using AV71 and AV73. The C-term Met18 (748-1032) was amplified off pAV29 using AV72 and AV74. The resulting mutated Met18 PCR products were then digested and ligated into the pRS316 plasmid as described above for the wild-type. These mutations were also confirmed by sequencing.

2.5 Expression and Purification of Cia1 Constructs

For N-terminally His-tagged Cia1 (HisCia1), the gene was amplified from plasmid ScCD00012999 obtained from DNASU stock center and inserted between EcoRI and NotI sites of pETDuet-1. For double-tagged Cia1 (dtCia1), the amino acids for a StrepII tag and a TEV protease site were inserted into the His-Cia1 vector by an inverse PCR amplification followed by circularization of the PCR product. The resulting dtCia1 vector encodes the following features in the following order: His tag, TEV protease site, StrepII-tag, Cia1.

HisCia1 and dtCia1 were expressed as described for dtCia2. Cells were resuspended in Buffer A with 5 mM betamercaptoethanol (BME) with protease inhibitor cocktail and DNase I. Following sonication and centrifugation, the clarified lysate was loaded on a HisBind column, washed with 50 CV resuspension buffer with 5 mM imidazole and eluted in the same buffer supplemented with 300 mM imidazole. Cia1 was dialyzed overnight against the resuspension buffer, concentrated, and stored at 80 1C. To obtain Strep-Cia1, the His-tag was removed from dtCia1 by the addition of His-tagged TEV protease (1 mg/mL). Following overnight incubation at room temperature, the

mixture was passed over a HisBind column and Strep-Cia1 was recovered from the flow-through (Figure A.3, Lane 1).

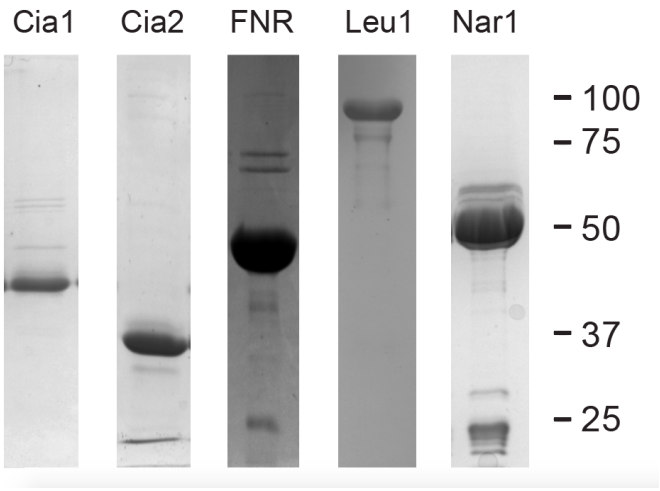

Figure A.3 Purification of CIA proteins and Targets.
SDS-PAGE of ^{His}Cia1 (Lane 1), refolded Cia2 (Lane 2), FNR^{SNAP} (Lane 3), ^{His}Leu1 (Lane 4), and ^{His}Nar1 as purified.

2.6 Expression and Purification of Cia2 Constructs

PCR amplified inserts were ligated into restriction enzyme digested vectors by the method of Gibson. DNA sequencing was used to confirm successful construction of the plasmids. For expression of untagged Cia2 in E. coli, the gene was amplified from yeast genomic DNA and ligated between the NcoI and NdeI digested pET15b plasmid. For double-tagged Cia2 (dtCia2), Cia2 was amplified and ligated between the BamHI and SalI sites of pET52b to encode a protein with the following features in the following order: Strep-II tag, thrombin protease cleavage site, Cia2, HRV3C protease cleavage site, and a 6xHis-tag. Δ102C-Cia2-forward and Cia2-reverse primers were used to delete the N-terminal domain of Cia2 via Q5 mutagenesis according to manufacturer's instructions (New England Biolabs). Forward and reverse primers containing the E208A and C161A

mutations for Cia2 were used to mutate these amino acids to alanine via Quikchange mutagenesis.[130] A forward primer containing a premature stop codon was used with a Cia2 reverse primer via Q5 mutagenesis to delete the last 5 amino acids of Cia2 and create the Δ5C construct. All constructs were confirmed by sequencing. E. coli BL21(DE3) transformed with the dtCia2 plasmid was grown at 37˚C, induced with IPTG (0.5 mM) at an OD600 of 0.7, and collected 4 h later.

Cells were lysed as described for ^{SUMO}Met18. The inclusion bodies were washed with 50 mM Tris pH 8, 100 mM NaCl, 1 mM EDTA, 1 mM DTT, 0.5% Triton X-100, 5% glycerol and a second time in the same buffer without the Triton X-100. The pellet was resuspended in 50 mM Tris pH 8, 200 mM NaCl, 2 mM EDTA, 7 M GuHCl. Denatured Cia2 (1 mL) was added dropwise to 49 mL of 50 mM Tris pH 8, 25 mM NaCl, 5% glycerol, 1 mM EDTA, 1 mM DTT. Refolding of the Cia2 mutants was enhanced by the additional inclusion of 500 mM arginine in the refolding buffer. Two hours after the rapid dilution, the mixture was centrifuged, concentrated, buffer exchanged, and stored at -80˚C. The refolded protein was assessed by circular dichroism (CD) to show the protein was properly folded and not random coil as described for Met18 above (Figure 2.5.1, Lane 2).

2.7 Expression of Cia2 Constructs in vivo in yeast

A yeast shuttle vector to express Cia2 with a C-terminal MYC tag from an *ADH* promoter was created by amplifying Cia2 from the BG1805 gateway destination vector (YSC3869-202333236, Dharmacon, GE Lifesciences) using primers yCia2-forward and -reverse (Table A1.1). The pRS313 (HIS3, centromeric) vector was amplified with

primers 313-forward and -reverse (Table A1.1). These two resulting PCR products were ligated by the Gibson Assembly method. To insert the ADH promoter, it was amplified by PCR from p316ADH using primers ADH-forward and -reverse (Table A1.1) and was cloned into the *EcoRV* and *SalI* digested vector also using the Gibson Assembly method.[126] The successful construction of pRS313-ADH-CIA2-MYC was confirmed by sequencing. The primers mentioned in the sections above were used with the p316ADH Cia2 plasmid to generate the other truncations and mutations and also confirmed by sequencing.

2.8 Expression and Purification of FNR

FNR was amplified from *E. coli* genomic DNA with primers JDG03 and JDG04 (Table A1.1) and inserted via Gibson assembly between the *NdeI* and *BamHI* sites of modified pET15b plasmid (see Leu1 cloning) to create pJDG04. The resulting His-TEV-FNR was subcloned between the *NdeI* and *HindIII* sites of pSNAP-tag(T7)-2 (New England Biolabs) by amplification with primers JDG16 and JDG17. This inserted His-TEV-FNR in frame with the C-terminal SNAP tag creating pCG05.

Expression of FNR was achieved as described ^{His}Met18. The cell paste was resuspended in Buffer C (50 mM potassium phosphate, 0.1 M KCl, 10% glycerol, pH 6.8) supplemented with 1mM PMSF, lysozyme (1mg/mL) and DNase nuclease. The cells were disrupted by sonication. The soluble lysate was batch absorbed to His-Bind resin. Resin was washed with Buffer C containing 5-20 mM imidazole over 40 CV, and eluted with Buffer C with 350 mM imidazole. FNR was concentrated, and dialyzed against Buffer C supplemented with 5mM DTT (Figure 2.5.1, Lane 3). Labeling of FNR with a

fluorescent SNAP substrate was carried out according to manufacturer's instructions (NEB).

2.9 Expression and Purification of Leu1

Leu1 was amplified from genomic DNA by primers MP01 and MP02 (Table S1) and inserted between the *NdeI* and *XhoI* sites of a modified pET15b vector where the thrombin protease site was replaced by a TEV protease site.[126] The resulting plasmid was used to express Leu1 with an N-terminal His-TEV tag. Leu1 was expressed as described above for ^{His}Met18 except the cells were induced for 16h at 15˚C.

To purify Leu1, cell paste was resuspended and lysed as described for ^{His}Met18. The soluble lysate was treated with streptomycin sulfate (1% w/v). The supernatant was then batch adsorbed to nickel affinity resin. The resin was washed with ≥100 CV Buffer A containing 5-30 mM imidazole and eluted with Buffer A supplemented with 300 mM imidazole. Leu1 was dialyzed and concentrated as described for ^{His}Met18. UV/Vis spectra of purified Leu1 and ferrozine iron assays did not reveal a significant amount of iron associated with Leu1, suggesting it is purified predominantly in the apo-form. To remove the His-tag, ^{His}Leu1 was incubated with His-tagged TEV protease then the mixture was passed over IMAC resin. Untagged Leu1 was recovered from the flow-through (Figure 2.5.1, Lane 4).

2.10 Expression and Purification of Nar1

Nar1 was amplified from plasmid ScCD00011645 obtained from DNASU (the DNA repository at Arizona State University) with primers AV05 and AV06 (Table A1.1)

and inserted between *NdeI* and *XhoI* sites of pRSF-Duet via Gibson ligation to create construct AV03, or untagged Nar1.[126] Next, Nar1 pRSFduet plasmid was amplified using primers MM01 and JC02 and the PCR product was circularized using Q5 mutagenesis (NEB). This placed His-TEV in frame with Nar1 on the N-terminus to generate construct MM01. ^{HisTEV}Nar1 expressed in *E. coli* BL21 (DE3) grown at 37˚C to an OD_{600} of 0.9-1.0. IPTG (1 mM) was added, the temperature was lowered to 30˚C and the cells were collected 4 h later.

To purify Nar1, cell paste was resuspended and lysed as described for ^{His}Met18. The soluble extract was added to nickel affinity resin. The resin was washed with ≥100 CV Buffer A containing 5-30 mM imidazole and eluted with Buffer A supplemented with 300 mM imidazole. The elution fractions were concentrated down by amicon filter and then buffer exchanged over a PD10 column and stored at -80˚C (Figure A.3, Lane 5).

2.11 Expression and Purification of Rad3

Rad3 was amplified from plasmid ScCD00012711 obtained from DNASU (the DNA repository at Arizona State University) with primers AV13 and AV14 (Table A1.1) and inserted between *NdeI* and *XhoI* sites of pRSF-Duet via Gibson ligation to create plasmid pAV08.[126] Expression for Rad3 was as described for ^{His}Met18 except the temperature was lowered to 25˚C after IPTG addition.

To refold Rad3, the cell paste was resuspended, lysed, and centrifuged as described for the Met18 refolding. The solubilized inclusion bodies were also prepared in the same way as the Met18 inclusions. Solubilized inclusions (1 mL) were added drop-wise to 49 mL of 50 mM Tris (pH 7.5), 10 µM betamercaptoethanol, 800 mM arginine,

and 100 mM KCl. The solution was incubated with gentle agitation for 2h, centrifuged, exchanged into Buffer B, concentrated, and stored at -80˚C. The refolded protein was assessed by circular dichroism (CD) to show the protein was properly folded and not random coil as described above for Cia2 and Met18 (Figure A.4).

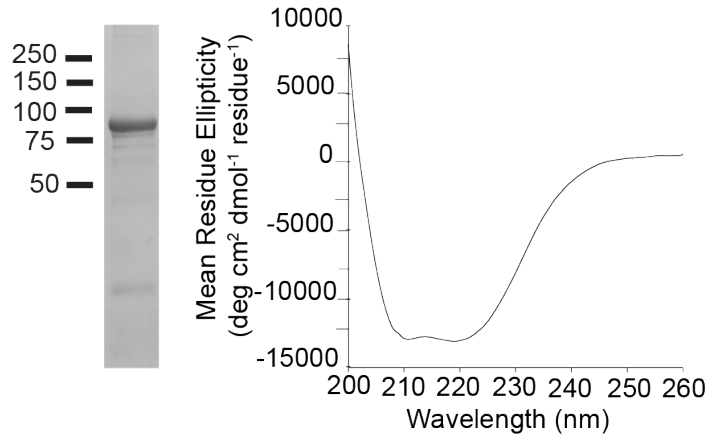

Figure A.4 SDS-PAGE and CD analysis of refolded Rad3
(89 kDa, migration of molecular weight standards in kDa are indicated). The CD spectrum of Rad3 (3 μM) was acquired in 10 mM KPO_4 and 100 mM NaCl buffer and demonstrates a significant amount of secondary structure content consistent with proper refolding of Rad3.

Appendix 3: Electron Microscopy Stoichiometry Conditions

Table A3.1 MCC Complex Mixture for EM samples 03/30/2016

Subunit	[Start] uM	ng/uL	uL	[Final] uM	Molar Ratio	[Final] ng/uL
Met18	4	472	150	1.2	0.4	150
Cia2	7	205	300	5.1	1.7	131
^{His} Cia1	70	2609	20	3	1.0	111
Total			470			393

Table A3.2 MCC Complex Mixture for EM samples 06/09/2016

Subunit	[Start] uM	ng/uL	uL	[Final] uM	Molar Ratio	[Final] ng/uL
Met18	10	1179	150	2.21	0.6	260
Cia2	20	514	500	14.71	3.8	378
^{His} Cia1	88	3432	30	3.88	1.0	151
Total			680			789

Table A3.3 MCC Complex Mixture for EM samples 11/16/2017

Subunit	[Start] uM	ng/uL	uL	[Final] uM	Molar Ratio	[Final] ng/uL
Met18	30	3536	120	3.43	0.8	404
Cia2	20	514	900	17.14	3.8	440
^{His} Cia1	160	6240	30	4.57	1.0	178
Total			1050			1023

Table A3.4 MCCN Complex Mixture for EM samples 11/16/2017

Subunit	[Start] uM	ng/uL	uL	[Final] uM	Molar Ratio	[Final] ng/uL
Met18	30	3536	80	2.29	0.8	269
Cia2	20	514	600	11.43	3.8	293
^{His} Cia1	160	5964	20	3.05	1.0	114
Nar1	20	1083	350	6.67	2.2	361
Total			1050			1037

Appendix 4: Investigations with other FeS Target Proteins

4.1 Original Plasmid Table

Table A4.1 Original Plasmids

Gene	Backbone	Antibiotic Resistance	Source/Description
Rli1	pYes2	Ampicillin	Rachel Greene
Rli1	pRSFduet	Kanamycin	Gene inserted into pRSFduet by Gibson Assembly using primers AV36 an AV37
RTEL1	Unknown	Ampicillin	Huang Ding
Dna2		Ampicillin	Jacqueline Barton and Judith Campell's Labs
Pol3	pRSFduet	Kanamycin	Genomic DNA C-terminal Domain () inserted into pRSFduet by Gibson Assembly using primers
^{SUMO}Pol3	pRSFduet	Kanamycin	Genomic DNA SUMO-tagged C-terminal Domain () inserted into pRSFduet by Gibson Assembly using primers CQ06 and CQ07
Chl1	pRSFduet	Kanamycin	Genomic DNA N-terminal Domain (1-612) inserted into pRSFduet by Gibson Assembly using primers AV57 and AV58

4.2 Primers to clone Target Proteins

Table A4.2 Primers to clone Target Proteins

Name	Backbone	Gene/Use	Sequence (5'→3')
AV36	pRSFduet	^{His}Rli1	AGCCATCACCATCATCACCACAG CCAGGATCCGAATTCGATGAGTGATAAA
AV37	pRSFduet	^{His}Rli1	TGTTCGACTTAAGCATTATGCGGC CGCAAGCTTGTCGACTTAAATACCGGT
AV57	pRSFduet	Chl1^{STREPx2}	GAAACCCTGTATTTCCAGGGCC ATATGGACAAAAAGGAATATTCG
AV58	pRSFduet	Chl1^{STREPx2}	CGCACGACGGGTTTCTTTACCAGAC TCGAGTTAATGATTGCAGCACAAGGT
CI01	pRSFduet	Pol3	AGCCATCACCATCATCACCACAGCCAGGATC CGAATTCGATGGGTATGTTCGTTGTGAAATCC
CI02	pRSFduet	Pol3	TGTTCGACTTAAGCATTACC ATTTGCTTAATTGTTCTAC
CQ01	pTB146	^{SUMO}Chl1	AGTTAAGTATAAGAAGGAGATATACA TATGAAGTTTTATATAGATGATTTACCA
CQ05	pTB146	^{SUMO}Chl1	AGTCACCCGGGCTCGAGTT TAATGATTGCACGACAAGG
CQ06	pTB146	^{SUMO}Pol3	CTCCGTCGACAAGCTTACGG TATGTTCGTTGTGAAATCCA
CQ07	pTB146	^{SUMO}Pol3	AGTCACCCGGGCTCGAGTTTA CCATTTGCTTAATTGTTCTAC

4.3 Bacterial Expression and Purification of Rli1

N-terminally His-tagged Rli1 (^{His}Rli1) was created by amplifying Rli1 from the plasmid from the Greene lab (Appendix Table 4.1) using primers AV36 and AV37 (Appendix Table 4.2) and inserting Rli1 between the EcoR1 and SalI sites of the pRSF-Duet vector via the Gibson DNA assembly method.[126] ^{His}Rli1 expressed in *E. coli* BL21(DE3) was grown at 37˚C to an OD_{600} of 0.7-0.8. IPTG (1 mM) and the cells were collected 4 h later.

Cells were resuspended in Buffer A (50 mM Tris (pH 8.0), 100 mM NaCl, 10% glycerol) with 5 mM betamercaptoethanol (BME) with protease inhibitor cocktail and DNase I. Following sonication and centrifugation, the clarified lysate was loaded on a HisBind column (Figure A.5A, Lanes 1-4), washed with 50 CV resuspension buffer with 5 mM imidazole (Figure A.5A, Lanes 5-7) and eluted in the same buffer supplemented with 300 mM imidazole. Rli1 was buffer exchanged by a PD10 column and stored at -80˚C.

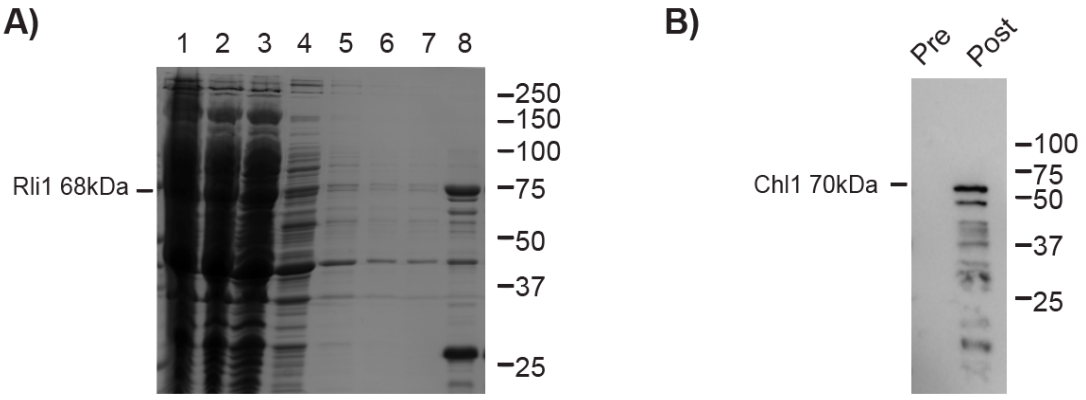

Figure A.5 Purification of Rli1 and Expression of Chl1.
A) An SDS PAGE gel shows Rli1 lysate (Lane 1) was clarified by centrifugation and the supernatant (Lane 2) was loaded onto the column and the pellet (Lane 3) was discarded. The flow-through for the column (Lane 4) indicated some protein bound to column and the proteins that were not of interest were washed off the column (Lane 5, 6, and 7). The purified Rli1

contained some IMAC binding contaminants (Lane 8). B) An anti-streptactin western blot shows that Chl1 expressed in the post induction sample, but expression was poor as it was not detected by SDS-PAGE and there appears to be some stalled translation products.

The resulting protein purification showed some contaminants and expression needs to be optimized to obtain a purer, larger quantity of the protein (Figure A.5A, Lane 8).

4.4 Bacterial Expression of NTD Chl1

N-terminally Double strep-tagged N-terminal domain Chl1 ($Chl1^{Strepx2}$) was created by amplifying Chl1 from yeast genomic DNA (Appendix Table 4.1) using primers AV57 and AV58 (Appendix Table 4.2) and inserting Chl1 in the XhoI site of the pRSF-Duet vector via the Gibson DNA assembly method. [126] The pRSF-Duet vector had a double strep-tag with a linker added previously with primers by Q5 mutagenesis, designed by John Grossman. $Chl1^{Strepx2}$ was expressed in *E. coli* BL21(DE3) was grown at 37˚C to an OD_{600} of 0.7-0.8. IPTG (1 mM) and the cells were collected 4 h later.

The expression of Chl1 needs to be optimized. An anti-strep western showed a small amount of expression of Chl1, but with N-terminally strep-tagged products that are likely due to prematurely terminated translation products (Figure A.5B, Lane 2). In attempt to increase protein expression we designed primers CQ01 and CQ05 to amplify Chl1 from genomic DNA and insert Chl1 in the NotI site of the pTB136 plasmid via Gibson Assembly so that the resulting plasmid would put the SUMO tag in frame with the Chl1 gene.[126] However, the construction of the plasmid was halted due to difficulties with obtaining the PCR product.

4.5 Bacterial Expression and Purification of CTD Pol3

CTD ^{SUMO}Pol3 was amplified from genomic DNA with primers CI01 and CI02 (Table 6.1) and inserted between *EcoRI* and *SalI* sites of pRSF-Duet via Gibson ligation. For SUMO Pol3 CTD ^{SUMO}Pol3 was amplified from the previously described plasmid with primers CQ06 and CQ07 and inserted in the *NotI* site of the pTB146 plasmid via Gibson ligation.[126] ^{SUMO}Pol3 was expressed in E. coli BL21(DE3) was grown at 37˚C to an OD600 of 0.7-0.8. IPTG (1 mM) and the cells were collected 4 h later.

To refold CTD ^{SUMO}Pol3, the cell paste was resuspended, lysed, and centrifuged as described for the previous protein refoldings (Figure A.6A). The solubilized inclusion bodies were also prepared in the same way. Solubilized inclusions (1 mL) were added drop-wise to 49 mL of 50 mM Tris (pH 7.5), 10 μM betamercaptoethanol, 800 mM arginine, 100 mM NDSB-195, and 100 mM NaCl. The solution was incubated with gentle agitation for 2h, centrifuged, exchanged into Buffer B, concentrated, and stored at -80˚C.

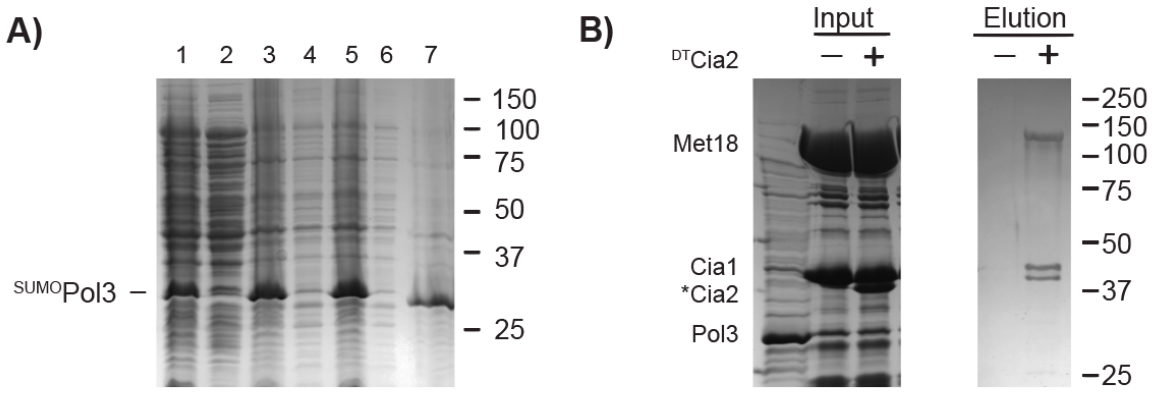

Figure A.6 Purification of Pol3
Denaturation of Pol3 and an SDS-PAGE analysis of affinity copurification to determine Pol3 binding with the core targeting complex. A) An SDS PAGE gel shows Pol3 cells were lysed (Lane 1), then centrifuged and the supernatant was discarded (Lane 2). The resulting pellet (Lane 3) was resuspended and excess protein was discarded in wash (Lane 4). This was repeated (Lane 5 and Lane 6). The protein was then denatured in GndHCl (Lane 7), which was then refolded. B) Refolded SUMOPol3 (Lane1), HisCia1, SUMOMet18, and DTCia2 were mixed (input) and separated via streptactin resin. DTCia2 can specifically retain HisCia1 and SUMOMet18, but not SUMOPol3 (elution) whereas no bands are detected in the control in which DTCia2 was omitted (Lane 4). Molecular weight standards in kDa are shown to the right of all the gels.

We explored CTD SUMOPol3's ability to bind to the core targeting complex. No CTD SUMOPol3 co-eluted with the targeting complex. This indicates to us that the C-terminal domain of SUMOPol3 does not bind or its interaction with the targeting complex is too weak to be detected by our co-affinity purification method (Figure A.6B).

REFERENCES

1. V. D. Paul and R. Lill, Biogenesis of cytosolic and nuclear iron–sulfur proteins and their role in genome stability, *Biochimica et Biophysica Acta - Molecular Cell Research*, 2015, **1853**, 1528-1539.

2. J. O. Fuss, C.-L. Tsai, J. P. Ishida and J. A. Tainer, Emerging critical roles of Fe-S clusters in DNA replication and repair, *Biochimica et Biophysica Acta* , 2015, **1853**, 1253-1271.

3. D. C. Johnson, D. R. Dean, A. D. Smith and M. K. Johnson, Structure, function, and formation of biological iron-sulfur clusters, *Annual Review of Biochemistry*, 2005, **74**, 247-281.

4. C. Ayala-Castro, A. Saini and F. W. Outten, Fe-S Cluster Assembly Pathways in Bacteria, *Microbiology and Molecular Biology Reviews*, 2008, **72**, 110-125.

5. A. D. Tsaousis, E. Gentekaki, L. Eme, D. Gaston and A. J. Roger, Evolution of the cytosolic iron-sulfur cluster assembly machinery in Blastocystis species and other microbial eukaryotes, *Eukaryotic Cell*, 2014, **13**, 143-153.

6. A. G. Albrecht, D. J. A. Netz, M. Miethke, A. J. Pierik, O. Burghaus, F. Peuckert, R. Lill and M. A. Marahiel, SufU Is an Essential Iron-Sulfur Cluster Scaffold Protein in Bacillus subtilis, *Journal of Bacteriology*, 2010, **192**, 1643-1651.

7. O. Stehling, J. Mascarenhas, A. A. Vashisht, A. D. Sheftel, B. Niggemeyer, R. Rösser, A. J. Pierik, J. A. Wohlschlegel and R. Lill, Human CIA2A-FAM96A and CIA2B-FAM96B integrate iron homeostasis and maturation of different subsets of cytosolic-nuclear iron-sulfur proteins., *Cell Metabolism*, 2013, **18**, 187-198.

8. T. A. Rouault, Biogenesis of iron-sulfur clusters in mammalian cells: new insights and relevance to human disease, *Disease Models & Mechanisms*, 2012, **5**, 155-164.

9. J. L. Weon, S. W. Yang and P. R. Potts, Cytosolic Iron-Sulfur Assembly Is Evolutionarily Tuned by a Cancer-Amplified Ubiquitin Ligase, *Molecular Cell*, **69**, 113-125.e116.

10. J.-L. Zhang, H.-Y. Wang, Q. Yang, S.-Y. Lin, G.-Y. Luo, R. Zhang and G.-L. Xu, Methyl-methanesulfonate sensitivity 19 expression is associated with metastasis and chemoradiotherapy response in esophageal cancer, *World Journal of Gastroenterology*, 2015, **21**, 4240-4247.

11. O. Levran, C. Attwooll, R. T. Henry, K. L. Milton, K. Neveling, P. Rio, S. D. Batish, R. Kalb, E. Velleuer, S. Barral, J. Ott, J. Petrini, D. Schindler, H.

Hanenberg and A. D. Auerbach, The BRCA1-interacting helicase BRIP1 is deficient in Fanconi anemia, *Nature Genetics*, 2005, **37**, 931.

12. D. J. A. Netz, J. Mascarenhas, O. Stehling, A. J. Pierik and R. Lill, Maturation of cytosolic and nuclear iron-sulfur proteins, *Trends in Cell Biology*, **24**, 303-312.

13. A. K. Sharma, L. J. Pallesen, R. J. Spang and W. E. Walden, Cytosolic Iron-Sulfur Cluster Assembly (CIA) System: Factors, Mechanism, and Relevance to Cellular Iron Regulation, *Journal of Biological Chemistry*, 2010, **285**, 26745-26751.

14. H. Li, D. T. Mapolelo, N. N. Dingra, S. G. Naik, N. S. Lees, B. M. Hoffman, P. J. Riggs-Gelasco, B. H. Huynh, M. K. Johnson and C. E. Outten, The yeast iron regulatory proteins Grx3/4 and Fra2 form heterodimeric complexes containing a [2Fe-2S] cluster with cysteinyl and histidyl ligation, *Biochemistry*, 2009, **48**, 9569-9581.

15. H. Li, M. Stümpfig, C. Zhang, X. An, J. Stubbe, R. Lill and M. Huang, The diferric-tyrosyl radical cluster of ribonucleotide reductase and cytosolic iron-sulfur clusters have distinct and similar biogenesis requirements, *Journal of Biological Chemistry*, 2017, **292**, 11445-11451.

16. U. Mühlenhoff, S. Molik, J. R. Godoy, M. A. Uzarska, N. Richter, A. Seubert, Y. Zhang, J. Stubbe, F. Pierrel, E. Herrero, C. H. Lillig and R. Lill, Cytosolic Monothiol Glutaredoxins Function in Intracellular Iron Sensing and Trafficking via Their Bound Iron-Sulfur Cluster, *Cell Metabolism*, 2010, **12**, 373-385.

17. D. J. A. Netz, M. Stümpfig, C. Doré, U. Mühlenhoff, A. J. Pierik and R. Lill, Tah18 transfers electrons to Dre2 in cytosolic iron-sulfur protein biogenesis, *Nature Chemical Biology*, 2010, **6**, 758.

18. D. J. A. Netz, A. J. Pierik, M. Stümpfig, U. Mühlenhoff and R. Lill, The Cfd1–Nbp35 complex acts as a scaffold for iron-sulfur protein assembly in the yeast cytosol, *Nature Chemical Biology*, 2007, **3**, 278.

19. A. Hausmann, D. J. Aguilar Netz, J. Balk, A. J. Pierik, U. Mühlenhoff and R. Lill, The eukaryotic P loop NTPase Nbp35: An essential component of the cytosolic and nuclear iron–sulfur protein assembly machinery, *Proceedings of the National Academy of Sciences of the United States of America*, 2005, **102**, 3266-3271.

20. A. Roy, N. Solodovnikova, T. Nicholson, W. Antholine and W. E. Walden, A novel eukaryotic factor for cytosolic Fe–S cluster assembly, *EMBO Journal*, 2003, **22**, 4826-4835.

21. K. Gari, A. M. León Ortiz, V. Borel, H. Flynn, J. M. Skehel and S. J. Boulton, MMS19 links cytoplasmic iron-sulfur cluster assembly to DNA metabolism., *Science*, 2012, **337**, 243-245.

22. O. Stehling, A. A. Vashisht, J. Mascarenhas, Z. O. Jonsson, T. Sharma, D. J. A. Netz, A. J. Pierik, J. A. Wohlschlegel and R. Lill, MMS19 Assembles Iron-Sulfur Proteins Required for DNA Metabolism and Genomic Integrity, *Science*, 2012, **337**, 195-199.

23. J. Balk, D. J. Aguilar Netz, K. Tepper, A. J. Pierik and R. Lill, The essential WD40 protein Cia1 is involved in a late step of cytosolic and nuclear iron-sulfur protein assembly, *Molecular and Cellular Biology*, 2005, **25**, 10833-10841.

24. J. Balk, A. J. Pierik, D. J. Netz, U. Muhlenhoff and R. Lill, The hydrogenase-like Nar1p is essential for maturation of cytosolic and nuclear iron-sulphur proteins, *EMBO Journal*, 2004, **23**, 2105-2115.

25. M. Seki, Y. Takeda, K. Iwai and K. Tanaka, IOP1 Protein Is an External Component of the Human Cytosolic Iron-Sulfur Cluster Assembly (CIA) Machinery and Functions in the MMS19 Protein-dependent CIA Pathway, *Journal of Biological Chemistry*, 2013, **288**, 16680-16689.

26. N. van Wietmarschen, A. Moradian, G. B. Morin, P. M. Lansdorp and E.-J. Uringa, The Mammalian Proteins MMS19, MIP18, and ANT2 Are Involved in Cytoplasmic Iron-Sulfur Cluster Protein Assembly. *Journal of Biological Chemistry*, 2012, **287**, 43351-43358.

27. J. Balk, A. J. Pierik, D. J. Aguilar Netz, U. Mühlenhoff and R. Lill, Nar1p, a conserved eukaryotic protein with similarity to Fe-only hydrogenases, functions in cytosolic iron-sulphur protein biogenesis, *Biochemical Society Transactions*, 2005, **33**, 86-89.

28. E. Urzica, A. J. Pierik, U. Mühlenhoff and R. Lill, Crucial Role of Conserved Cysteine Residues in the Assembly of Two Iron−Sulfur Clusters on the CIA Protein Nar1, *Biochemistry*, 2009, **48**, 4946-4958.

29. Y. Nicolet and J. C. Fontecilla-Camps, Structure-Function Relationships in [FeFe]-Hydrogenase Active Site Maturation, *Journal of Biological Chemistry*, 2012, **287**, 13532-13540.

30. D. S. Horner, B. Heil, T. Happe and T. M. Embley, Iron hydrogenases – ancient enzymes in modern eukaryotes, *Trends in Biochemical Sciences*, **27**, 148-153.

31. E. L. Bastow, K. Bych, J. C. Crack, N. E. Le Brun and J. Balk, NBP35 interacts with DRE2 in the maturation of cytosolic iron-sulphur proteins in Arabidopsis thaliana, *The Plant Journal*, 2017, **89**, 590-600.

32. V. Srinivasan, D. J. A. Netz, H. Webert, J. Mascarenhas, A. J. Pierik, H. Michel and R. Lill, Structure of the yeast WD40 domain protein Cia1, a component acting late in iron-sulfur protein biogenesis, *Structure*, 2007, **15**, 1246-1257.

33. P.-Y. Goh and U. Surana, Cdc4, a Protein Required for the Onset of S Phase, Serves an Essential Function during G(2)/M Transition in Saccharomyces cerevisiae, *Molecular and Cellular Biology*, 1999, **19**, 5512-5522.

34. D. G. Lambright, J. Sondek, A. Bohm, N. P. Skiba, H. E. Hamm and P. B. Sigler, The 2.0 Å crystal structure of a heterotrimeric G protein, *Nature*, 1996, **379**, 311.

35. I. Garcia-Higuera, C. Gaitatzes, T. F. Smith and E. J. Neer, Folding a WD Repeat Propeller: Role of highly conserved aspartic acid residues in the G protein β subunit and Sec13, *Journal of Biological Chemistry*, 1998, **273**, 9041-9049.

36. C. E. Ford, N. P. Skiba, H. Bae, Y. Daaka, E. Reuveny, L. R. Shekter, R. Rosal, G. Weng, C.-S. Yang, R. Iyengar, R. J. Miller, L. Y. Jan, R. J. Lefkowitz and H. E. Hamm, Molecular Basis for Interactions of G Protein βγ Subunits with Effectors, *Science*, 1998, **280**, 1271.

37. B. H. Jennings and D. Ish-Horowicz, The Groucho/TLE/Grg family of transcriptional co-repressors, *Genome Biology*, 2008, **9**, 205.

38. O. Goldenberg, E. Erez, G. Nimrod and N. Ben-Tal, The ConSurf-DB: pre-calculated evolutionary conservation profiles of protein structures, *Nucleic Acids Research*, 2009, **37**, D323-D327.

39. D. Luo, D. G. Bernard, J. Balk, H. Hai and X. Cui, The DUF59 Family Gene AE7 Acts in the Cytosolic Iron-Sulfur Cluster Assembly Pathway to Maintain Nuclear Genome Integrity in <em>Arabidopsis</em&gt, *The Plant Cell*, 2012, **24**, 4135.

40. A. T. Vo, N. M. Fleischman, M. D. Marquez, E. J. Camire, S. U. Esonwune, J. D. Grossman, K. A. Gay, J. A. Cosman and D. Perlstein, Defining the domains of Cia2 required for its essential function in vivo and in vitro, *Metallomics*, 2017, DOI: 10.1039/C7MT00181A.

41. S. Hunter, R. Apweiler, T. K. Attwood, A. Bairoch, A. Bateman, D. Binns, P. Bork, U. Das, L. Daugherty, L. Duquenne, R. D. Finn, J. Gough, D. Haft, N. Hulo, D. Kahn, E. Kelly, A. Laugraud, I. Letunic, D. Lonsdale, R. Lopez, M. Madera, J. Maslen, C. McAnulla, J. McDowall, J. Mistry, A. Mitchell, N. Mulder, D. Natale, C. Orengo, A. F. Quinn, J. D. Selengut, C. J. A. Sigrist, M. Thimma, P. D. Thomas, F. Valentin, D. Wilson, C. H. Wu and C. Yeats, InterPro: the integrative protein signature database, *Nucleic Acids Research*, 2009, **37**, D211-D215.

42. K. Zumbrennen, M. Wallander, S. Romney and E. Leibold, Cysteine Oxidation Regulates the RNA-Binding Activity of Iron Regulatory Protein 2, *Molecular and Cellular Biology*, 2009, **29**, 2219.

43. A. A. Mashruwala, S. Bhatt, S. Poudel, E. S. Boyd and J. M. Boyd, The DUF59 Containing Protein SufT Is Involved in the Maturation of Iron-Sulfur (FeS) Proteins during Conditions of High FeS Cofactor Demand in Staphylococcus aureus, *PLoS Genetics*, 2016, **12**, e1006233.

44. A. M. Grishin, E. Ajamian, L. Tao, L. Zhang, R. Menard and M. Cygler, Structural and Functional Studies of the Escherichia coli Phenylacetyl-CoA Monooxygenase Complex, *The Journal of Biological Chemistry*, 2011, **286**, 10735-10743.

45. S. Schwenkert, D. J. A. Netz, J. Frazzon, A. J. Pierik, E. Bill, J. Gross, R. Lill and J. Meurer, Chloroplast HCF101 is a scaffold protein for [4Fe-4S] cluster assembly, *Biochemical Journal*, 2010, **425**, 207-214.

46. E. Weerapana, C. Wang, G. M. Simon, F. Richter, S. Khare, M. B. D. Dillon, D. A. Bachovchin, K. Mowen, D. Baker and B. F. Cravatt, Quantitative reactivity profiling predicts functional cysteines in proteomes, *Nature*, 2010, **468**, 790-795.

47. E. Weerapana, C. Wang, G. M. Simon, F. Richter, S. Khare, M. B. D. Dillon, D. A. Bachovchin, K. Mowen, D. Baker and B. F. Cravatt, Quantitative reactivity profiling predicts functional cysteines in proteomes, *Nature*, 2010, **468**, 790-795.

48. K.-E. Chen, A. A. Richards, J. K. Ariffin, I. L. Ross, M. J. Sweet, S. Kellie, B. Kobe and J. L. Martin, The mammalian DUF59 protein Fam96a forms two distinct types of domain-swapped dimer, *Acta Crystallographica. Section D-Biological Crystallography*, 2012, **68**, 637-648.

49. L. Prakash and S. Prakash, Three additional genes involved in pyrimidine dimer removal in Saccharomyces cerevisiae: RAD7, RAD14 and MMS19, *Molecular and General Genetics*, 1979, **176**, 351-359.

50. H. Kou, Y. Zhou, R. M. C. Gorospe and Z. Wang, Mms19 protein functions in nucleotide excision repair by sustaining an adequate cellular concentration of the TFIIH component Rad3, *Proceedings of the National Academy of Sciences of the United States of America*, 2008, **105**, 15714.

51. S. Ito, L. J. Tan, D. Andoh, T. Narita, M. Seki, Y. Hirano, K. Narita, I. Kuraoka, Y. Hiraoka and K. Tanaka, MMXD, a TFIIH-independent XPD-MMS19 protein complex involved in chromosome segregation, *Molecular Cell*, 2010, **39**, 632-640.

52. S. H. Askree, T. Yehuda, S. Smolikov, R. Gurevich, J. Hawk, C. Coker, A. Krauskopf, M. Kupiec and M. J. McEachern, A genome-wide screen for Saccharomyces cerevisiae deletion mutants that affect telomere length, *Proceedings of the National Academy of Sciences of the United States of America*, 2004, **101**, 8658.

53. C.-G. Duan, X. Wang, K. Tang, H. Zhang, S. K. Mangrauthia, M. Lei, C.-C. Hsu, Y.-J. Hou, C. Wang, Y. Li, W. A. Tao and J.-K. Zhu, MET18 Connects the Cytosolic Iron-Sulfur Cluster Assembly Pathway to Active DNA Demethylation in Arabidopsis, *PLoS Genetics*, 2015, **11**, e1005559.

54. H. Takano and J. F. Gusella, The predominantly HEAT-like motif structure of huntingtin and its association and coincident nuclear entry with dorsal, an NF-kB/Rel/dorsal family transcription factor, *BMC Neuroscience*, 2002, **3**, 15-15.

55. A. Grinthal, I. Adamovic, B. Weiner, M. Karplus and N. Kleckner, PR65, the HEAT-repeat scaffold of phosphatase PP2A, is an elastic connector that links force and catalysis, *Proceedings of the National Academy of Sciences of the United States of America*, 2010, **107**, 2467.

56. Y. Nobumori, G. P. Shouse, L. Fan and X. Liu, HEAT Repeat 1 Motif Is Required for B56γ-containing Protein Phosphatase 2A (B56γ-PP2A) Holoenzyme Assembly and Tumor-suppressive Function, *The Journal of Biological Chemistry*, 2012, **287**, 11030-11036.

57. A. F. Neuwald and T. Hirano, HEAT Repeats Associated with Condensins, Cohesins, and Other Complexes Involved in Chromosome-Related Functions, *Genome Research*, 2000, **10**, 1445-1452.

58. Y. Cheng, X. Dai and Y. Zhao, AtCAND1, A HEAT-Repeat Protein That Participates in Auxin Signaling in Arabidopsis, *Plant Physiology*, 2004, **135**, 1020-1026.

59. L. Queimado, M. Rao, R. A. Schultz, E. V. Koonin, L. Aravind, T. Nardo, M. Stefanini and E. C. Friedberg, Cloning the human and mouse MMS19 genes and functional complementation of a yeast mms19 deletion mutant, *Nucleic Acids Research*, 2001, **29**, 1884-1891.

60. D. C. Odermatt and K. Gari, The CIA Targeting Complex Is Highly Regulated and Provides Two Distinct Binding Sites for Client Iron-Sulfur Proteins, *Cell Reports*, 2017, **18**, 1434-1443.

61. A. T. V. Vo, N. M. Fleischman, M. J. Froehlich, C. Y. Lee, J. A. Cosman, C. A. Glynn, Z. O. Hassan and D. L. Perlstein, Identifying the protein interactions of the cytosolic iron sulfur cluster targeting complex essential for its assembly and recognition of apo-targets, *Biochemistry*, 2017, DOI: 10.1021/acs.biochem.7b00072.

62. A. A. Vashisht, C. C. Yu, T. Sharma, K. Ro and J. A. Wohlschlegel, The Association of the Xeroderma Pigmentosum Group D DNA Helicase (XPD) with Transcription Factor IIH Is Regulated by the Cytosolic Iron-Sulfur Cluster Assembly Pathway, *Journal of Biological Chemistry*, 2015, **290**, 14218-14225.

63. T. N. Moiseeva, A. M. Gamper, B. L. Hood, T. P. Conrads and C. J. Bakkenist, Human DNA polymerase ε is phosphorylated at serine-1940 after DNA damage and interacts with the iron-sulfur complex chaperones CIAO1 and MMS19, *DNA Repair*, 2016, **43**, 9-17.

64. A. S. Upadhyay, K. Vonderstein, A. Pichlmair, O. Stehling, K. L. Bennett, G. Dobler, J. T. Guo, G. Superti-Furga, R. Lill, A. K. Overby and F. Weber, Viperin is an iron-sulfur protein that inhibits genome synthesis of tick-borne encephalitis virus via radical SAM domain activity, *Cellular Microbiology*, 2014, **16**, 834-848.

65. X.-H. Wu, Y. Wang, Z. Zhuo, F. Jiang and Y.-D. Wu, Identifying the Hotspots on the Top Faces of WD40-Repeat Proteins from Their Primary Sequences by β-Bulges and DHSW Tetrads, *PLoS ONE*, 2012, **7**, e43005.

66. I. Lev, M. Volpe, L. Goor, N. Levinton, L. Emuna and S. Ben-Aroya, Reverse PCA, a Systematic Approach for Identifying Genes Important for the Physical Interaction between Protein Pairs, *PLoS Genetics*, 2013, **9**, e1003838.

67. F. Sievers, A. Wilm, D. Dineen, T. J. Gibson, K. Karplus, W. Li, R. Lopez, H. McWilliam, M. Remmert, J. Söding, J. D. Thompson and D. G. Higgins, Fast, scalable generation of high-quality protein multiple sequence alignments using Clustal Omega, *Molecular Systems Biology*, 2011, **7**, 539-539.

68. M. D. Hatfield, A. M. C. Reis, D. Obeso, J. R. Cook, D. M. Thompson, M. Rao, E. C. Friedberg and L. Queimado, Identification of MMS19 domains with distinct functions in NER and transcription, *DNA Repair*, 2006, **5**, 914-924.

69. S. J. Ciesielski, B. A. Schilke, J. Osipiuk, L. Bigelow, R. Mulligan, J. Majewska, A. Joachimiak, J. Marszalek, E. A. Craig and R. Dutkiewicz, Interaction of J-Protein Co-Chaperone Jac1 with Fe–S Scaffold Isu Is Indispensable In Vivo and Conserved in Evolution, *Journal of Molecular Biology*, 2012, **417**, 1-12.

70. C. Voisine, Y. C. Cheng, M. Ohlson, B. Schilke, K. Hoff, H. Beinert, J. Marszalek and E. A. Craig, Jac1, a mitochondrial J-type chaperone, is involved in the biogenesis of Fe/S clusters in Saccharomyces cerevisiae, *Proceedings of the National Academy of Sciences of the United States of America*, 2001, **98**, 1483-1488.

71. W. Voos and K. Röttgers, Molecular chaperones as essential mediators of mitochondrial biogenesis, *Biochimica et Biophysica Acta - Molecular Cell Research*, 2002, **1592**, 51-62.

72. R. Dutkiewicz, B. Schilke, S. Cheng, H. Knieszner, E. A. Craig and J. Marszalek, Sequence-specific Interaction between Mitochondrial Fe-S Scaffold Protein Isu and Hsp70 Ssq1 Is Essential for Their in Vivo Function, *Journal of Biological Chemistry*, 2004, **279**, 29167-29174.

73. N. Maio, A. Singh, H. Uhrigshardt, N. Saxena, W.-H. Tong and Tracey A. Rouault, Cochaperone Binding to LYR Motifs Confers Specificity of Iron Sulfur Cluster Delivery, *Cell Metabolism*, **19**, 445-457.

74. S. A. Cory, J. G. Van Vranken, E. J. Brignole, S. Patra, D. R. Winge, C. L. Drennan, J. Rutter and D. P. Barondeau, Structure of human Fe–S assembly subcomplex reveals unexpected cysteine desulfurase architecture and acyl-ACP–ISD11 interactions, *Proceedings of the National Academy of Sciences of the United States of America*, 2017, **114**, E5325.

75. K. S. Kim, N. Maio, A. Singh and T. A. Rouault, Cytosolic HSC20 integrates de novo iron–sulfur cluster biogenesis with the CIAO1-mediated transfer to recipients, *Human Molecular Genetics*, 2018, DOI: 10.1093/hmg/ddy004, ddy004-ddy004.

76. Y. Wu and R. M. Brosh, DNA helicase and helicase-nuclease enzymes with a conserved iron-sulfur cluster., *Nucleic Acids Research*, 2012, **40**, 4247-4260.

77. E. Weerapana, C. Wang, G. M. Simon, F. Richter, S. Khare, M. B. Dillon, D. A. Bachovchin, K. Mowen, D. Baker and B. F. Cravatt, Quantitative reactivity profiling predicts functional cysteines in proteomes, *Nature*, 2010, **468**, 790-795.

78. P. C. Havugimana, G. T. Hart, T. Nepusz, H. Yang, A. L. Turinsky, Z. Li, P. I. Wang, D. R. Boutz, V. Fong, S. Phanse, M. Babu, S. A. Craig, P. Hu, C. Wan, J. Vlasblom, V. U. Dar, A. Bezginov, G. W. Clark, G. C. Wu, S. J. Wodak, E. R. Tillier, A. Paccanaro, E. M. Marcotte and A. Emili, A census of human soluble protein complexes, *Cell*, 2012, **150**, 1068-1081.

79. Y. Ho, A. Gruhler, A. Heilbut, G. D. Bader, L. Moore, S.-L. Adams, A. Millar, P. Taylor, K. Bennett, K. Boutilier, L. Yang, C. Wolting, I. Donaldson, S. Schandorff, J. Shewnarane, M. Vo, J. Taggart, M. Goudreault, B. Muskat, C. Alfarano, D. Dewar, Z. Lin, K. Michalickova, A. R. Willems, H. Sassi, P. A. Nielsen, K. J. Rasmussen, J. R. Andersen, L. E. Johansen, L. H. Hansen, H. Jespersen, A. Podtelejnikov, E. Nielsen, J. Crawford, V. Poulsen, B. D. Sørensen, J. Matthiesen, R. C. Hendrickson, F. Gleeson, T. Pawson, M. F. Moran, D. Durocher, M. Mann, C. W. V. Hogue, D. Figeys and M. Tyers, Systematic identification of protein complexes in Saccharomyces cerevisiae by mass spectrometry, *Nature*, 2002, **415**, 180-183.

80. T. Ito, T. Chiba, R. Ozawa, M. Yoshida, M. Hattori and Y. Sakaki, A comprehensive two-hybrid analysis to explore the yeast protein interactome, *Proceedings of the National Academy of Sciences of the United States of America*, 2001, **98**, 4569-4574.

81. N. J. Krogan, G. Cagney, H. Yu, G. Zhong, X. Guo, A. Ignatchenko, J. Li, S. Pu, N. Datta, A. P. Tikuisis, T. Punna, J. M. Peregrin-Alvarez, M. Shales, X. Zhang,

M. Davey, M. D. Robinson, A. Paccanaro, J. E. Bray, A. Sheung, B. Beattie, D. P. Richards, V. Canadien, A. Lalev, F. Mena, P. Wong, A. Starostine, M. M. Canete, J. Vlasblom, S. Wu, C. Orsi, S. R. Collins, S. Chandran, R. Haw, J. J. Rilstone, K. Gandi, N. J. Thompson, G. Musso, P. St Onge, S. Ghanny, M. H. Lam, G. Butland, A. M. Altaf-Ul, S. Kanaya, A. Shilatifard, E. O'Shea, J. S. Weissman, C. J. Ingles, T. R. Hughes, J. Parkinson, M. Gerstein, S. J. Wodak, A. Emili and J. F. Greenblatt, Global landscape of protein complexes in the yeast Saccharomyces cerevisiae, *Nature*, 2006, **440**, 637-643.

82. P. Uetz, L. Giot, G. Cagney, T. A. Mansfield, R. S. Judson, J. R. Knight, D. Lockshon, V. Narayan, M. Srinivasan, P. Pochart, A. Qureshi-Emili, Y. Li, B. Godwin, D. Conover, T. Kalbfleisch, G. Vijayadamodar, M. Yang, M. Johnston, S. Fields and J. M. Rothberg, A comprehensive analysis of protein-protein interactions in Saccharomyces cerevisiae, *Nature*, 2000, **403**, 623-627.

83. J. W. Peters, G. J. Schut, E. S. Boyd, D. W. Mulder, E. M. Shepard, J. B. Broderick, P. W. King and M. W. Adams, [FeFe]- and [NiFe]-hydrogenase diversity, mechanism, and maturation, *Biochimica et Biophysica Acta*, 2015, **1853**, 1350-1369.

84. K. E. Chen, A. A. Richards, J. K. Ariffin, I. L. Ross, M. J. Sweet, S. Kellie, B. Kobe and J. L. Martin, The mammalian DUF59 protein Fam96a forms two distinct types of domain-swapped dimer, *Acta Crystallographica. Section D Biological Crystallography,* 2012, **68**, 637-648.

85. A. C. Gavin, M. Bosche, R. Krause, P. Grandi, M. Marzioch, A. Bauer, J. Schultz, J. M. Rick, A. M. Michon, C. M. Cruciat, M. Remor, C. Hofert, M. Schelder, M. Brajenovic, H. Ruffner, A. Merino, K. Klein, M. Hudak, D. Dickson, T. Rudi, V. Gnau, A. Bauch, S. Bastuck, B. Huhse, C. Leutwein, M. A. Heurtier, R. R. Copley, A. Edelmann, E. Querfurth, V. Rybin, G. Drewes, M. Raida, T. Bouwmeester, P. Bork, B. Seraphin, B. Kuster, G. Neubauer and G. Superti-Furga, Functional organization of the yeast proteome by systematic analysis of protein complexes, *Nature*, 2002, **415**, 141-147.

86. A. D. Tsaousis, E. Gentekaki, L. Eme, D. Gaston and A. J. Roger, Evolution of the cytosolic iron-sulfur cluster assembly machinery in Blastocystis species and other microbial eukaryotes, *Eukaryotic Cell*, 2014, **13**, 143-153.

87. A. H. Kachroo, J. M. Laurent, C. M. Yellman, A. G. Meyer, C. O. Wilke and E. M. Marcotte, Evolution. Systematic humanization of yeast genes reveals conserved functions and genetic modularity, *Science*, 2015, **348**, 921-925.

88. J. Balk, A. J. Pierik, D. J. Aguilar Netz, U. Mühlenhoff and R. Lill, Nar1p, a conserved eukaryotic protein with similarity to Fe-only hydrogenases, functions in cytosolic iron-sulphur protein biogenesis, *Biochemical Society Transactions*, 2005, **33**, 86-89.

89. N. D. Lanz, T. L. Grove, C. B. Gogonea, K.-H. Lee, C. Krebs and S. J. Booker, in *Methods in Enzymology*, ed. D. A. Hopwood, Academic Press, 2012, vol. 516, pp. 125-152.

90. J. D. Grossman, E. J. Camire and D. L. Perlstein, in *Methods in Enzymology*, Academic Press, 2018, DOI: https://doi.org/10.1016/bs.mie.2017.11.005.

91. H. Beinert, Semi-micro methods for analysis of labile sulfide and of labile sulfide plus sulfane sulfur in unusually stable iron-sulfur proteins, *Analytical Biochemistry*, 1983, **131**, 373-378.

92. A. Yan and P. J. Kiley, in *Methods in Enzymology*, eds. R. R. Burgess and M. P. Deutscher, Academic Press, 2009, vol. 463, pp. 787-805.

93. Y. Wu and R. M. Brosh, DNA helicase and helicase-nuclease enzymes with a conserved iron-sulfur cluster, *Nucleic Acids Research*, 2012, DOI: 10.1093/nar/gks039.

94. S. Ito, L. J. Tan, D. Andoh, T. Narita, M. Seki, Y. Hirano, K. Narita, I. Kuraoka, Y. Hiraoka and K. Tanaka, MMXD, a TFIIH-independent XPD-MMS19 protein complex involved in chromosome segregation, *Molecular Cell*, 2010, **39**, 632-640.

95. V. Desiree Paul, U. Muhlenhoff, M. Stumpfig, J. Seebacher, K. G. Kugler, C. Renicke, C. Taxis, A. C. Gavin, A. J. Pierik and R. Lill, The deca-GX proteins Yae1-Lto1 function as adaptors recruiting the ABC protein Rli1 for iron-sulfur cluster insertion, *Elife*, 2015, **4**.

96. J. Crack, J. Green and A. J. Thomson, Mechanism of Oxygen Sensing by the Bacterial Transcription Factor Fumarate-Nitrate Reduction (FNR), *Journal of Biological Chemistry*, 2004, **279**, 9278-9286.

97. D. M. Bates, C. V. Popescu, N. Khoroshilova, K. Vogt, H. Beinert, E. Münck and P. J. Kiley, Substitution of Leucine 28 with Histidine in theEscherichia coli Transcription Factor FNR Results in Increased Stability of the [4Fe-4S]2+ Cluster to Oxygen, *Journal of Biological Chemistry*, 2000, **275**, 6234-6240.

98. N. Maio and T. A. Rouault, Iron-sulfur cluster biogenesis in mammalian cells: New insights into the molecular mechanisms of cluster delivery, *Biochimica et Biophysica Acta*, 2015, **1853**, 1493-1512.

99. T. R. Hughes, M. J. Marton, A. R. Jones, C. J. Roberts, R. Stoughton, C. D. Armour, H. A. Bennett, E. Coffey, H. Dai, Y. D. He, M. J. Kidd, A. M. King, M. R. Meyer, D. Slade, P. Y. Lum, S. B. Stepaniants, D. D. Shoemaker, D. Gachotte, K. Chakraburtty, J. Simon, M. Bard and S. H. Friend, Functional Discovery via a Compendium of Expression Profiles, *Cell*, 2000, **102**, 109-126.

100. S. Mnaimneh, A. P. Davierwala, J. Haynes, J. Moffat, W.-T. Peng, W. Zhang, X. Yang, J. Pootoolal, G. Chua, A. Lopez, M. Trochesset, D. Morse, N. J. Krogan, S. L. Hiley, Z. Li, Q. Morris, J. Grigull, N. Mitsakakis, C. J. Roberts, J. F. Greenblatt, C. Boone, C. A. Kaiser, B. J. Andrews and T. R. Hughes, Exploration of Essential Gene Functions via Titratable Promoter Alleles, *Cell*, 2004, **118**, 31-44.

101. P. Tompa, Intrinsically unstructured proteins, *Trends in Biochemical Sciences*, 2002, **27**, 527-533.

102. M. S. Almeida, T. Herrmann, W. Peti, I. A. Wilson and K. Wüthrich, NMR structure of the conserved hypothetical protein TM0487 from Thermotoga maritima: Implications for 216 homologous DUF59 proteins, *Protein Science*, 2005, **14**, 2880-2886.

103. P. C. Dos Santos, A. D. Smith, J. Frazzon, V. L. Cash, M. K. Johnson and D. R. Dean, Iron-Sulfur Cluster Assembly: NifU-directed activations of the nitrogenase Fe protein, *Journal of Biological Chemistry*, 2004, **279**, 19705-19711.

104. J. N. Agar, P. Yuvaniyama, R. F. Jack, V. L. Cash, A. D. Smith, D. R. Dean and M. K. Johnson, Modular organization and identification of a mononuclear iron-binding site within the NifU protein, *Journal of Biological Inorganic Chemistry*, 2000, **5**, 167-177.

105. B. Py, C. Gerez, S. Angelini, R. Planel, D. Vinella, L. Loiseau, E. Talla, C. Brochier-Armanet, R. Garcia Serres, J.-M. Latour, S. Ollagnier-de Choudens, M. Fontecave and F. Barras, Molecular organization, biochemical function, cellular role and evolution of NfuA, an atypical Fe-S carrier, *Molecular Microbiology*, 2012, **86**, 155-171.

106. S. Angelini, C. Gerez, S. Ollagnier-de Choudens, Y. Sanakis, M. Fontecave, F. Barras and B. Py, NfuA, a new factor required for maturing Fe/S proteins in Escherichia coli under oxidative stress and iron starvation conditions, *Journal of Biological Chemistry*, 2008, **283**, 14084-14091.

107. S. Bandyopadhyay, K. Chandramouli and M. K. Johnson, Iron-sulfur cluster biosynthesis, *Biochemical Society Transactions*, 2008, **36**, 1112-1119.

108. S. Bandyopadhyay, S. G. Naik, I. P. O'Carroll, B.-H. Huynh, D. R. Dean, M. K. Johnson and P. C. Dos Santos, A proposed role for the Azotobacter vinelandii NfuA protein as an intermediate iron-sulfur cluster carrier, *The Journal of Biological Chemistry*, 2008, **283**, 14092-14099.

109. L. H. L. M. Laakso, Dali server update, *Nucleic Acids Research*, 2016, **44**, W361-355

.

110. T. Yabe, E. Yamashita, A. Kikuchi, K. Morimoto, A. Nakagawa, T. Tsukihara and M. Nakai, Structural analysis of Arabidopsis CnfU protein: an iron-sulfur cluster biosynthetic scaffold in chloroplasts, *Journal of Molecular Biology*, 2008, **381**, 160-173.

111. K. E. Chen, A. A. Richards, J. K. Ariffin, I. L. Ross, M. J. Sweet, S. Kellie, B. Kobe and J. L. Martin, The mammalian DUF59 protein Fam96a forms two distinct types of domain-swapped dimer, *Acta Crystallographica. Section D Biological Crystallography* , 2012, **68**, 637-648.

112. I. Lev, M. Volpe, L. Goor, N. Levinton, L. Emuna and S. Ben-Aroya, Reverse PCA, a systematic approach for identifying genes important for the physical interaction between protein pairs, *PLoS Genetics*, 2013, **9**, e1003838.

113. B. Ouyang, L. Wang, S. Wan, Y. Luo, L. Wang, J. Lin and B. Xia, Solution structure of monomeric human FAM96A, *Journal of Biomolecular NMR*, 2013, **56**, 387-392.

114. J. Crack, A. Jervis, A. A Gaskell, G. White, J. Green, A. Thomson and N. Le Brun, *Signal perception by FNR: The role of the iron-sulfur cluster*, 2009.

115. B. Kobe, T. Gleichmann, J. Horne, I. G. Jennings, P. D. Scotney and T. Teh, Turn up the HEAT, *Structure*, 1999, **7**, R91-R97.

116. G. E. Crooks, G. Hon, J.-M. Chandonia and S. E. Brenner, WebLogo: A Sequence Logo Generator, *Genome Research*, 2004, **14**, 1188-1190.

117. E. A. Winzeler, D. D. Shoemaker, A. Astromoff, H. Liang, K. Anderson, B. Andre, R. Bangham, R. Benito, J. D. Boeke, H. Bussey, A. M. Chu, C. Connelly, K. Davis, F. Dietrich, S. W. Dow, M. El Bakkoury, F. Foury, S. H. Friend, E. Gentalen, G. Giaever, J. H. Hegemann, T. Jones, M. Laub, H. Liao, N. Liebundguth, D. J. Lockhart, A. Lucau-Danila, M. Lussier, N. M'Rabet, P. Menard, M. Mittmann, C. Pai, C. Rebischung, J. L. Revuelta, L. Riles, C. J. Roberts, P. Ross-MacDonald, B. Scherens, M. Snyder, S. Sookhai-Mahadeo, R. K. Storms, S. Véronneau, M. Voet, G. Volckaert, T. R. Ward, R. Wysocki, G. S. Yen, K. Yu, K. Zimmermann, P. Philippsen, M. Johnston and R. W. Davis, Functional characterization of the S. cerevisiae genome by gene deletion and parallel analysis, *Science*, 1999, **285**, 901-906.

118. A. Drozdetskiy, C. Cole, J. Procter and G. J. Barton, JPred4: a protein secondary structure prediction server, *Nucleic Acids Research*, 2015, **43**, W389-W394.

119. Y. Zhang, I-TASSER server for protein 3D structure prediction, *BMC Bioinformatics*, 2008, **9**, 40.

120. L. A. Kelley, S. Mezulis, C. M. Yates, M. N. Wass and M. J. E. Sternberg, The Phyre2 web portal for protein modeling, prediction and analysis, *Nature Protocols*, 2015, **10**, 845.

121. M. Masselot and Y. Surdin-Kerjan, *Methionine biosynthesis in Saccharomyces cerevisiae. II. Gene-enzyme relationships in the sulfate assimilation pathway*, 1977.

122. L. J. Pallesen, N. Solodovnikova, A. K. Sharma and W. E. Walden, Interaction with Cfd1 Increases the Kinetic Lability of FeS on the Nbp35 Scaffold, *Journal of Biological Chemistry*, 2013, **288**, 23358-23367.

123. X. Tang, G. R. Munske, W. F. Siems and J. E. Bruce, Mass Spectrometry Identifiable Cross-Linking Strategy for Studying Protein−Protein Interactions, *Analytical Chemistry*, 2005, **77**, 311-318.

124. M. Brosch, L. Yu, T. Hubbard and J. Choudhary, Accurate and Sensitive Peptide Identification with Mascot Percolator, *Journal of Proteome Research*, 2009, **8**, 3176-3181.

125. B. Clifford-Nunn, H. D. H. Showalter and P. C. Andrews, Quaternary Diamines as Mass Spectrometry Cleavable Crosslinkers for Protein Interactions, *Journal of the American Society for Mass Spectrometry*, 2012, **23**, 201-212.

126. D. G. Gibson, L. Young, R. Y. Chuang, J. C. Venter, C. A. Hutchison, 3rd and H. O. Smith, Enzymatic assembly of DNA molecules up to several hundred kilobases, *Nat Methods*, 2009, **6**, 343-345.

127. F. W. Studier, Protein production by auto-induction in high-density shaking cultures, *Protein Expression and Purification*, 2005, **41**, 207-234.

128. R. van der Lee, M. Buljan, B. Lang, R. J. Weatheritt, G. W. Daughdrill, A. K. Dunker, M. Fuxreiter, J. Gough, J. Gsponer, D. T. Jones, P. M. Kim, R. W. Kriwacki, C. J. Oldfield, R. V. Pappu, P. Tompa, V. N. Uversky, P. E. Wright and M. M. Babu, Classification of intrinsically disordered regions and proteins, *Chemical Reviews*, 2014, **114**, 6589-6631.

129. M. D. Hatfield, A. M. Reis, D. Obeso, J. R. Cook, D. M. Thompson, M. Rao, E. C. Friedberg and L. Queimado, Identification of MMS19 domains with distinct functions in NER and transcription, *DNA Repair*, 2006, **5**, 914-924.

130. H. Liu and J. H. Naismith, An efficient one-step site-directed deletion, insertion, single and multiple-site plasmid mutagenesis protocol, *BMC Biotechnology*, 2008, **8**, 91-91.

CURRICULUM VITAE